COMPUTATIONAL FLUID DYNAMICS STUDY OF HYDROGEN GENERATION BY LOW TEMPERATURE STEAM METHANE REFORMING IN A MEMBRANE REACTOR

BY

MOHAMMED WASEEUDDIN

A Thesis Presented to the
DEANSHIP OF GRADUATE STUDIES

KING FAHD UNIVERSITY OF PETROLEUM & MINERALS
DHAHRAN, SAUDI ARABIA

In Partial Fulfillment of the
Requirements for the Degree of

MASTER OF SCIENCE

In

MECHANICAL ENGINEERING

KING FAHD UNIVERSITY OF PETROLEUM & MINERALS

DHAHRAN- 31261, SAUDI ARABIA

DEANSHIP OF GRADUATE STUDIES

This thesis, written by **MOHAMMED WASEEUDDIN** under the direction his thesis advisor and approved by his thesis committee, has been presented and accepted by the Dean of Graduate Studies, in partial fulfillment of the requirements for the degree of **MASTER OF SCIENCE IN MECHANICAL ENGINEERING.**

Dr. Syed A.M. Said
(Advisor)

Dr.Zuhair Gasem
Department Chairman

Dr. Shakeel Ahmed
(Co-Advisor)

Dr. Salam A. Zummo
Dean of Graduate Studies

Dr. Mohamed. A. Habib
(Member)

3/3/15
Date

Dr. Esmail M. A. Mokheimer
(Member)

Dr.Habib I. Abualhamayel
(Member)

To my beloved parents, Wahab and Rahmath,

And my ever encouraging brothers Wali, Wajhee and Wafi

ACKNOWLEDGMENTS

All praise is to ALLAH (S.W.T), the Compassionate, the Merciful, and the Lord of the Worlds and the Hereafter, to Him we belong and to Him shall we return. May ALLAH shower his countless blessings and bounties on Prophet MUHAMMED (S.A.W.S), the Mercy to all Mankind. May ALLAH (S.W.T) send HIS blessings on all the COMPANIONS (R.A) and the AHLUL BAYT (R.A) of Prophet MUHAMMED (S.A.W.S) who are indeed better than us in Emaan and Taqwaa.

I would like to extend my thanks to Dr. S. A. M. Said, my thesis advisor, who supported, motivated and nurtured me time and again from my arrival to departure from KFUPM. I would also like to thank my thesis co-advisor, Dr. Shakeel Ahmed for sharing his experience and knowledge throughout my work. I thank my entire thesis committee for the valuable suggestions provided to me during the numerous group meetings and discussions held. My heartfelt thanks to Dr. David Simakov from MIT for his endless help and suggestions during this work.

My profound gratitude goes to my family *(Daddy, Ammi, Bhaipasha, Wajhee and Wafi)* who were extremely patient during my stay at KFUPM when they needed me the most. I whole heartedly appreciate the support from my friends *Azhar, Mujtaba, Imtiyaz, Sami, Azharuddin, Pervez Ahmed.* My extended thanks to *Mr. Ibrar Hussain* for all the help provided during computational difficulties.

To all other individuals who in one way or the other had contributed to the success of this work, to you all, and from the bottom of my heart I say thank you and may you continue to enjoy the blessings of ALLAH.

TABLE OF CONTENTS

LIST OF TABLES

LIST OF FIGURES

LIST OF ABBREVIATIONS

AMG	Aggressive Advanced Multigrid
ATR	Auto Thermal Reforming
BCGSTAB	Bi-Conjugate Gradient Stabilized Method
CCS	Carbon Capture and Sequestration
ECBM	Enhanced Coal Bed Methane Recovery
GHSV	Gas Hourly Space Velocity
IPCC	Intergovernmental Panel on Climate Change
SIMPLE	Semi-Implicit Method for Pressure-Linked Equations
SMR	Steam Reforming of Methane
UDF	User-Defined Function
WGS	Water Gas Shift

ABSTRACT

NAME : MOHAMMED WASEEUDDIN

TITLE : COMPUTATIONAL FLUID DYNAMICS STUDY OF HYDROGEN GENERATION BY LOW TEMPERATURE METHANE REFORMING IN A MEMBRANE REACTOR

MAJOR : MECHANICAL ENGINEERING

DATE : DECEMBER 2014

The world energy sector is dominated by the combustion of fossil fuels, leading to excessive carbon dioxide emissions and environmental pollution. Hydrogen is a more efficient and cleaner combustion fuel. It is mainly produced via methane reforming – a highly endothermic process that requires combusting ~30% of the fuel input to provide the heat to drive the reaction. This fraction can be saved by the use of concentrated solar energy via solar thermal reforming. An attractive route is the parabolic trough technology, which is mature and inexpensive but restricted to temperatures below 600 °C. Although at such temperatures methane conversion is low, removing hydrogen from the reactive stream by a permselective membrane drives the equilibrium towards products and high conversions are accessible. In this study, low temperature methane reforming in a membrane reactor is analyzed numerically by computational fluid dynamics. Effects of temperature, steam-to-carbon ratio and space velocity on conversion, hydrogen recovery and carbon monoxide selectivity are specifically investigated. Our results show that below 500 °C the reactor performance is kinetically limited by the reforming reaction,

while above this temperature hydrogen separation is a limiting factor. High hydrogen recovery is achievable even at high, industrially relevant space velocities. Importantly, hydrogen separation enhances water gas shift, reducing the concentration of carbon monoxide, the main source of coke formation at low temperatures.

MASTER OF SCIENCE DEGREE

KING FAHD UNIVERSITY OF PETROLEUM & MINERALS

Dhahran, Saudi Arabia

ملخص الرسالة

الاسم الكامل: محمد وصي الدين

عنوان الرسالة: دراسة انتاج الهيدروجين عند درجات حرارة اصلاح الميثان المنخفضة في مفاعلات الأغشية باستخدام طرق حوسبة الموائع.

التخصص: الهندسة الميكانيكية

تاريخ الدرجة العلمية: ربيع الأول 1436هـ

يهيمن احتراق المحروقات الأحفوري على قطاع انتاج الطاقة في العالم مما يتسبب في انبعاثات ثاني أوكسيد الكربون والتلوث البيئي. يعتبر الهيدروجين وقود نظيف وذو كفاءة عالية. يتم انتاج الهيدروجين بصورة أساسية من عملية اصلاح الميثان والتي تصنف كعمليه ماصة للحرارة تستهلك حوالي 30% من الوقود المستخدم لتوفير الحرارة للتفاعل. هذه النسبة يمكن توفيرها بواسطة مركزات الطاقة الشمسية. تعتبر تقنية القطع المكافئ الشمسي جاذبه لأنها تقنية ناضجه وغير مكلفة ولكنها محدودة لدرجات الحرارة الأقل من 600 درجة مئوية. بالرغم من أنه عند هذه الدرجة تكون عملية تحويل الميثان منخفضة، فان استخراج الهيدروجين من البخار المتفاعل بواسطة الأغشية يقود الى الاتزان في المواد الناتجة من التفاعل ويمكن من الوصول الى عمليات التحويل عالية. في هذه الدراسة تم تحليل عملية اصلاح الميثان، بدرجة حرارة منخفضه في مفاعل أغشية، عدديا وباستخدام العمليات الحاسوبية لميكانيكا الموائع. تم دراسة أثر درجة الحرارة، نسبة البخار/الكربون والسرعة على عملية التحويل. تم تحديدا الاستقصاء عن درجة استعادة الهيدروجين وانتقائية ثاني أول الكربون. أظهرت النتائج في درجات الحرارة أقل من 500 درجة أن أداء المفاعل يكون محدودا بإصلاح التفاعل، بينما في درجات الحرارة الأعلى يكون فصل الهيدروجين هو العامل المهم. أيضا، يمكن استعادة الهيدروجين حتى في السرعات العالية. الأكثر أهمية، أن فصل الهيدروجين يؤدي الى خفض تركيز أول أكسيد الكربون والذي يعتبر العامل الأساسي في تكوين الفحم عند درجات الحرارة المنخفضة.

CHAPTER 1

INTRODUCTION

1.1 Research Background

The energy sector worldwide is largely dominated by the burning of fossil fuels which leads to the emissions of CO_2 into the atmosphere and is known to contribute to the undesired global warming. It is generally accepted that the increase in the temperature of the earth is linked to the increase in greenhouse gases, mostly CO_2, in the atmosphere. Saudi Arabia has ratified the Kyoto protocol [1], which sets strict limits on emissions of CO_2 and imposes penalties.

CO_2 is a major greenhouse gas released whenever fuels containing hydrocarbon, such as methane, are burned. Most of the world's energy needs are currently met by combustion of hydrocarbon fuels. Renewable energies are alternatives which provide a favourable solution to the problem of greenhouse gas emissions. But these technologies are currently not mature enough in comparison to fossil fuel based technologies. Still more research is required on renewables to produce a major portion of our energy. Another method of power production is nuclear technology that does not contribute to the global warming problem. However acceptance of nuclear power by the public is quite low, particularly in Saudi Arabia.

Fossil fuels are heavily used in power industry as it is relatively cheap and abundant. The Hubbert oil peak is the maximum production of oil. In theory it coincides with the midpoint of the available oil in a region. Various current estimates place the world peak

between 2009 and 2035 [2], implying that there is at least as much oil still available in the world as has been consumed since the industrial revolution. The discovery of methane hydrates in vast quantities indicates that fossil fuel will continue to be used for decades to come. Unfortunately combustion of these fuels produces pollutants and CO_2, the main contributor to global warming. One of the main challenge facing engineers now is how to reduce or prevent the negative impact of CO_2 on the climate caused from power plants, while allowing the continued use of fossil fuels for power production.

The statement given by IPCC [3]: 'Emissions of CO_2 due to fossil fuel burning are virtually certain to be the dominant influence of the trends in atmospheric CO_2 concentration during the 21st century'. CO_2 is considered to be the greenhouse gas that makes the largest contribution from human activities. With the on-going debate on global warming and climate changes there is a clear incentive to investigate strategies to reduce the emissions of CO_2 to the atmosphere. One way to achieve this is to remove CO_2 from exhaust gases from the power plants and store it away from the atmosphere, i.e. CO_2-capture and sequestration.

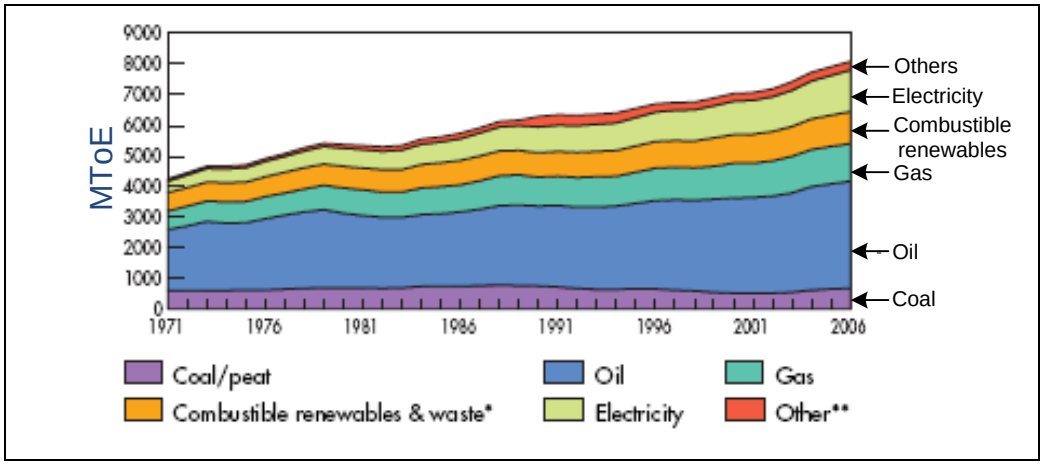

Figure 1.1: World Energy consumption based on the types of fuel (Mtoe) [4]

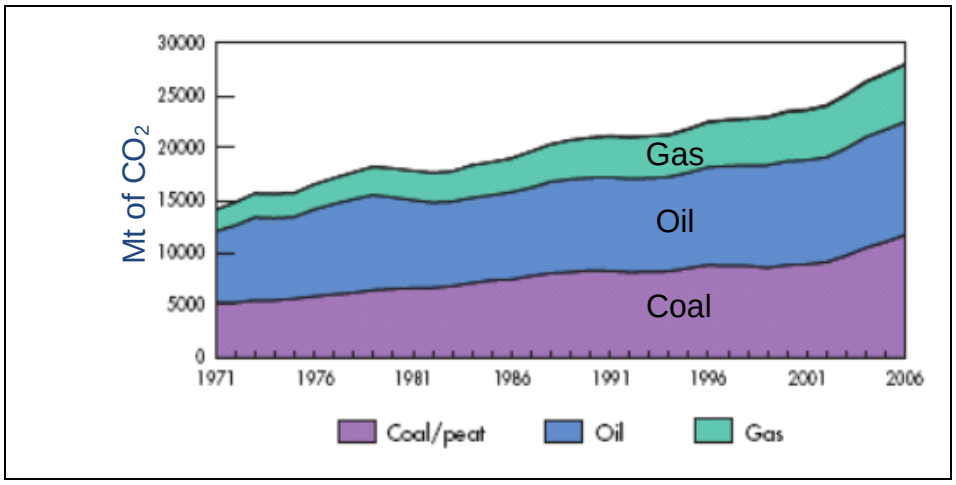

Figure 1.2: World CO_2 emissions from different types of fuels (Mt of CO_2) [4]

Figure 1.1 show how the world energy is produced in the last few decades [4]. As most of the energy is produced from fossil fuels, this also causes an increase in CO_2 emissions which can be seen clearly in Figure 1.2. According to IPCC [5], the average yearly growth in CO_2 emissions during the period 1995-2001 was 1.4%, a number that was higher than the five year period before that.

Carbon capture and sequestration (CCS) means capturing CO_2 and trapping it away from the atmosphere. There are many methods of sequestering CO_2 either by utilization in industrial processes or by storage underground or in deep seas. Enhanced Oil Recovery (EOR) is another option which involves injecting CO_2 into partially depleted oil wells to increase oil production. This is currently a common practice in many oil companies. Over 40 Million cubic feet of CO_2 can be injected daily into oil well in Ghawar, Saudi Arabia by 2012 which was reported by Minister of Petroleum, Saudi Arabia [6].

CO_2 is also utilized in Enhanced Coal Bed Methane Recovery (ECBM) for harvesting methane from unmineable coal by injecting CO_2 into the coal bed. The neutralization of alkali pollutants can be done by using CO_2 in polluted areas. Yet another method is to

absorb CO_2 into coal beds that are inaccessible and cannot be mined. Some minerals will react with CO_2 to form a solid product. There are two methods of doing this; the first is mining the reactant mineral and the second is reacting it with CO_2 to produce a product which can be used in road pavement, or injecting CO_2 into subterranean caverns containing the reactant mineral, and allowing it to slowly react over time. Other methods of CO_2 storage include injection into some geological formations, particularly porous rock.

Until now, many methods have been proposed for capturing CO_2 produced by combustion of fossil fuels for production of electricity. The fuel may be burned in air, and the exhaust products separated to capture CO_2. This usually involves either cryogenic or chemical processes, or use of membranes to separate gases. These methods are costly and consume a large amount of energy, thus resulting in reducing the power plant efficiency. Since it is now necessary to look for a clean energy source, the available choices are hydrogen and green solutions. The carbon is removed from hydrocarbon fuel before combustion, by conversion of methane to syngas, a mixture of carbon monoxide (CO) and hydrogen (H_2), followed by separation of H_2 from the mixture. This process is called the steam methane reforming process which is the cheapest, oldest and most widely used method to produce hydrogen commercially worldwide [7]. It is possible to produce pure H_2 by this method, so that the H_2-using technology is emission free. This mixture is also an energy rich fuel source, having the potential to replace the existing fossil fuel sources used in the power industry. Hydrocarbons usually used for hydrogen production are natural gas, liquid gas, naphtha, coal and methane among which methane

is highly used due to its high hydrogen content and low capital costs compared to other hydrocarbons. Steam reforming of methane of methane is given by the reactions:

$$CH_4 + H_2O \rightleftharpoons CO + 3H_2 \qquad \Delta H^{o}_{298} = 206 \text{ kJ/mol} \qquad (1)$$

$$CO + H_2O \rightleftharpoons CO_2 + H_2 \qquad \Delta H^{o}_{298} = -41.1 \text{ kJ/mol} \qquad (2)$$

$$CH_4 + 2H_2O \rightleftharpoons CO_2 + 4H_2 \qquad \Delta H^{o}_{298} = 164.9 \text{ kJ/mol} \qquad (3)$$

The first reaction that is the steam methane reforming reaction is highly endothermic and requires large amounts of heat energy for the process to take place. This heat energy is provided by firing the catalyst filled reforming reactor tubes from outside and the feed to flow from inside the tubes. SMR process is always followed by the Water Gas Shift reaction where the CO produced in the first reaction is reacted with steam over a catalyst to produce H_2 and CO_2. Though the WGS reaction is exothermic, the highly endothermic nature of SMR process over shadows the amount of heat produced by the WGS reaction. The third reaction is simply the overall reaction known as Methanation reaction which is also endothermic. Steam reforming of methane is also a reversible reaction and in order to obtain higher methane conversions, it is necessary to conduct the reforming reaction at high temperatures, low pressures and relatively high steam to carbon ratios [8].

1.2 Problem Statement

A steam methane reforming reactor with a palladium based hydrogen permeable membrane for selective removal of hydrogen has been studied focusing the low temperatures generated by solar parabolic troughs. The inlet feed to the reforming reactor consists of CH_4 and H_2O which convert into H_2, CO and CO_2 at the exit when heat is applied at the boundary wall of the reactor. The hydrogen formed by the steam methane

reforming process is allowed to permeate through the membrane wall and thus pure hydrogen can be obtained at exit of the permeate side. Effect of gas hourly space velocities, steam to carbon ratio in the inlet feed on fractional methane conversion, the H_2/CO ratio and hydrogen recovery for the membrane reactor are focused in the analyses. The membrane considered in this work is a palladium membrane which is highly selective to hydrogen. The outcome of this study illustrates the performance of a membrane reformer under different reforming conditions which can be the first step in designing a reforming reactor for low temperature solar applications.

1.3 Objectives

The overall objective of this work is to investigate the performance of steam methane reforming process in a hydrogen permeable palladium membrane reforming reactor for low temperature solar applications. However, the specific objectives of this thesis are listed as:

1. To develop a computational fluid dynamics model for low temperature steam methane reforming process.
2. To validate of the model developed using experimental data in the literature.
3. To incorporate the effect of hydrogen permeation in the developed model by creating source and sink terms at the membrane boundary cells in the continuity and species transport equation.
4. To study the effect of operating temperatures, gas hourly space velocities and steam methane ratios of the feed on the performance parameters fractional methane conversion, H_2/CO ratio and hydrogen recovery.

1.4 Thesis Outline

This thesis contains six chapters.

Chapter 1 introduces the subject of global warming and the remedies to mitigate greenhouse gases specially CO_2. The utilization of CO_2 in various industrial processes is also presented. The problem statement and objectives of the present thesis are discussed.

Chapter 2 is mainly a literature review and is divided in three sections. First section is about the process of steam reforming of methane. The second section discusses the membranes for steam reforming. The last section highlights the numerical schemes that were applied by previous researchers for steam reforming and H_2 separation technologies.

In Chapter 3, a membrane permeation model for steam reforming of methane has been developed in order to study separation of H_2 from the reforming reaction mixture.

In Chapter 4 the numerical method used for solving the flow, species transport and steam methane reforming processes is discussed. The results of grid independence test and validation of the computational code are presented.

Chapter 5 is divided into two sections. This chapter focuses on discussion of results in the membrane in tube model (2-Compartment model) developed in Chapter 3.

In Chapter 6, the conclusions of this study are presented. The recommendations of possible future research in this area also presented.

CHAPTER 2

LITERATURE REVIEW

The literature review presented in this chapter is divided into three sections. The first section presents the steam reforming of methane process focusing the different kinds of reforming process and the chemical kinetics. In the second section, solar steam reforming systems have been discussed. In the third section, the numerical investigations carried out in the area of steam reforming have been presented.

2.1 Steam Reforming of Methane

2.1.1 The Reforming Process:

Steam reforming of methane is a catalytically promoted highly endothermic reaction. In this process, mixture of methane and steam is passed over the surface of catalyst. Hydrogen and carbon monoxide are formed as products whereas some CO_2 is also formed as a byproduct. The reaction is reversible in nature so methane and steam are also present in the product mixture. The steam reforming process produces syngas with a ratio $H_2/CO = 3$. Steam reacts with methane in a catalyst bed to produce syngas [9]. The steam methane reforming reaction is as follows.

$$CH_4 + H_2O \rightleftharpoons CO + 3H_2 \qquad \Delta H^{o}_{298} = 206 \text{ kJ/mol} \qquad (4)$$

Since the hydrogen to CO ratio in steam reforming of methane is high, it is considered to obtain highly pure hydrogen. For the reaction to occur, steam reforming requires very high thermal energy which escalates the cost of the process, since the process is highly endothermic. To lower these costs of hydrogen production via fossil fuel burning,

alternative methods of methane reforming are being studied by several researchers considering the quality and requirement of syngas and moreover the economic viability [9-11]. With the aforementioned concerns, alternative methane reforming processes like dry reforming, partial oxidation and autothermal reforming are being suggested for production of syngas.

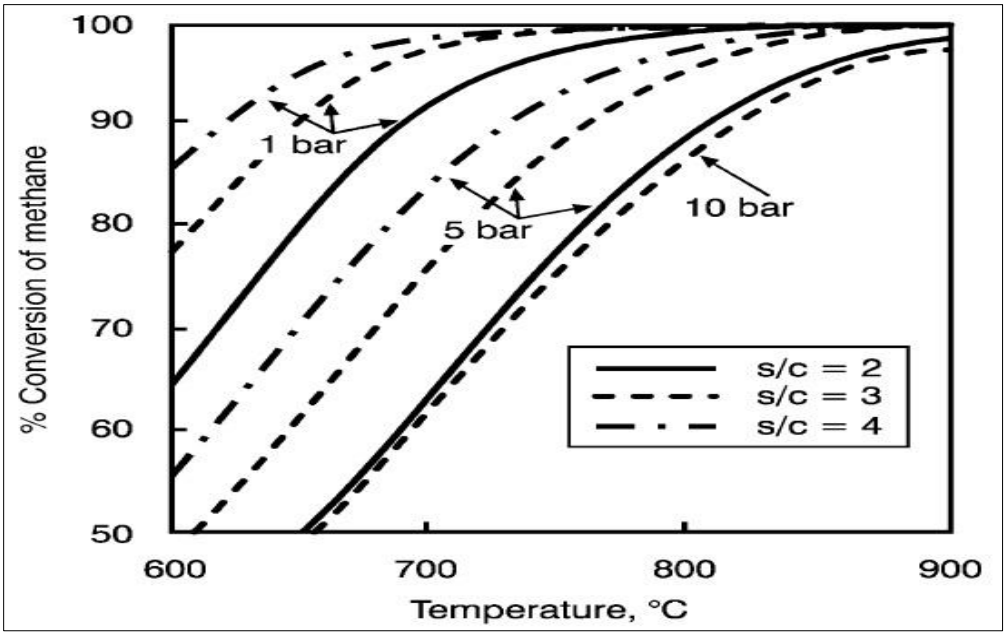

Figure 2.1: Steam reforming of methane. Equilibrium conversion against temperature, pressure and steam/carbon ratio [8]

Dry reforming is another process which produces syngas; with hydrogen to CO ratio of 1. The process is similar to steam reforming but with a variation of methane reacting with carbon dioxide instead of steam and produce syngas [9, 12]. The dry reforming of methane reaction is shown below.

$$CH_4 + CO_2 \rightleftharpoons 2CO + 2H_2 \qquad \Delta H^{\circ}_{298} = 247 \text{ kJ/mol} \qquad (5)$$

This process is considered for reforming when the use of syngas produced is for material synthesis and require syngas as raw materials. Coke, which is deposited on the surface of

the catalyst, reduces the activity of the reaction and is considered as a disadvantage as it reduces its useful life. Coke formation is due to the presence of CO_2 as a reagent in the reaction. Thus, dry reforming is affected by the two carbon containing elements namely CH_4 and CO_2 [9, 12, 13]. There are likely more chances of coke formation in this process due to the low H/C ratio when compared to steam reforming [14]. Low coke formation rate on the catalyst surface is one of the main challenges for dry reforming for which active catalysts need to be developed. Use of supports which favor the dissociation reaction of CO_2 into CO and O can reduce the coke formation to some extent [15].

Another method for production of syngas is the partial oxidation of methane. In this process, methane reacts with oxygen to produce syngas. The resultant syngas obtained by this process is of good hydrogen to CO ratio [16].The reaction for partial oxidation of methane is as follows.

$$CH_4 + \tfrac{1}{2} O_2 \rightleftharpoons CO + 2H_2 \qquad \Delta H^{o}_{298} = -22.6 \text{ KJ/mol} \qquad (6)$$

Unlike steam reforming and dry reforming, partial oxidation of methane is an exothermic process which releases heat when the reaction occurs. Also the process requires a lower amount of thermal energy, it is considered to be economical than other reforming processes. From another point of view, the process is considered expensive as it requires a flow of pure oxygen for combustion of methane. Specific care must be taken during the process since the gases involved (CH_4 and O_2) are highly explosive when combusted and may prove to be dangerous [17].

Steam Reforming and partial oxidation methods were combined to give a new process to produce syngas namely Autothermal reforming. Thus, in the steam reforming there is contact with a flow of gaseous oxygen, in the presence of a catalyst [10-12]. The three

reagents for autothermal reforming of methane are CH_4, H_2O and O_2. The thermal energy required for the steam methane reforming process is generated by the partial oxidation method and thus saves a significant amount of energy. Since this method produces syngas by consuming the thermal energy it generates, it is named Autothermal [18]. Hydrogen to CO ratio in the syngas depends on the inlet gaseous feed and usually a value of H_2/CO ratio for the process ranges between 1 and 2 [17].

$$CH_4 + \tfrac{1}{2}O_2 \rightleftharpoons CO + 2H_2 \qquad \Delta H^{o}_{298} = -22.6 \text{ kJ/mol} \qquad (7)$$

$$CH_4 + H_2O \rightleftharpoons CO + 3H_2 \qquad \Delta H^{o}_{298} = 206 \text{ kJ/mol} \qquad (8)$$

In general, methane reforming process is used to obtain high-purity gaseous hydrogen; however, the type of method used in the conversion process of methane in syngas influences on H_2/CO ratio obtained. The most common type reforming processes is the steam reforming process [9, 10, 19], because it generates syngas with the highest H_2/CO ratio. However, alternative methods for natural gas reforming were developed to save money by employing the best suitable reforming method; steam reforming is found to be an efficient one for bulk hydrogen production. Thus, the choice of the most appropriate catalytic chemical process of methane reforming should account for the economic viability of the process with regard to the purpose given to the syngas produced. In other words, it can be said in short that the choice of the type of catalytic chemical process of reforming to be used in the conversion of methane to syngas should be made based on the final application that will be given to syngas obtained.

Steam reforming is, in industrial practice, mainly carried out in reactors referred to as steam reformers, which are essentially fired heaters with catalyst filled tubes placed in the radiant part of the heater. The process may also be carried out in reactors referred to as

heat exchange reformers wherein the heat from a process gas or flue gas or any other heating medium is transferred to the reactants for the reaction to take place. These are essentially heat exchangers with catalyst-filled tubes.

Tubes and burners are ideally arranged in the furnace box in such a way that adjustment and control of temperature and heat flux along the tube length can be obtained. Reformers are designed with a variety of tube and burner arrangements. Basically there are four types of reformers namely:

1. Radiant Wall Reformer
2. Top Fired Reformer
3. Bottom Fired Reformer
4. Terrace Fired Reformer

The radiant wall or side fired reformer contains tubes mounted in a single row along the centerline of the furnace. Burners are mounted in several levels in the furnace walls, and the flames are directed backwards towards the walls. Heating of the tubes is by radiation from the furnace walls and the flue gas and to a minor extent by convection. The flue gas leaves the furnace at the top so that the flow of process gas and flue gas is counter-current.

The top fired reformer burners are mounted in the furnace ceiling between the tube rows and between the tubes and the furnace wall. From the burners, long flames are directed downwards, and the tubes are heated by radiation from the flames and the hot flue gas and by convection.

The bottom fired type has easy access to the burners and gives an almost constant heat flux profile along the length of the tube. Since the tubes are hot in the bottom a

substantial margin is required on the tube design temperature limiting the outlet temperature.

The terrace wall fired type reformer is a modification of the bottom fired type, having slightly lower tube wall temperatures. Problems can arise at the 'pinch point' in the middle of the furnace where the tubes are subject to both radiations from the burners and to enhanced convection from the flue gas. Different tube and burner arrangements are illustrated in Figure 2.2.

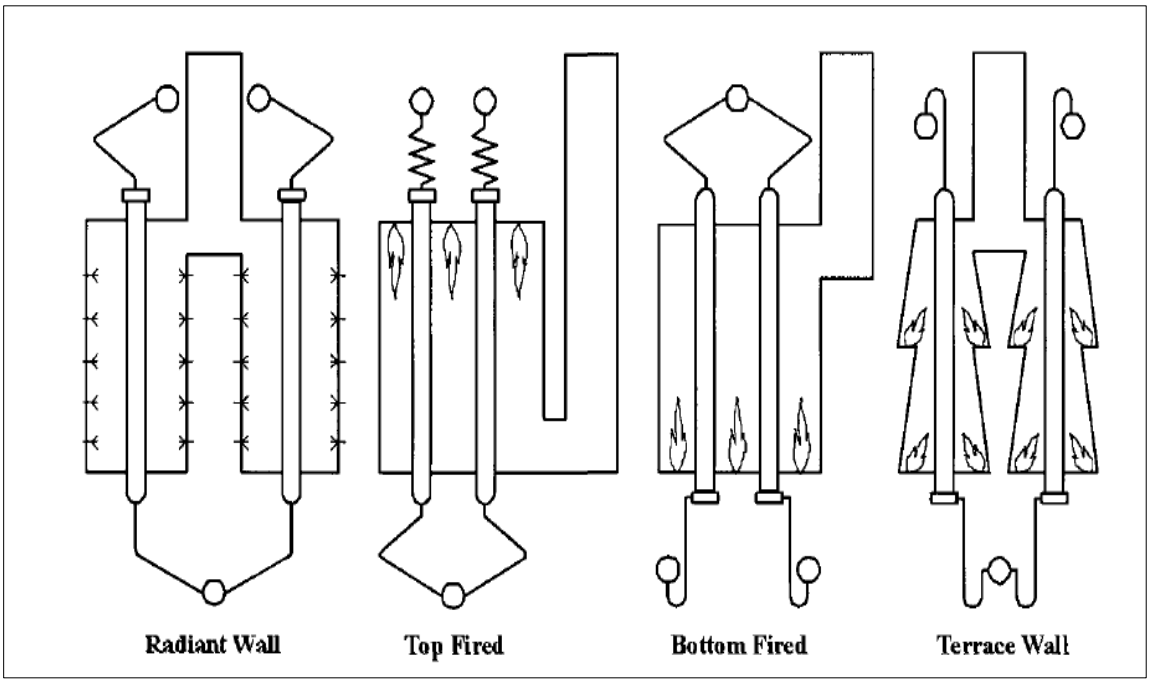

Figure 2.2: Tube and Burner Arrangements

2.1.2 Catalysts for Steam Methane Reforming:

Steam reforming uses nickel based catalysts as the active material. However, cobalt and other noble metals also catalyze the steam reforming reaction but are generally too expensive to find widespread use. Ruthenium and Rhodium have higher activity per metal area than nickel but are usually not considered due to their high costs being rare

earth metals. A number of different carriers including alumina, magnesium-aluminium spinel, and zirconia are employed. Some of the problems faced by SMR process are low methane conversion due to reversibility, coke formation, catalyst deactivation, heat transfer issues and diffusion limitations [8, 20-23]. Being catalytically promoted, the process is sensitive to the catalyst used not only chemically but also due to the physical phenomena taking place. Thus, complete insight of the phenomena is necessary to run the process efficiently and economically.

As mentioned, the most commonly used catalyst for steam methane reforming (SMR) is Nickel. Ni is used unsupported as well as supported on certain supports such as SiO_2, Al_2O_3, Al_2O_4, ZrO_2, Ce-ZrO_2 [24-28]. Low conversion, deactivation and coke formation are issues that makes certain catalysts unsuitable for the SMR process since in real life, reformers operate far away from ideal conditions. Usually operating pressure ranges from 20 to 40 bars to get high pressure required in synthesis loop but at the same time, reduce conversion. Presence of higher hydrocarbons and sulfur content along with high pressure make the environment severe for the catalyst. Ni supported on certain supports such as Al_2O_4, Al_2O_3 and SiO_2 were reported to be deactivated severely due to oxidation of Ni [31]. It was found that $NiAl_2O_3$ [38] catalyst deactivated severely even when operated under different reaction systems to check the dependence of heat transfer mechanism [29]. Also, pretreatment of the catalyst with other metals like Rh was found to give higher activity also at elevated temperatures after undergoing certain oxidation reduction reactions for Al_2O_3 [28].

A comparative study of Ni supported over Ni/Ce–ZrO_2, Ni/ZrO_2, Ni/CeO_2, Ni/$MgAl_2O_4$ and Ni/Al_2O_3 [30] indicated that Ni over Ce-ZrO_2 catalyst have higher activity due to

high interaction between Ni and Ce-ZrO_2 supports and also due to high oxygen carrying capacity. In another study, Ni/Ce–ZrO_2θ-Al_2O_3 catalyst was tested against the steam treatment effects and it was found that catalyst deactivated in steam due to formation of inactive Ni- Al_2O_4 reduced to Ni and Al_2O_3 in presence of H_2. Same effect was reported to be the reason for the deactivation of Ni-Al_2O_3 catalysts but this deactivation was low due to the coverage provided by ZrO_2. Thus, the catalyst was found to be highly active by using low steam concentrations in the reactor feed initially so that the process proceeds in the forward direction and some hydrogen is produced [31].(

Since steam methane reforming occurs on the surface of the catalyst (surface reactions), increasing the amount of active metal will increase the surface area for species to absorb resulting in higher reaction rates. However, the loading of active metal is limited due heat and mass transfer effects. Ni loading on reduced NiAl_2O_3 catalyst was optimized to 12% within a range of 6 to 15% loading and also it was reported that below 3% loading of Ni, inactive Ni Al_2O_4 is formed. Also, reduction of the catalyst makes it liable for higher conversion and thus conversion of 80% was reported at atmospheric pressure, temperature of 1023 K and S/C of 1 [32].

Sintering is another problem associated with the steam reforming catalyst. It is the loss of surface area of the active species of the catalyst due to migration and coalescence of nickel particles on the carrier surface and is a complex process influenced by several parameters including chemical environment, catalyst structure and composition [33-37]. Factors like high temperature and high steam partial pressure enhance sintering. Also, steam reforming catalysts are susceptible to sulphur poisoning. At steam reforming

conditions, all sulphur compounds are converted into hydrogen sulphide, which is chemically absorbed on the nickel surface, enhancing the phenomena.

It is reported that for Ni supported over $MgAl_2O_4$ catalyst, sintering occurs in the initial 200 hours of the reaction, after which, change in the size of Ni particles is small. The size of the nickel particles is limited after sintering and is related to the support surface area and Ni loading yielding to sintering being proportional to nickel loading [38]. The sintering process is more affected by temperature than time and at higher temperatures, particle migration is dominant whereas atomic migration dominates at low temperatures [39].

The operating conditions in a reformer depend on the type of feedstock and the application. The typical inlet temperature is between 350°C and 550°C. The selection of the operating conditions is in many cases dictated by the limits of carbon formation on the catalyst. For a given feedstock and pressure, the reformer must be operated within a certain temperature window. The formation of a whisker type of carbon will occur above the upper temperature limit whereas operation below the lower temperature limit may result either in a polymeric type of carbon formation (gum) or lack of sufficient catalyst activity.

2.1.3 Kinetics for Steam Methane Reforming:

Chemical kinetics plays an important role in the steam methane reforming process. For a system to be in chemical equilibrium depends on whether the time constants of the controlling chemical reactions are short compared with time scales over which the system conditions i.e. the temperature and pressures change. As mentioned earlier, steam methane reforming is a well-developed technology with a large number of catalysts been

developed to overcome different problems associated with this reaction such as coke formation, low methane conversion etc. but the kinetics of SMR over these catalysts have always been a main concern for the researchers. It is quite impossible to obtain a rate expression for SMR which is independent of the catalyst used due to difference in the catalytic composition. Simple kinetic rate expressions were developed in the beginning studies [40-42] of steam methane reforming kinetics wherein the rate of reaction was proportional to the partial pressure of methane.

$$-r = k_o e^{\frac{-E}{RT}} P_{CH_4} \quad (9)$$

Where; k_o =127 kmol/(h kg_{cat} atm) , E = 8778 cal/mol

Some kinetic models were based on the power law fit [43, 44] of the experimental data which required a less insight into the process. These models were relatively less accurate for example the power law kinetic model developed by Steel et al. [43] in the temperature range of 773 to 953 K and pressure range of 1 to 10 torr, the rate of reaction depended on the partial pressure of methane and water but was independent of product's concentration. Order of the reaction rate was positive with respect to steam but negative with respect to water. The rate expression was reported to be applicable after 30 seconds from the start of the reaction. It was also reported that the consumption of methane and mole fraction of CO_2 were way less than the mole fraction of CO. This was due to the production of oxygen from the catalyst and error in the measurements of mole fraction of water. Moreover, the rate of reaction was made independent of the amount of catalyst present as well as the flow velocity and other flow parameters.

$$r = k_o e^{\frac{-E}{RT}} P_{CH_4}^{n} P_{H_2O}^{m} \quad (10)$$

Where; n = 1, m = -0.5, k_o = 1.78*10^{17} g-mol/g_{cat}.h, E=29 kcal/g mol

SMR is a surface based catalytically assisted endothermic reaction in which the species adsorb on the surface of catalyst and undergo the reaction scheme to form the products followed by desorption of products from the catalyst surface [31]. One of the main assumptions in the power law based models is the applicability of rate expression after a certain contact time, limits of which are usually such that the changes in the concentration of species are very small or the reaction is close to thermodynamic equilibrium. To predict the rate of reaction from the beginning, an insight of how the reactants behave when they are in contact with certain amount of catalyst and the reaction mechanism is necessary. The consumption of reactants depends on the slowest process from the adsorption of species, formation of products and desorption of products from the catalyst surface. This slowest process of SMR mechanism is called the rate determining step.

As mentioned earlier, a kinetic model should explain the reaction mechanism correctly by picking the correct reaction path depending on the operating conditions. It should explain the non-monotonic behaviour of the reaction rate with respect to the partial pressure of water and should take diffusion limitations into account. Taking the reaction of carbon intermediate with absorbed oxygen as the rate determining step, Xu and Froment [45] developed a kinetic model with 21 sets of rate expressions on the possible reaction mechanism. The best rate expression that explained the experimental data accurately was reported to be the rate of reaction for the SMR process in the operating range of

temperature and pressure. Diffusion limitations were catered by taking into account the Knudsen and molecular diffusion with mass conservation equation solved on the particle surface by assuming radial diffusion only. The developed pressure gradients were then used to calculate the reduction in reaction rate due to diffusion [46]. This model also takes care of non-monotonic behaviour of the rate of reaction with respect to steam and hence is more generalized. It was also observed that the rate of reaction 1, 2 and 3 increased with increase in steam's partial pressure and then decreased in the latter part. The kinetic reaction rates given by [45]are:

$$R_1 = \frac{k_1}{p_{H_2}^{2.5}}\left(p_{CH_4} p_{H_2O} - \frac{p_{H_2}^3 p_{CO}}{K_{1,eq}} \right)\frac{1}{\text{den}^2} \tag{11a}$$

$$R_2 = \frac{k_2}{p_{H_2}}\left(p_{CO} p_{H_2O} - \frac{p_{H_2} p_{CO_2}}{K_{2,eq}} \right)\frac{1}{\text{den}^2} \tag{11b}$$

$$R_3 = \frac{k_3}{p_{H_2}^{3.5}}\left(p_{CH_4} p_{H_2O}^2 - \frac{p_{H_2} p_{CO_2}}{K_{3,eq}} \right)\frac{1}{den^2} \tag{11c}$$

$$\text{den} = 1 + K_{CO} p_{CO} + K_{H_2} p_{H_2} + K_{CH_4} p_{CH_4} + \frac{K_{H_2O} p_{H_2O}}{p_{H_2}} \tag{11d}$$

Different models have been developed for the steam methane reforming reaction to predict the extent of reaction under certain operating conditions and to serve for optimization purposes [47]. The intrinsic kinetic rates depend on the scheme of reaction and are independent of other flow factors such as diffusion, inertial and viscous resistances to the flow, resistance to heat transfer etc. In actual cases, the rates of reactions are different from the intrinsic reaction rates due to the diffusion limitations. The ratio of observable reaction rate to intrinsic reaction rate is called the effectiveness factor. Depending on the evaluation of effectiveness factor, three types of models are

found in the literature, which are the homogenous model, the pseudo homogenous model and the heterogeneous model.

The homogenous model assumes a predefined constant value of the effectiveness factor [48-50]. Thus observable rate are directly obtained by multiplying the intrinsic rate with the effectiveness factor. In this model, the whole domain is considered to be filled with reaction mixture with no catalyst pellets hindering the flow as well as thermal homogeneity is maintained. The pseudo homogenous model is the same as that of homogenous model except that a profile of effectiveness factor is taken into account instead of a constant value. In these models, a correlation for effectiveness factor is used that usually depends on the catalyst particle's shape. Thus, effectiveness factor remains constant for one catalyst bed profile [51-54]. The heterogeneous model is the most realistic one in which the presence of catalyst pellet is taken into account. Thus effectiveness factor is determined at every location in the reactor by solving species transport equation over the catalyst pellet [47, 55-60]. Heterogeneous models are very sensitive to diffusion limitations, thus often misleading if the diffusion limitations are not handled carefully. These models are complex and require the solution of separate continuity equations over the catalyst pellet. Pseudo homogenous models are catalyst bed specific and usually are insignificant while using reformers of smaller length. Homogenous models are simple and are of good choice as long as the diffusion limitations are modelled precisely. Homogenous models are used extensively by researchers by choosing different values of effectiveness factors for the reactions R_1, R_2 and R_3.

2.1.4 Reforming Using Membranes:

The main drawbacks of conventional SMR, partial oxidation and auto-thermal conventional reactors are that all these reactions are equilibrium limited and (even in case of complete fuel conversion) produce a hydrogen rich gas mixture containing carbon oxides and other by-products. Consequently, in order to produce pure hydrogen, these chemical processes are carried out in a number of reaction units (typically high temperature reformer, high and low temperature shift reactors) followed by separation units (mostly pressure swing adsorption). The large number of different process steps decreases the system efficiency and makes scale-down uneconomical. A typical reaction process scheme is shown in Figure 2.3. Using this process, high hydrogen yields are achieved, but costly high temperature heat exchangers and complex energy integration among different process units are required to obtain hydrogen at the desired high purity. Among different technologies related to production, separation and purification of H_2, membrane technologies seem to be the most promising and membrane separation is nowadays increasingly considered as a good candidate for substituting conventional systems. The specific thermodynamic constrains limiting traditional reactors can be circumvented by using innovative integrated systems, such as the so-called membrane reactors (MRs), systems in which both reaction and separation are carried out in the same device.

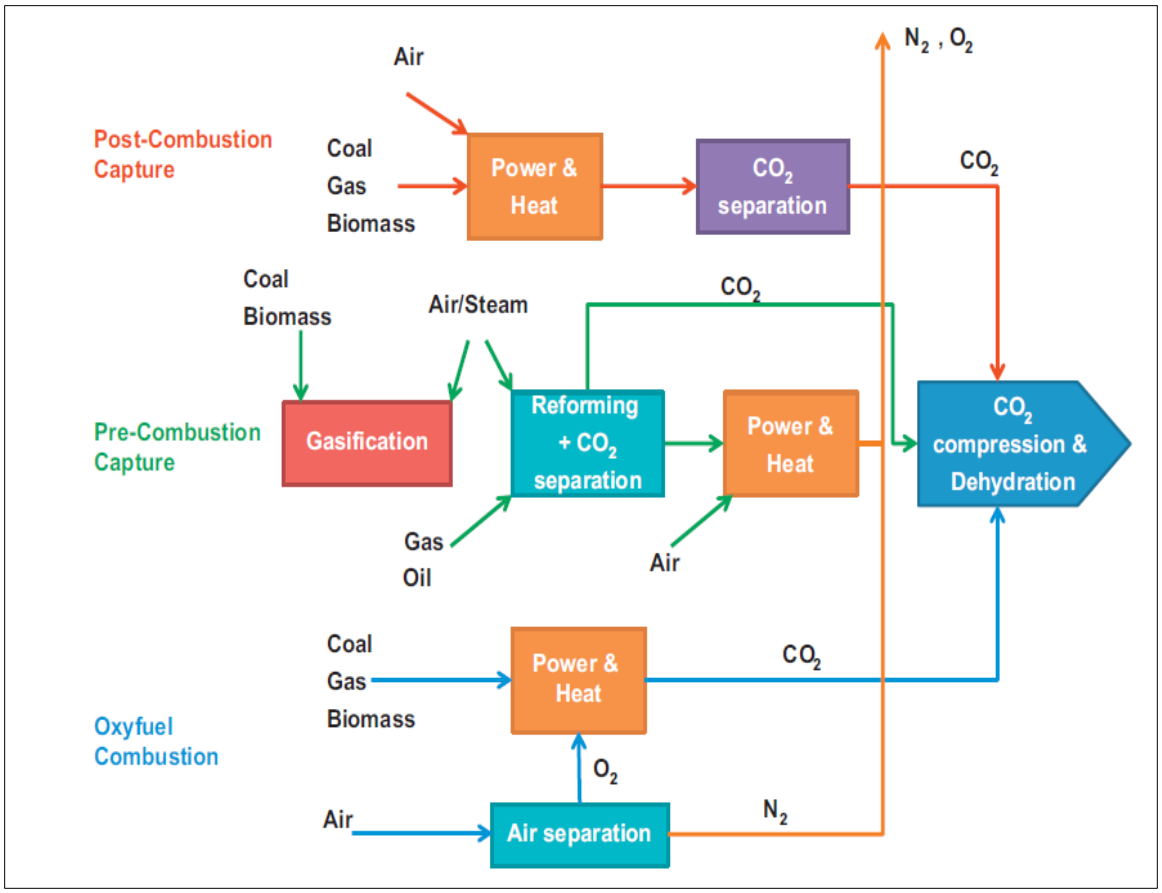

Figure 2.3: CO_2 capture routes [66]

Basically, membranes are barriers which allow the flow of a specific component in the gas stream to the other side. The permeated component is known as permeate while the retained mixture is the retentate. High selectivity, high flux, low cost and high mechanical and chemical stability are some of the characteristics which a separation membrane should possess.

As mentioned, steam reforming of methane reactions can be performed at lower temperatures than the conventional ones by removing the hydrogen formed from the products stream, thus shifting the equilibrium towards the product side and promoting the reaction kinetics according to Le Chatelier's principle. The removal of hydrogen is done by use of membranes which are highly selective to hydrogen within or outside the

vicinity of the reactor. The hydrogen flux across the membrane is governed by Sivert's Law [61] according to which the flux across the membrane is proportional to the difference of the square root of hydrogen partial pressures at the two sides of the membrane. The Sivert's law is given by:

$$J_{H_2} = A_{H_2} \exp\left(-\frac{E_{H_2}}{R_g T}\right)\left(p_{H_2}^{0.5} - p_{H_2,\mathrm{M}}^{0.5}\right) \qquad (12)$$

Where, J_{H2} is the hydrogen flux, A_{H2} is the pre-exponential factor, P_{H2} and $P_{H,M}$ are the partial pressures of hydrogen at the feed and permeate side.

In order to attain high purity hydrogen, dense metal membranes like Pd and its alloys are currently the most suitable due to remarkably high hydrogen selectivity. Recent developments in Pd and Pd alloy membranes [62, 63] allow the use of these membranes to a temperature range of 300-700 ^{o}C. The Pd-based membranes which characterize the high hydrogen selectivity follow a solution diffusion mechanism as shown in Figure 2.4.

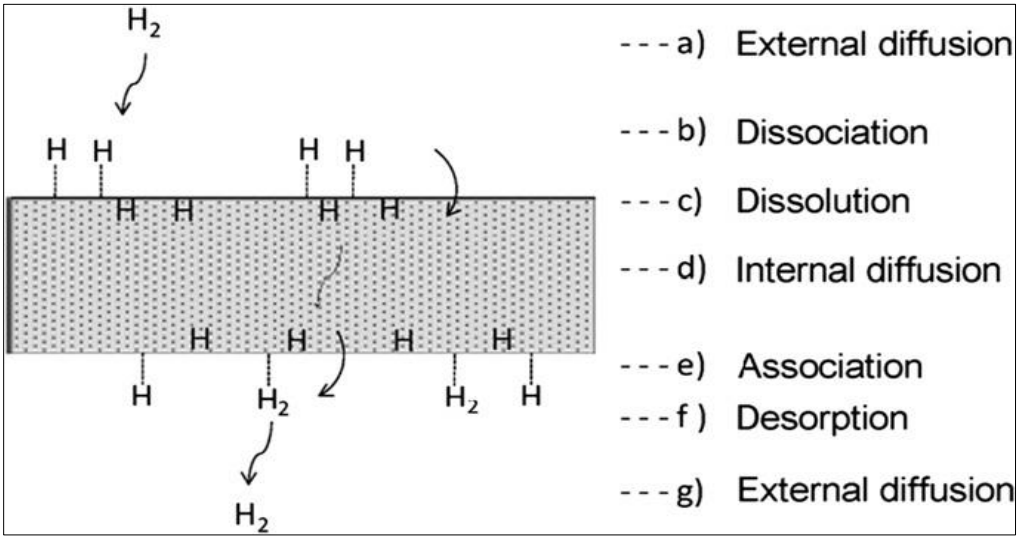

Figure 2.4: Solution-diffusion mechanism [67]

This solution diffusion mechanism can be explained as follows:

a) Dissociation of the hydrogen molecule at the gas – metal interface.

b) Adsorption of the atomic hydrogen on the membrane surface.

c) Dissolution of the atomic hydrogen into the palladium membrane.

d) Diffusion of the atomic hydrogen through the membrane matrix.

e) Recombination of atomic hydrogen to form hydrogen molecules at the other side of the gas-metal interface.

f) Desorption of hydrogen molecules.

g) Diffusion of hydrogen molecules away from the surface.

The materials used for hydrogen separation are polymeric, porous membranes, dense metal membranes and proton exchange membranes. The application of the right material depends on factors like selectivity, hydrogen flux and the temperature range within which they operate. A comparison of different membrane types is shown in Table 1.

Table 1: Properties of Hydrogen Selective Membranes [64]

Material	Dense Polymer	Micro porous Ceramic	Dense Ceramic	Porous Carbon	Dense Metallic
Temperature Range	<100 ^{o}C	200-600 ^{o}C	600-900 ^{o}C	500-900 ^{o}C	300-600 ^{o}C
H_2 Selectivity	Low	Moderate	Very High	Low	Very High
H_2 Flux	Low	High	Moderate	Moderate	High
Poisoning Issues	HCl, SO_2, CO_2	-	H_2S	Strong Vapors, Organics	H_2S, HCl, CO
Example Materials	Polymers	Si, Al_2O_3, Zr, Titania, Zeolites	$SrCeO_{3-\delta}$, $BaCeO_{3-\delta}$	Carbon	Palladium Alloys, Pd-Cu, Pd-Ag, Pd-Au
Transport Mechanism	Solution diffusion	Molecular sieving	Solution diffusion	Surface diffusion, Molecular sieving	Solution diffusion

Different types of membrane reactors have been proposed in the literature for hydrogen production amongst which packed bed membrane reactor are the most studied followed by fluidized bed membrane reactors and micro membrane reactors [64]. Packed membrane reactors configuration focus on the effect of hydrogen permeation through membranes on the reaction system and thus are the most studied compared to fluidized bed membrane system which involve complicated and complex fluid dynamics.

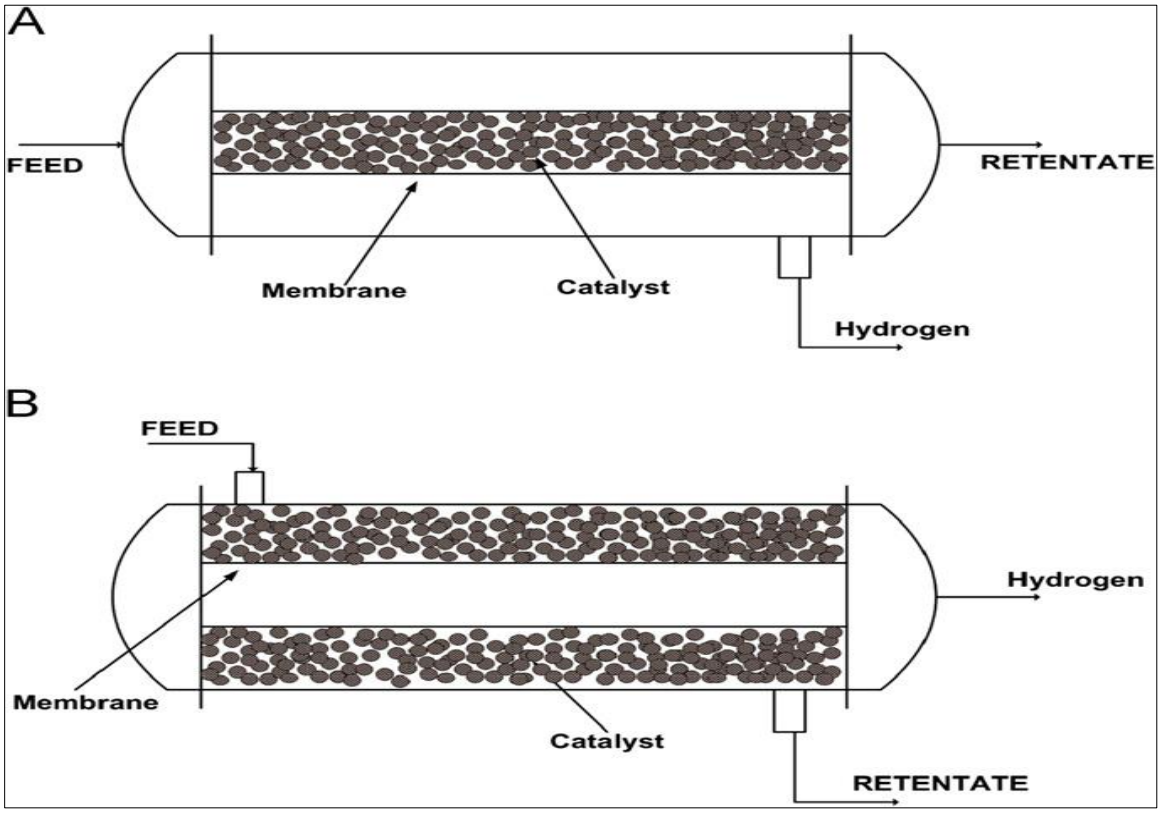

Figure 2.5: Catalyst in tube (A) and catalyst in shell (B) configurations [64]

In order to keep the pressure in the permeation zone as low as possible, a sweep gas is often used to sweep out the permeated hydrogen from the reforming reactor. Gases like helium, argon, nitrogen etc. are used which sweep the permeated hydrogen from the reactor. The sweep gas plays an important role in packed bed membrane reactors and can

be used in the co-current and counter-current flow direction. Also, the catalyst within the reactor can be arranged in the shell or the tube of the reactor as shown in Figure 2.5. For multi-tubular membrane reactor configurations, the catalyst in tube configuration can be preferred especially for construction reasons and for the extent of bed-to-wall mass and heat transfer limitations which can be very detrimental when the catalyst is positioned in shell configuration.

2.2 Solar Steam Reforming of Methane

2.2.1 Solar Energy:

Solar energy is by far the most abundant energy resource for our planet earth. However, it is intermittent and does not necessarily match the variations in demand. Solar energy, to become a major contributor of our energy supply, needs some form of storage. Conversion of solar energy into chemical fuels is an attractive method of solar energy storage. Solar fuels, such as hydrogen, can be used for upgrading fossil fuels, burned to generate heat, further processed into electrical or mechanical work by turbines and generators or internal combustion engines. Nevertheless, solar fuels are among the most promising technologies to curb the growing demand for fossil fuels and to mitigate the effects of climate change. The challenge is to produce large amounts of chemical fuels directly from sunlight in robust, cost-effective ways while minimizing the adverse effects on the environment.

The success of solar thermal power generation known as ‘Concentrating Solar Power’ (CSP) is already moving towards sustainable, large scale fuel production. This is done by concentrating solar radiation with reflecting mirrors providing high temperature process heat for driving efficient thermochemical processes. To achieve the technical feasibility

of various technologies, it is recommended that commercial implementation steadily evolves, starting from the current state of- the-art fossil fuel production technologies.

Different solar technologies used nowadays are parabolic troughs, linear Fresnel collectors, parabolic dish and solar tower technologies. Parabolic systems use trough-shaped mirrors to focus sunlight onto an absorber tube (receiver) placed in the trough's focal line. The receivers contain a heat transfer fluid (e.g. synthetic thermal oil, molten salt) which is heated by the focused sunlight. It is circulated in these tubes and pumped through heat exchangers to produce steam. The parabolic trough technology is currently the best proven and most used technology.

Figure 2.6: Parabolic Trough Technology [65]

The Linear Fresnel technology uses long, flat or slightly curved mirrors to focus sunlight onto a linear receiver located at a common focal point of the reflectors. The receiver runs parallel to and above the reflectors and collects the heat to boil water in the tubes, generating high-pressure steam to power the steam turbine (water/direct steam generation, no need for heat exchangers). The reflectors make use of the Fresnel lens effect, which allows for a concentrating mirror with a large aperture and short focal length. This reduces the plant costs since sagged-glass parabolic reflectors are typically

much more expensive. Since the optical efficiency as well as the working temperatures are considerably lower than with other CSP concepts, saturated steam conditions have to be considered for this technology.

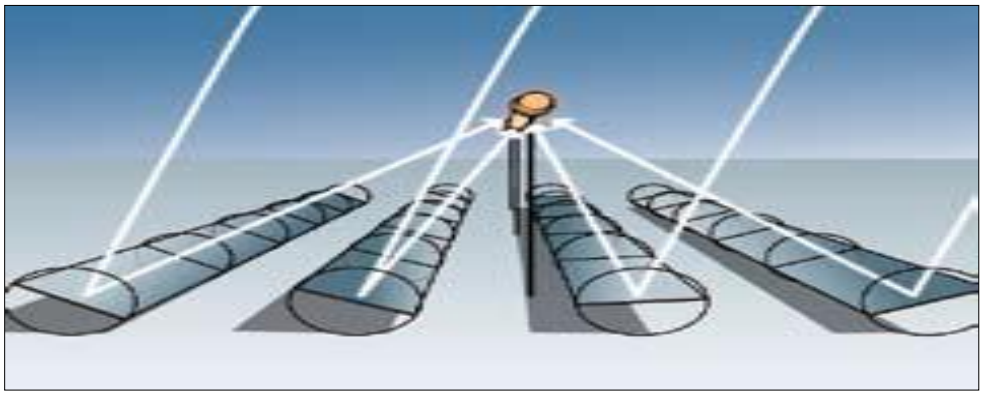

Figure 2.7: Linear Fresnel Technology [65]

A circular array of flat heliostats (sun tracking mirrors) concentrates sunlight on to a central receiver at the top of a tower. A heat transfer medium (water/steam, molten salt or air) in the receiver absorbs the thermal energy and transfers it into the steam cycle to generate superheated steam for the turbine. The advantage of solar tower over the parabolic trough or Fresnel collector concept is that the sunlight on the central receiver is focused to a smaller area, and the heat transfer medium does not have to be piped around the large solar field. This means that higher working fluid temperatures in the receiver (up to 1000°C) and better steam parameters are feasible, even supercritical steam can be expected. The main advantage of solar power towers in comparison to line-focusing systems is the ability to provide high-temperature superheated steam, with inlet temperatures to the turbine being very high, leading to higher power generation efficiencies. Another point is its flexibility when it comes to plant construction, because heliostats do not need to be sited on an even surface.

Figure 2.8: Central Tower Technology [65]

Today, however, more than 90% of hydrogen produced is by using high temperature processes from fossil resources, mainly natural gas. If hydrogen is generated from solar energy, it is a completely clean technology; no hazardous wastes or climate changing by products are formed and only sunshine and water are required as inputs to the process.

2.2.2 Solar Reforming:

Research in the last two decades has demonstrated the efficient use of solar thermal energy for driving chemical reforming reactions [66-76]. In these highly endothermic reactions, hydrocarbons are reacted with steam or carbon dioxide (CO_2) over a catalyst to form a synthesis gas (syngas) composed primarily of hydrogen (H_2) and carbon monoxide (CO) in a reforming reactor which is coupled with a solar facility. The solar heat is applied to the reactor either indirectly through a working fluid (molten salt, heated air) or directly via reactor tubes or a porous catalytic reactor exposed to concentrated solar radiation. In open loop systems, solar energy is applied to upgrade the energy content of the hydrocarbon feedstock whereas energy upgrade and transportation of the hydrocarbon feedstock takes place for a closed loop system. Advantage of the closed loop system is that the syngas formed can be stored and transported and the stored solar heat

can be recovered via methanation reaction which can further be used for industrial processes for energy generation.

The high temperatures required for solar reforming effectively limit the concentrator choices to dishes and central receivers. The dish technology is modular and is well suited to distributed applications such as the destruction of toxic wastes. On the other hand, bulk energy production, whether in closed-loop or open-loop configuration, probably must be carried out on a large scale to compete with fossil fuels and probably requires the tower (central receiver) technology. In recent years, several basic solar reformer concepts have been investigated. These reformers can be classified as the indirectly heated reformer, the tubular reformer-receiver, and the windowed or volumetric reformer-receiver [66].

The indirectly heated reformer consists of a tube bundle containing catalyst within the tubes through which the process gas is circulated, and heated by a secondary fluid that gets its thermal energy from a solar receiver. Heating agents that have been considered are air, helium and condensing sodium vapor. The indirectly heated steam reformer has potential advantages of utilizing commercially proven tubes and catalyst, and can be equipped with thermal storage or auxiliary fossil firing to give extended or 24-hour operation. This mode of operation is desirable to reduce capital costs and provide a uniform product. The process pressure can be optimized independent of the solar receiver pressure. On the contrary, the indirectly heated system has more equipment, and the secondary fluid introduces additional pumping and temperature losses.

The tubular reformer/receiver incorporates the catalyst-bearing tubes directly into the solar furnace where they are heated by solar radiation. While this concept eliminates the costs and energy losses associated with the secondary heat transport loop, a larger and

more costly solar receiver is required. A limited amount of heat storage is associated with the receiver, sufficient to damp the effect of solar transients. Auxiliary fossil-fuel or electrical heating can be used to extend the heating time, and there is freedom in selecting the optimal process pressure.

The windowed or volumetric reformer/receiver places the reforming catalyst in a position where it is heated directly by the solar beam, making very high volumetric reaction rates possible. As a result, the receiver is quite compact and potentially inexpensive. However, this technology requires good matching of flow rate with solar flux and also the development of reliable windows (which may limit operating pressure) and does not lend itself to energy storage or non-solar operation. Nevertheless, prospects for low capital costs and a good match to dish concentrators make this concept attractive. The individual receiver cells are limited in capacity by the window area, but large modular arrays are feasible for solar towers.

ASTERIX [69, 70] experiment for solar steam reforming of methane was conducted in the early 90's for investigating the details and problems associated with the process heat demand for an industrial chemical process with solar-generated high temperature heat, using an indirectly heated reformer. The specific objectives of the ASTERIX experiment were to collect and store an optimum amount of solar energy, to obtain maximum conversion of methane and to produce consistently high-quality synthesis gas. A Gas-Cooled Solar Tower (GAST) system [70] was used to produce hot air and drive a separate steam reformer which was again fed into the GAST cycle. The results of this test indicated that the reformer developed was more temperature dependent than pressure

dependent and the reformer can be used effectively when used as reactor in series operations.

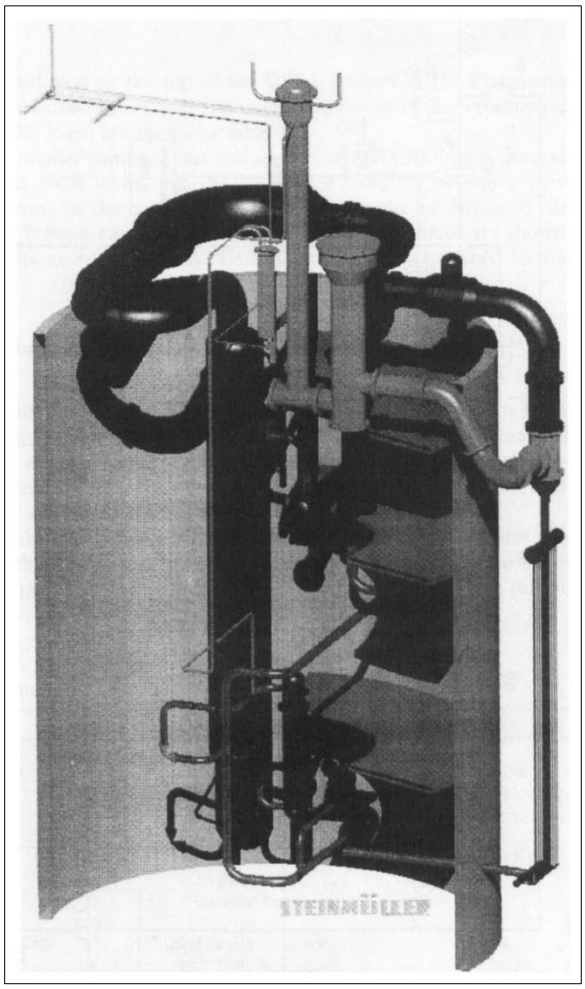

Figure 2.9: Cross-section of ASTERIX [76] heat exchange reformer

The Catalytically Enhanced Solar Absorption Receiver (CAESAR) [66-68] test was conducted to determine the thermal, chemical, and mechanical performance of a commercial-scale, dish mounted, direct catalytic absorption receiver (DCAR) reactor over a range of steady state and transient (cloud) operating conditions. The focus of the test was to demonstrate "proof-of-concept" and determine global performance such as reactor efficiencies and overall methane conversion. The objectives of the project were to demonstrate the solar DCAR concept using a commercial-scale receiver/reactor on a

parabolic dish, and to develop numerical simulation models capable of predicting the global performance of the receiver/reactor unit and the thermal, chemical and mechanical performance of the absorber. The focus, therefore, was on obtaining global and absorber performance data over a range of steady-state and transient operating conditions (e.g., cloud transients) and comparing these results with model predictions.

The system was operated during both steady-state and solar transient (cloud passage) conditions with total solar power absorbed value of 97 kW and maximum methane conversion of 70%. Receiver thermal efficiencies ranged up to 85% and chemical efficiencies peaked at 54%. Global model predictions such as reactor efficiencies and CH_4 conversion compared well with test data. For example, model predictions of 71.9%, 48.2%, and 46.5% for thermal efficiency, chemical efficiency, and CH_4 conversion, respectively, for one of the CAESAR tests, compared favorably with the corresponding test values of 79.3%, 50.7%, and 45.9%. A photograph of the CAESER unit is shown in the Figure 2.10.

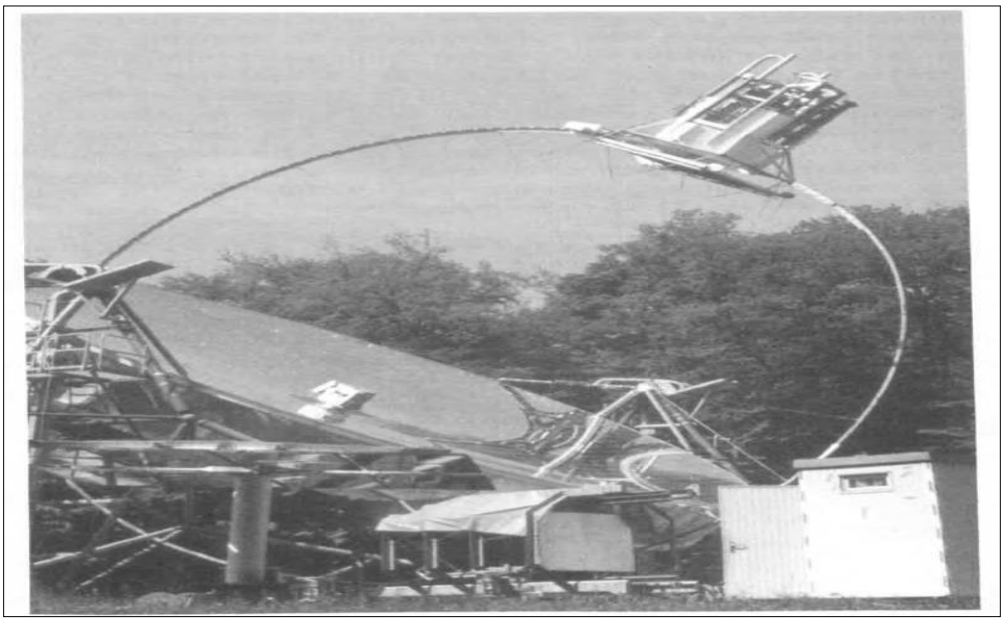

Figure 2.10: The CAESER Unit [67]

A 480 KW testing facility of reformers was developed at Weizmann Institute of Science [71]. A solar receiver with storage and transportation, for development of high temperature technology was designed for both carbon dioxide (CO_2) and steam reforming. The test facility operated between 1 to 18 bars pressure, coupled with a methanator system that recovers the heat energy from the reverse reaction. The cavity receiver contained eight vertical reformer tubes (2-inch schedule 80), 4.5 m long (active length). The overall dimensions of the device were about 5 m high, 4.5 m wide and 3 m deep. The reactor was designed to produce syngas at 800°C which resembled commercial reformers except that a solar cavity receiver had replaced the conventional gas-fuelled radiant furnace. The solar cavity is shown in the Figure 2.11.

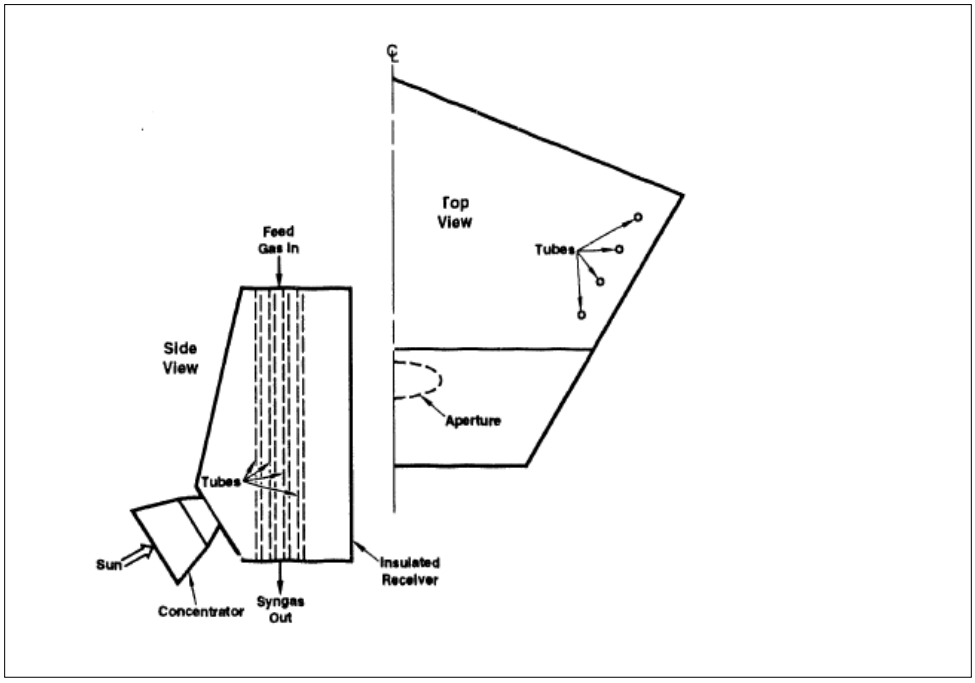

Figure 2.11: The Weizmann Institute 480 KW Reformer/Receiver [71]

Another chemical reactor was integrated into a sodium reflux heat pipe receiver for carbon dioxide reforming of methane and tested in the solar furnace of the Weizmann

Institute of Science [72]. The receiver/reactor was a heat pipe containing seven tubes inside an evacuated metal box containing sodium. Two of the tubes were filled with catalyst, 0.5 wt% Rh on alumina and the front surface of the box served as the solar absorber. In operation, concentrated sunlight heated the front plate and vaporized sodium from a wire mesh wick attached to the other side of the plate. Sodium vapor condensed on the reactor tubes, releasing latent heat and returning to the wick by gravity. Adequate performance of the receiver system was observed during many tests under varying flow conditions. The maximum power absorbed was 7.5 kW at temperatures above 800°C. The feasibility of operating a heat pipe receiver/reactor under solar conditions was proven, and the advantages of reflux devices were confirmed.

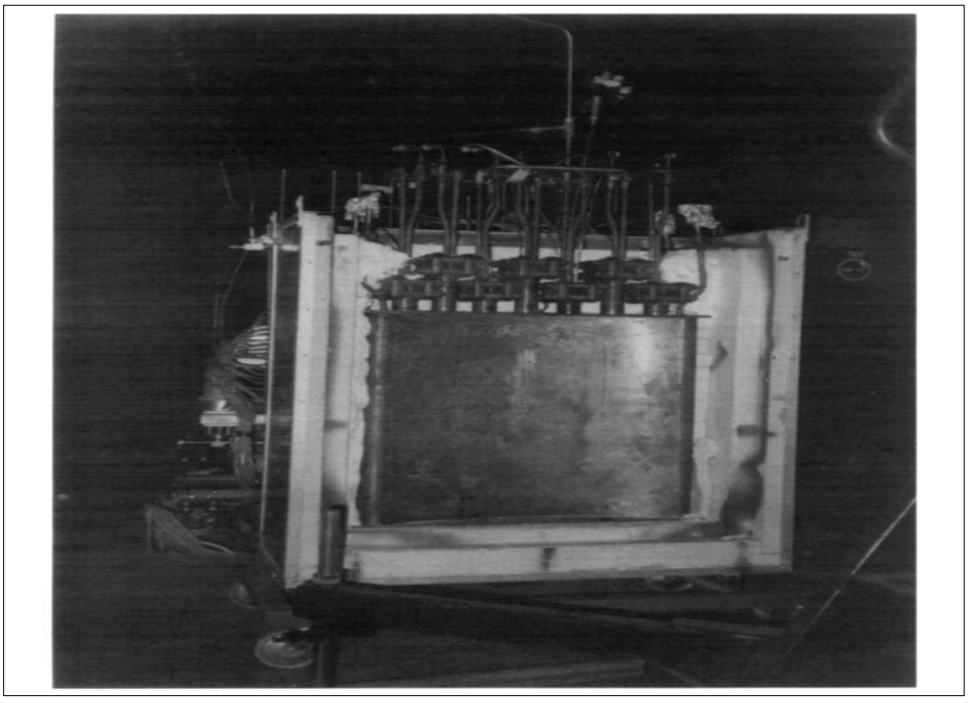

Figure 2.12: Sodium Heat Pipe Reformer [72]

A DIAPR system which uses steam reforming of methane with a Ru/Al_2O_3 catalyst promoted by Mn oxides was studied by Berman et al [80]. A directly irradiated annular

pressurized receiver reactor was used as the receiver reactor which was used in conjunction with a field of heliostats. The absorber of the receiver consisted of pins arranged in the shape of a porcupine made of sintered alumina (99.7 % Al_2O_3). The catalyst activity and stability was tested for methane conversion at different reforming temperatures ranging from 500-1100 ^oC using fresh catalyst and catalyst that has been used for 506 hours at 1100 ^oC. It was found that the activity of the catalyst does not change significantly even after prolonged use which suggested that the catalyst was thermally stable. The same tests when conducted with the same catalyst but without Mn oxides showed that the activity of the catalyst decreases drastically at higher temperatures.

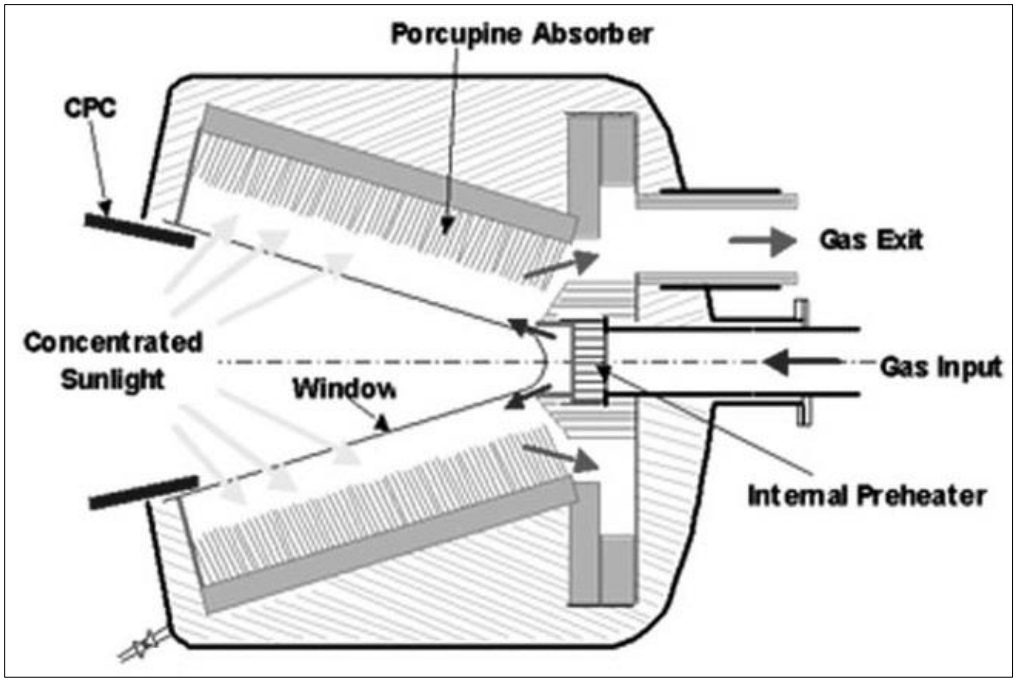

Figure 2.13: Schematic of DIAPR solar facility [74]

A receiver reactor paired with a solar furnace with heliostats to collect the solar radiation and reflected onto the parabolic reflector was studied [76] . The catalyst used in this study

was 10 % Ni deposited on Al_2O_3 pellets. The reformer was tested for different steam to methane ratios (1-3) and temperatures (680-750 ^oC) at atmospheric pressure. It was found that at the highest temperature studied (750 ^oC), methane conversion was within 20 % of the equilibrium and the heating value of the product gases was approximately 20% higher than that of the input methane. The experimental set up along with the solar facility is shown in Figure 2.14.

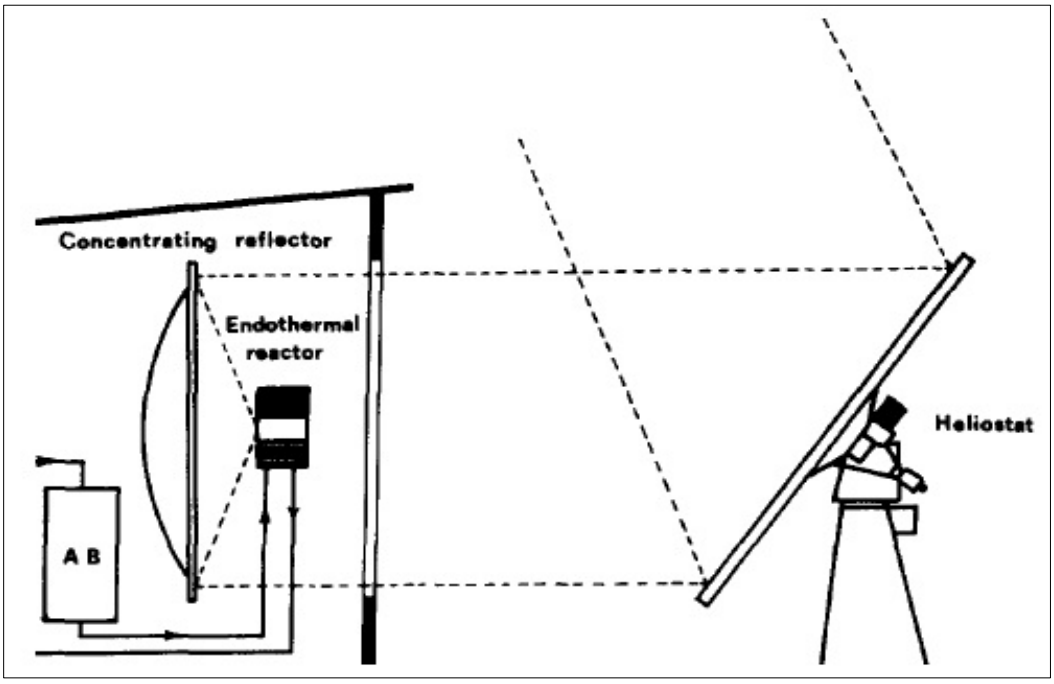

Figure 2.14: Experimental set up of DeMaria et al [76]

To convert solar energy into chemical energy, an infrared furnace was designed and tested with FeO powder as catalyst for the dry reforming of methane [73]. The FeO powder was suspended in a molten salt solution wherein the reactants were flown and observed at different flow rates. It was observed that the product consisted of CO, H_2 and H_2O with a ratio of 3:1:1 respectively at a flow rate of 200 ml/min and that of CO and H_2 with a 2:1 ratio at a flowrate of 50 ml/min. theoretical dry reforming of methane was

attained at a flowrate of 50 ml/min due to the contact efficiency between the catalyst (FeO powder) and CH_4/CO_2 mixed gases. This experiment of methane reforming reaction with CO_2 also demonstrated the use of FeO as catalyst in the molten salt medium for converting solar into chemical energy. Schematic of the process diagram is shown in Figure 2.15.

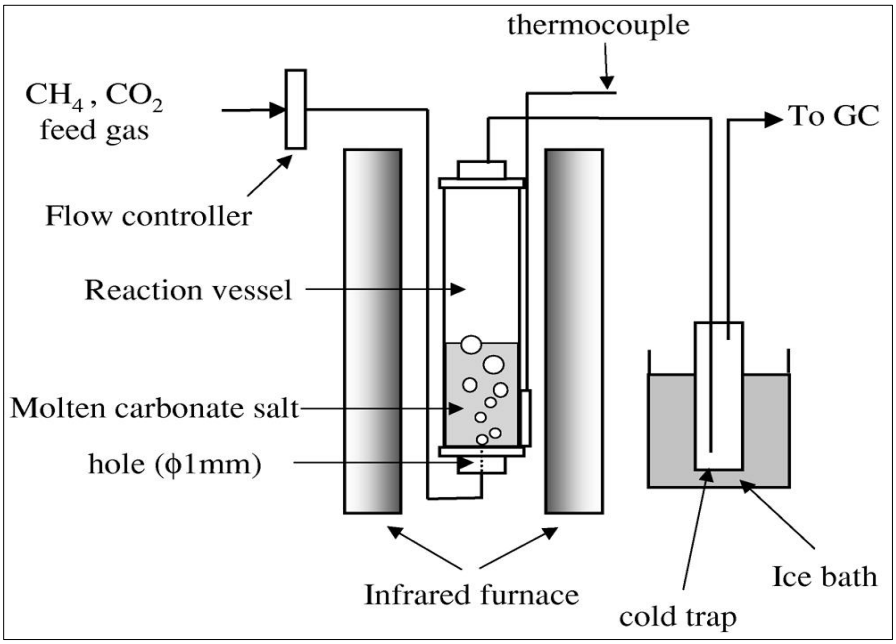

Figure 2.15: Dry reforming with FeO as Catalyst set up [73]

Economic viability of the process equipment should also be weighed while applying the solar facilities like solar towers and dishes for performing solar reforming. Another mature and relatively inexpensive solar technology is the solar parabolic trough but the temperatures generated by them (max. 600 ^oC) are below the operating temperatures of the reforming process and thus are not found in the literature. Although solar parabolic troughs do not generate the temperatures required for reforming (850-950 ^oC), this technology can be applied for solar reforming processes by developing a reformer which operates at lower temperatures than reforming temperatures.

2.3 Numerical work in the area of steam reforming of methane

There has been an extensive work on the numerical analysis of the steam reforming in order to study and improve the process. Numerical investigation was made on a reforming system consisting of a combustion zone, steam methane reforming zone (SMR) and water gas shift (WGS) bed [48]. Concentration of the species at the exit, temperature in the WGS bed, heat transfer to the catalyst bed and the steam methane reforming reactions were studied depending on the operating parameters. Analysis was made on the outer wall of the system by providing a cooling flux, effect of which reduced the methane conversion and carbon monoxide yield in the SMR bed. Increasing steam to methane ratio showed increase in the methane conversion along with a decrease in the carbon dioxide concentration.

A simulation model was developed for the steam methane reforming reaction in a micro reactor consisting of a combustion channel and a reaction channel [49]. The SMR reaction was Rh-catalyzed whereas the combustion was Pt-catalyzed. The CFD model built included the elementary reaction kinetics for the SMR reactions and global reaction kinetics was applied for combustion. Heat conduction ability of the wall was given importance in the study which affects the interplay between the endothermic and exothermic reactions occurring simultaneously in the reactor. A characteristic value of 0.5 mm was suggested by the authors for the thickness of the walls.

A simulation study was conducted on the Zone Flow Reactor [56]. Zone Flow is a tubular reactor having two types of internals: a core type and a casing type which is adjacent to the wall, having a thin layer of catalyst over them. A very complex reactor with corrugations, blades and cones was studied in order to improve the heat transfer. Higher

catalyst efficiency per unit reactor volume was achieved due to the higher geometric surface area. Also, a judicious design for the relative position of the internals and their geometrical characteristics and higher catalyst effectiveness, higher energy efficiency and lower steam to carbon ratios was aimed in the study.

Numerical analysis was performed on the steam methane reforming reactions in a monolith reactor using surface based and volume based reaction models [50]. In the surface based approach, the reaction takes place near the wall where the catalyst is coated whereas reaction of chemical species through penetration inside a thin catalyst layer occurs in a volumetric approach. The numerical models developed utilized the Langmuir-Hinshelwood type of kinetic reaction rates for the SMR and Water Gas Shift reactions. The modelling results of the surface based reactions were found to be more accurate with the experimental data. However volumetric reaction models are of good choice as long as they predict the experimental data closely.

A study was made on steam reforming of methane in a packed bed reactor considering the dynamic behavior of the process [47]. A set of partial differential equations were developed and validated against experimental results for the physico-chemical process. The physico-chemical process taking place in the solid and gaseous phase were set to the operating conditions of an actual reformer with high temperatures and pressures. The heat at the reactor wall was optimized for hydrogen yield. The dynamic conversion, temperature and partial pressures profile at the bed and particle level were well demonstrated by the use of 2 – phase reactor concept and optimized wall temperature profile.

A 1 – dimensional model for the steam reforming of methane in a Pd membrane reactor was studied and analyzed [77]. The performance of the steam reforming reaction was evaluated by the methane conversion, hydrogen to carbon monoxide ratio and the hydrogen recovery. For the study conducted, reactor performance was found optimal for the temperature range of 580-600 ^{o}C, steam methane ratio of 3, pressure range of 300-600 KPa and a sweep gas ratio of 3. Similarly, the simulation study [78] showed that the membrane thickness is an important parameter for methane conversion and that methane conversions can enhance up to 95% with the use of thin membranes (<1.0 μm). A one dimensional non-isothermal model of the autothermal Pd membrane reformer and studied systematically the effects of various design and operation parameters on the reformer performance. The simulations mapped the acceptable domain of operation and the optimal set of operating parameters [79-81].

Numerical simulations of membrane reforming using finite-volume approach are very few. A hydrogen perm-selective membrane reactor was modelled and studied [55]. The catalyst considered for the study was Ru/SiO2 which is favourable for steam methane reforming at low temperatures and steam to methane ratios whereas the membrane for hydrogen permeation was that of palladium. Analysis was made on the inlet temperature, space velocities, pressures and sweep gas rate. The inlet temperature and space velocity showed significant effect on methane conversion among the operating variables considered. At a space velocity of 8900 h^{-1}, hydrogen permeation rate was found to be maximum, however to attain complete conversion of methane, space velocity of 6000 h^{-1} was suggested by the authors.

Numerical and experimental investigation of mass transfer performance of Pd-Ag Membrane Modules for Hydrogen separation [61] was made. In the analysis, concentration polarization and non-ideal flow on design of membrane separation units was evaluated by using CFD. The source and sink terms were introduced on either side of the membrane boundary cell in order to account for the permeation of hydrogen in the numerical study developed [82]. The study covered different module configuration for H_2 and N_2 mixture and compared with the experimental results which were found to be in good agreement. The analysis extended to the use of baffles which permits the production of compartments inside the module, avoiding mixing and increase permeation driving force. An increase in the number of baffles resulted in increased separation performance also giving maximum permeates of H_2.

A composite palladium membrane was analyzed to study the effect of hydrogen permeation rate tubular configurations [83]. A palladium film was coated on composite membrane tube and analysis was done for increasing temperatures for two different modes. In the first mode, H_2 was passed through the tube and pressure was reduced in shell side. Therefore, H_2 permeates first through the ceramic tube then palladium film. In the second mode, H_2 was passed from shell side and pressure inside the membrane tube was reduced and H_2 permeates first through palladium film then composite tube. The numerical models were based on the combined resistances of both palladium film and composite support. From the results it showed that with increase of temperature, permeation rate increases under the first mode.

A CFD analysis [82] was made on inorganic membrane modules for gas mixture separation to derive the permeation coefficient, based on the transport mechanisms for

the gas molecules across the membrane. The basics of molecular diffusion, Knudsen diffusion and viscous (Poiseulle) flow, and used in the source term formulation in the continuity and species transport equations. Of all the mechanisms, the molecular diffusion was dominant on H_2 permeation at high pressures. The mole fraction and permeation rate of hydrogen increases with increase of working pressure and a good agreement with the experimental results was found.

Simulative analysis of mass transfer effects in gas and vapor permeation modules were conducted in the work by [84]. The study relates the effect of concentration polarization and flow distribution with spacers between two membrane surfaces. Calculations of permeation as a function of temperature, pressure and composition were done using finite-volume method. The use of baffles in the model which separates membrane into a number of compartments helped in velocity control of feed. The flow through the membrane was implemented as a sink in the basic transport equation for each finite cell. A user-defined function (UDF) was implemented for the transport from the membrane using a function for flux proportional to partial pressures. Similarly, it was found from the results that the driving force obtained was due to concentration polarization and the use of spacers which affects the performance of membrane.

CHAPTER 3

MODEL DEVELOPMENT

This chapter consists of two sections. The first section gives detailed information about formulating the model for steam reforming reaction coupled with hydrogen permeation. The second section of this chapter defines the numerical scheme and boundary conditions.

3.1 Model for Steam Reforming of Methane

CFD (Computational Fluid Dynamics) is becoming a preferred tool for modeling and simulation of steam reformers. Developments in CFD modeling are rapid and more comprehensive as accurate models are being elaborated. Tubular steam reforming is a complex interaction of heat transfer and coupled chemical reactions. The heat released by the burners is transferred via convection to the reformer tubes, then passes through the tube walls by conduction and is finally transferred to the catalyst bed by convection and radiation. At the same time, a network of chemical reactions creates temperature and concentration gradients in the radial direction of the tube and around and within the porous catalyst particles. For these purposes, a CFD model needs to be developed which can predict the entire steam reforming process without actually running the process.

3.1.1 Governing Equations:

The basis of the numerical simulations conducted are on the CFD models developed by Seo et al [48] for the SMR catalyst bed and Coroneo et al [61] for hydrogen permeation through the membrane, both of which are based on finite volume method. The numerical solutions of mass, momentum, energy and the species transport equations are used to

obtain velocity, pressure and concentration of the gas mixture due to steam methane reforming process. The reaction rates are calculated by the chemical kinetics given by Xu and Froment [45] for the steam methane reforming process. The convection diffusion equations consisting of a source term for mass flow of hydrogen across the membrane is used for the calculation of hydrogen permeation fluxes at the feed and permeates sides. The flow equations in steady state are given as:

Continuity Equation:

$$\nabla.(\rho_f \vec{V}) = S_i \tag{13}$$

Momentum Equation:

$$\nabla.\left(\rho_f \vec{V}\vec{V}\right) = -\nabla\left(P\right) + \nabla\left(\vec{\vec{\tau}}\right) - \frac{150}{d_p^2}\frac{(1-\varepsilon)^2}{\varepsilon^3}.\mu_f \vec{V} \tag{14}$$

Energy Equation:

$$\nabla.(\rho_f \vec{V}E + \vec{V}P) = \nabla.(k_e \nabla T - \sum_i h_i j_i + (\vec{\vec{\tau}}.\vec{V})) + (1-\varepsilon)\sum_i h_i \eta_i R_i \tag{15}$$

Species Transport Equation:

$$\nabla.\left(\rho_i \vec{V} Y_i\right) = -\nabla.J_i + (1-\varepsilon)\eta_i R_i + S_i \tag{16}$$

where; V is the velocity , ρ_f is the fluid mixture density, P is the pressure, μ_f is the fluid mixture viscosity and S_i is the source/sink term. The last term in the RHS of the momentum equation is the Blake-Kozeny equation [85] which is used to calculate the pressure drop in porous media in packed beds and represents the permeability and inertial loss within the reactor since the SMR is modeled as a porous media which in turn reflects that the reactor is filled with catalyst. S_i in the continuity and species transport equations represents the mass flow of species across the membrane. The species are allowed to

disappear from the feed side of the reactor through the sink term and to come out on the permeate side through the source term. A thorough understanding of the permeability characteristics of the membrane is required to formulate the source term. The palladium membrane considered in this work is permeable to hydrogen only, therefore the source term in equations (13) & (16) takes into account only hydrogen permeation and are expressed as:

$$S_i = \begin{cases} +\dfrac{J_{H_2} \cdot A_{cell} \cdot MW_{H_2}}{V_{cell}} & \text{at low partial pressure of } H_2 \\ -\dfrac{J_{H_2} \cdot A_{cell} \cdot MW_{H_2}}{V_{cell}} & \text{at high partial pressure of } H_2 \end{cases} \tag{17}$$

The term Si is equivalent to zero unless i=H_2 and the computational cell is adjacent to the membrane. The hydrogen mass flux across the membrane is governed by Sievert's Law and is given by the following equation.

$$J_{H_2} = A_{H_2} \exp\left(-\frac{E_{H_2}}{R_g T}\right)\left(p_{H_2}^{0.5} - p_{H_2,M}^{0.5}\right) \tag{18}$$

Wherein $p_{H_2,M}$ denotes the H_2 partial pressure in the permeate zone, $E_{H_2} = 6.6$ kJ/mol, $A_{H_2} = 0.4$ mol/(m^2 s bar$^{0.5}$) [81].

The density, viscosity, specific heat and thermal conductivity calculated for the mixture [85] are given by the following equations:

The equation of state [48]for reaction mixture is given as follows.

$$P = \rho_f RT \sum_i \frac{Y_i}{M_i} \tag{19}$$

Where the effective density of reaction mixture (ρ_f) is calculated using volume weighted mixing law [85] and is written as follows.

$$\rho_f = \frac{1}{\sum_i \frac{Y_i}{\rho_i}} \tag{20}$$

The specific heat capacity of the species is calculated using a fourth order polynomial fit of temperature [85] as follows.

$$C_{pi} = \sum_{i=1}^{5} A_{C_p,i} T^{i-1} \tag{21}$$

Effective specific heat capacity of the reaction mixture is calculated using mass weighted mixing law [85] and expressed as:

$$C_p = \sum_i Y_i C_{pi} \tag{22}$$

The viscosity of each species is calculated using a power law [85] expression as:

$$\mu_i = \mu_{i,o} \left(\frac{T}{T_o} \right)^n \tag{23}$$

Effective viscosity of reaction mixture is calculated using mass weighted mixing law [85] and is given as follows.

$$\mu = \sum_i Y_i \mu_i \tag{24}$$

The temperature dependent thermal conductivity [85] of each species is calculated by the following formula:

$$k_i = \frac{15R\mu_i}{4M_i}\left(\frac{5C_{pi}M_i}{R} + \frac{1}{3}\right) \tag{25}$$

Fluid mixture's thermal conductivity is calculated by mass weighted mixing law [85] as follows.

$$k_f = \sum_i Y_i k_i \tag{26}$$

Effective thermal conductivity [48] is calculated as follows

$$k_e = \varepsilon k_f + (1-\varepsilon)k_s \tag{27}$$

Binary mass diffusion coefficient is calculated using Chapman-Enskog formula on the basis of the kinetic theory [85].

$$\varphi_{i,j} = \frac{\left[1+(\mu_i/\mu_j)^{1/2}(M_j/M_i)^{1/4}\right]^2}{\left[8(1+(M_i/M_j)\right]^{1/2}} \tag{28}$$

Diffusive flux, J_i, consists of mass and thermal fluxes [49]and is given as

$$J_i = \rho_i D_{i,e}\nabla Y_i + D_{i,T}\frac{\nabla T}{T} \tag{29}$$

The effective diffusion coefficient, $D_{e,i}$, is obtained from Knudsen, $D_{n,i}$, and molecular diffusion, $D_{m,i}$, coefficients by using parallel pore model [46].

$$\frac{1}{D_{e,i}} = \frac{1}{D_{n,i}} + \frac{1}{D_{m,i}} \tag{30}$$

The kinetic reaction rates r_1, r_2 and r_3 for the steam methane reforming process are calculated using Xu & Froment's reaction kinetics [86] given by

$$R_1 = \frac{k_1}{p_{H_2}^{2.5}}\left(p_{CH_4} p_{H_2O} - \frac{p_{H_2}^3 p_{CO}}{K_{1,eq}} \right)\frac{1}{\text{den}^2} \tag{31a}$$

$$R_2 = \frac{k_2}{p_{H_2}}\left(p_{CO} p_{H_2O} - \frac{p_{H_2} p_{CO_2}}{K_{2,eq}} \right)\frac{1}{\text{den}^2} \tag{31b}$$

$$R_3 = \frac{k_3}{p_{H_2}^{3.5}}\left(p_{CH_4} p_{H_2O}^2 - \frac{p_{H_2} p_{CO_2}}{K_{3,eq}} \right)\frac{1}{den^2} \tag{31c}$$

$$\text{den} = 1 + K_{CO} p_{CO} + K_{H_2} p_{H_2} + K_{CH_4} p_{CH_4} + \frac{K_{H_2O} p_{H_2O}}{p_{H_2}} \tag{31d}$$

The activation energies and pre-exponential factors for the reaction rate constants k_1, k_2 and k_3, the adsorption enthalpy change and their pre-exponential factors K_{CO}, K_{H2}, K_{CH4} and K_{H2O} along with thermal properties of the reactants and species are given in Tables 2, 3, 4 and 5.

Reaction rate constants for Arrhenius equation;

$$k_{o,i} = A_i \exp\left(\frac{-E_i}{RT}\right)$$

Table 2: Rate Constants for Arrhenius Equation

Activation Energy, E_i (kJmol^{-1})	**E_1**	**E_2**	**E_3**
	240.1	67.13	243.9
Pre-Exponential factor, A_i	**A_1**	**A_2**	**A_3**
	4.225×10^{15}	1.955×10^{6}	1.020×10^{15}

Constants for Van't Hoff's equation;

$$K_i = B_i \exp(\frac{-H_i}{RT})$$

Table 3: Rate Constants for Van't Hoff Equation

Absorption Enthalpy Change, H_i ($kJmol^{-1}$)	**H_{H2O}**	**H_{CH4}**	**H_{CO}**	**H_{H2}**
	88.68	-38.28	-70.61	-82.90
Pre-Exponential factor, B_i	**B_{H2O}**	**B_{CH4}**	**B_{CO}**	**B_{H2}**
	1.77×10^{5}	6.65×10^{-4}	8.23×10^{-5}	6.12×10^{-9}

Table 4: Coefficients of polynomial functions* belonging to temperature-dependent thermal properties of species, taken from the material property database given by Fluent Inc. [95]

Species	**a_0**	**a_1**	**a_2**	**a_3**	**a_4**
CH_4	403.5847	9.057335	-0.01442509	1.58×10^{-5}	-6.34×10^{-9}
H_2O	1563.077	1.603755	-0.002932784	3.22×10^{-6}	-1.16×10^{-9}
CO	968.3898	0.4487877	-0.001152217	1.66×10^{-6}	-7.35×10^{-10}
H_2	13602.45	3.402317	-0.003358423	-3.91×10^{-7}	1.71×10^{-9}
CO_2	429.9289	1.874473	-0.001966485	1.30×10^{-6}	-4.00×10^{-10}

*Polynomial functions are defined as $\psi(T) = a_0+a_1T^1+a_2T^2+a_3T^3+a_4T^4$

Table 5: Properties of reactants and products species.

Species	**H^a (J/Kmol)**	**M^a (Kg/mol)**
CH_4	$-7.489518 * 10^7$	16.04303
H_2O	$-2.418379 * 10^8$	18.01534
CO	$-1.105396 * 10^8$	28.01055

H_2	0	2.01594
CO_2	$-3.935324 * 10^8$	44.00995

[a] taken from the material property database given by Fluent Inc.

3.1.2 User Defined Function (UDF):

Due to the deficiency of the model in Fluent 14.0, the kinetic reaction rates of the reforming process [45] inside the tube is modelled by user-defined functions (UDF) written in visual studio C++. This data is then used in the species transport equation to provide the concentration profiles of the species. Permeation of hydrogen across the membrane is also modeled using a user-defined function written in visual studio C++ and the two UDF's are compiled and hooked in FLUENT software. The reaction and permeate zones on either side of the membrane are patched with two different values of initial partial pressures (using mole fraction) of the species. "VR Rate" Macro [95] was used to calculate the volumetric reaction rates of the steam reforming of methane taking into consideration the catalyst density and molecular mass for calculation of the kinetic reaction rates. Also, mass fractions of the species were converted into mole fraction values for the calculation of reaction rates based on mole fractions rather than being calculated on mass fraction basis which is usually done by FLUENT [85]. 'Define Initialize', 'Define Source' and 'Define Adjust' Macros were used by the permeation UDF as defined in FLUENT . With these macros, the cell index across the membrane is allowed to add and subtract the source term in the continuity and species transport equations and furthermore, the solver data is updated at the membrane wall for each iteration. The issue of hydraulic jump across the membrane was resolved by patching the cells from the upper and lower zones with two different values of initial partial pressures of species. The solution strategy of the present work is shown in Figure 3.1.

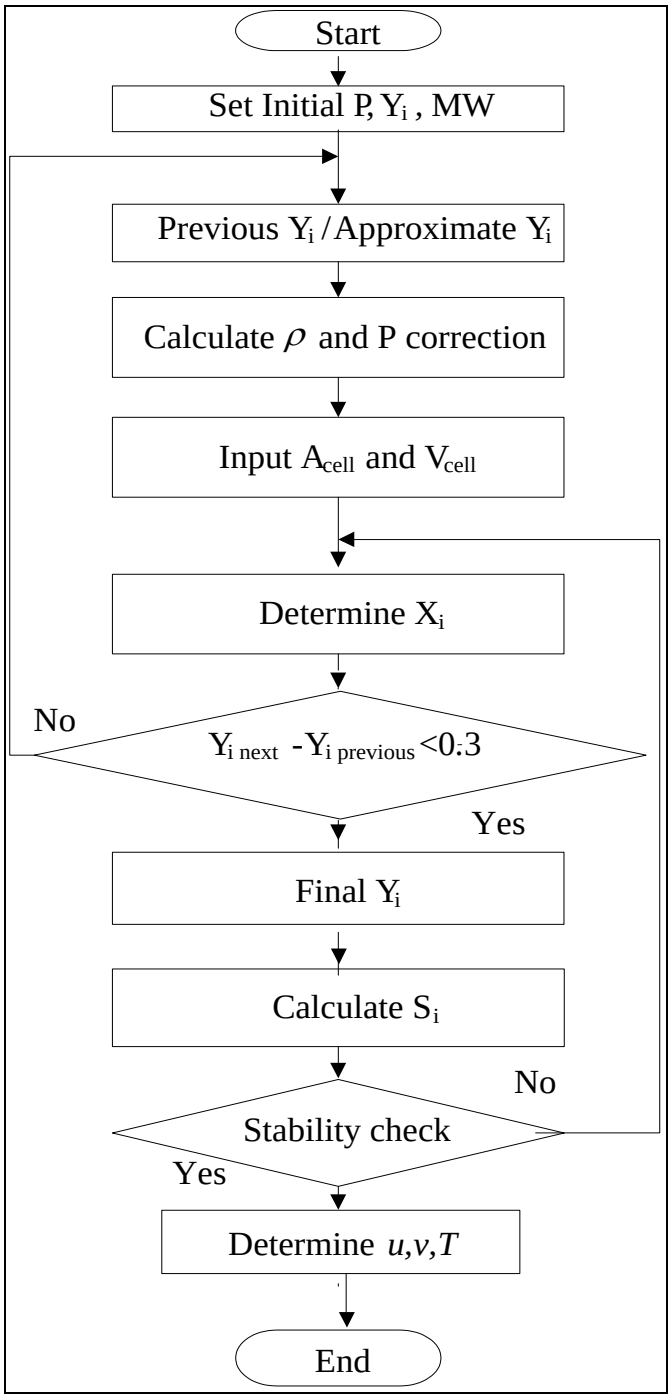

Figure 3.1: Solution strategy for steam reforming of methane in a membrane reactor

3.2 Numerical Scheme and Boundary conditions

In these simulations, the governing equations were solved using a segregated solver and the pressure velocity correction was done using the Semi-Implicit Method for Pressure-

Linked Equations (SIMPLE) formulation [87]. The convergence criteria for the continuity, momentum, energy and species variables were set to 10^{-9} for complete convergence. The gas mixture density is calculated using the volume weighted mixing law and the viscosity, specific heat and thermal conductivity are calculated as a mass fraction-weighted average of all species. The specific heat of each species is calculated using a piecewise polynomial fit of temperature [48, 50]. Pressure and velocity under-relaxation factors were set to 0.3 and 0.7 at all nodes within the computational domain in order to obtain a stable solution. Standard pressure interpolation scheme was used for pressure and the momentum, energy and species transport were discretized using the second order upwind scheme [48, 50] The Aggressive Advanced Multigrid (AMG) scheme with a fixed F-cycle was used for the governing equations in order to enhance convergence [85]. To avoid irregular convergence patterns 'Biconjugate Gradient Stabilized Method' (BCGSTAB) was employed. In the membrane reformer, the reforming reactions takes place inside the reaction zone which is filled with catalyst. The modelling of the catalyst within the reaction zone was done by setting the reaction zone as a porous zone [48]with a specific porosity based on the particle size diameter d_p. The inlet boundary condition in each channel (reaction and permeation zones) is set uniform, i.e., the velocity inlet boundary. To be noted, the net transport of temperature and species at the inlet consists of only convection components in the modeling system. Then the outlet condition of each channel is set as pressure outlet boundary condition as recommended by FLUENT Inc. [85] for flow exits. The top wall of the reformer is set a constant temperature boundary condition so as to imply a isothermally heated wall. In the simulations, we can therefore choose a representative element as the simplified geometry.

Only half of reforming channel and permeation channel is adopted in the simulation domain, and the boundaries are set axisymmetric as shown by the dashed lines in Figure 3.2. The wall medium between the reaction and permeation channels is the membrane which allows flow of hydrogen mass flux from the reaction zone to the permeation zone. The boundary conditions of the computational domain are shown in a pictorial way which is relevant to the Fluent Inc. software [85].

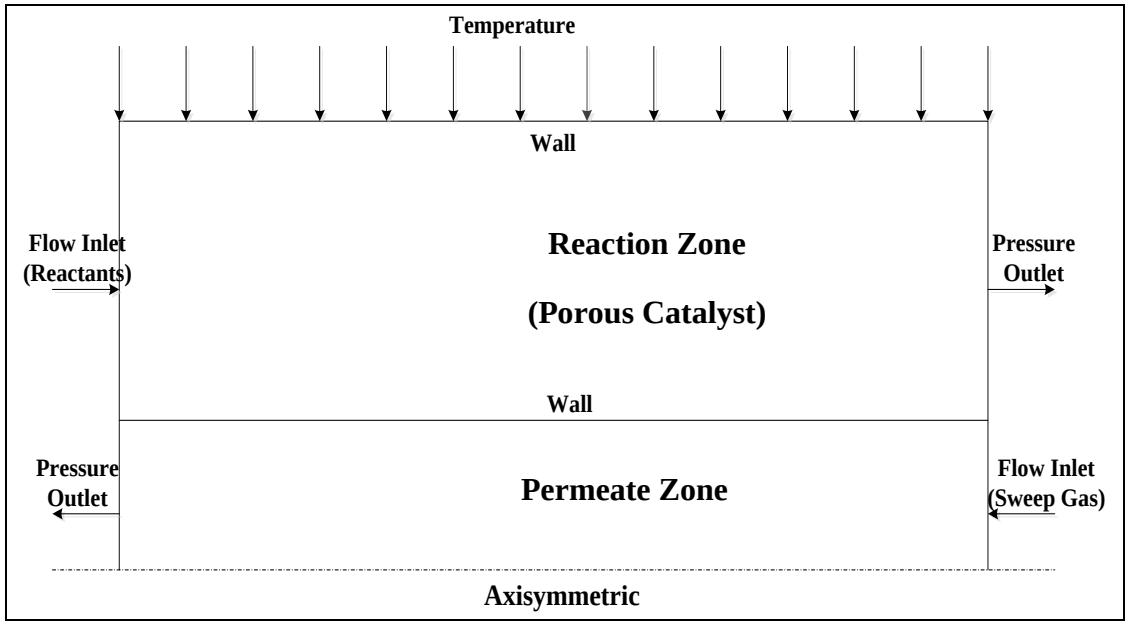

Figure 3.2: Schematic of the membrane reformer with boundary conditions

CHAPTER 4

NUMERICAL STUDY

The control volume approach is used to discretize the governing equations using FLUENT^{TM} 14.0 code [85]. All variables are computed at each grid point except the velocities, which are determined midway between the grid points. A staggered grid arrangement is used in the present study, which links the pressure through the continuity equation and is known as SIMPLE algorithm [87].

The steam reforming of methane process and the permeation of hydrogen through the palladium membranes is solved as a two dimensional axisymmetric problem using the double-precision solver. In addition to the scaled residuals, the fractional conversion of methane, mass fraction of H_2 at the reaction and the sweep side are monitored at the outlet using surface monitors to ensure convergence. Second order upwind schemes are used for discretization of momentum and energy equations.

4.1 Model Validation:

In order to verify the accuracy of the computational model developed in Chapter 3 (Eq. 13 to Eq. 16), performance of the reforming reactor with the dimensions given in Figure 4.1 was compared with the experimental data given Xu and Froment [45]. It is to be noted that in the study made by Xu and Froment, a non-membrane reactor was used in which permeation of hydrogen was not accounted for (S_{H2} = 0). Thus, the reformer domain in Figure 4.1 does not consist of the permeation zone although the boundary conditions applied were the same (without the permeate zone) as discussed in the previous chapter (see Figure 3.2).

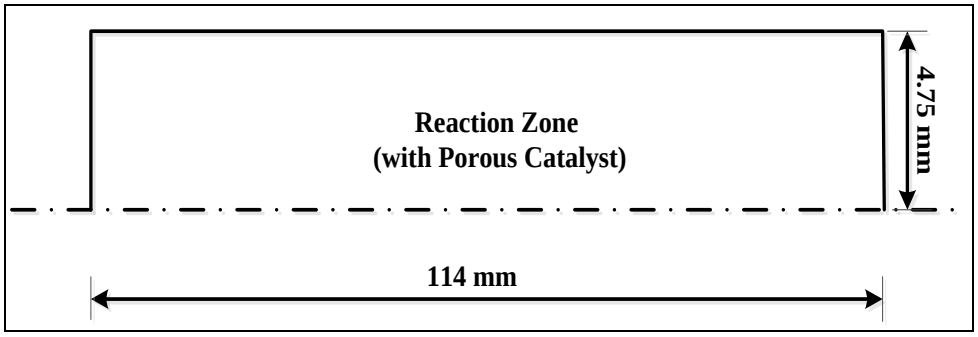

Figure 4.1: Axisymmetric view of geometry for validation

In this problem, fractional methane conversion is investigated at different operating temperatures at the wall of the reformer. The inlet feed consisted of CH_4, H_2O and H_2 with a steam to methane ratio of 3 and hydrogen to methane ratio of 1.25. Porosity of the catalyst bed is set to be 0.528. Simulations were carried out at four different operating temperatures of 848 K, 823 K, 798 K and 773 K and exit pressure of 10 bar. Figure 4.2 shows the variation of fractional methane conversion in the reactor at different reforming temperatures and found to be in good agreement with the experimental values. As mentioned earlier, steam reforming of methane is endothermic and proceeds with increase in temperature. Thus, increase in temperature makes the reaction more favourable, therefore, having more conversion of reactants to products. The fractional methane conversion is obtained from carbon balance and is defined as

$$\text{Fractional Methane Conversion} = \frac{F_{CO} + F_{CO_2}}{F_{CO} + F_{CO_2} + F_{CH_4}} \tag{32}$$

where; F_{co}, F_{co2} and F_{ch4} are the values of mole fractions of carbon monoxide, carbon dioxide and methane at the exit of the reactor.

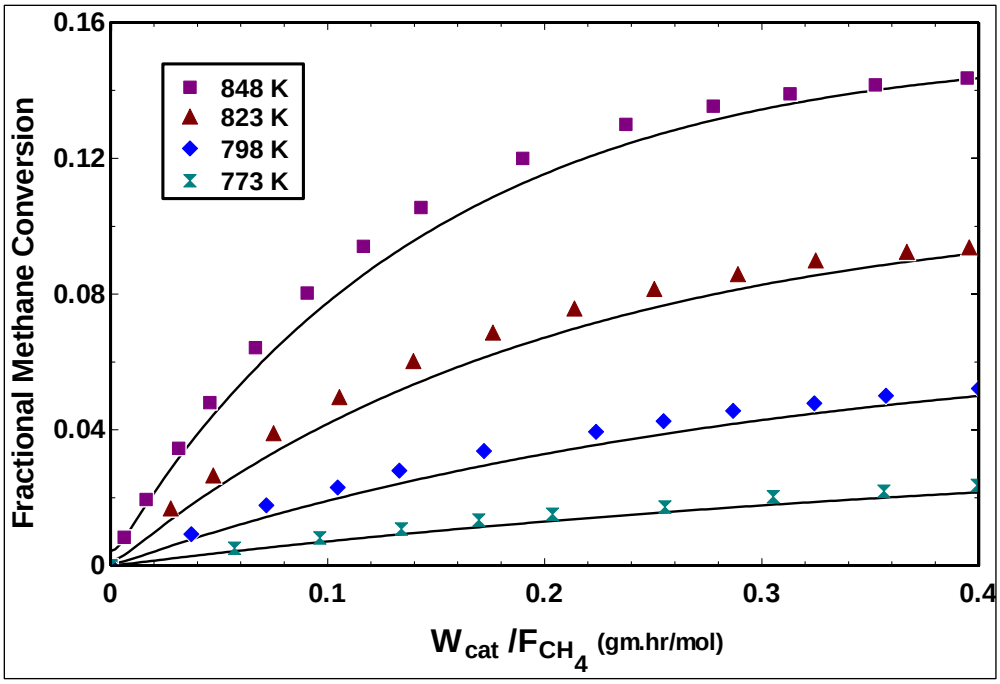

Figure 4.2: Variation of Fractional Methane Conversion vs W_{cat}/F_{CH4} at F_{H2O}/F_{CH4} = 3, F_{H2}/F_{CH4} = 1.25, P = 10 bar; (■▲◆⧗) Experimental Data; (——) Present Simulation Results

Figure 4.3 shows the variation of mass fraction of species along the centerline of the reactor for reaction conditions of T = 773 K and P = 10 bar. It is evident through the plot that there are gradients in concentration of the species along the axial direction although there is a negligible variation in the mass fraction of methane (CH_4) and carbon monoxide (CO). This negligible variation in the concentrations can be explained as the slow reforming kinetics at low temperatures and high pressures. The same can also be confirmed from Figure 4.2 wherein low methane conversions are achieved at low temperatures and high pressures (T = 773 K & P = 10 bar).

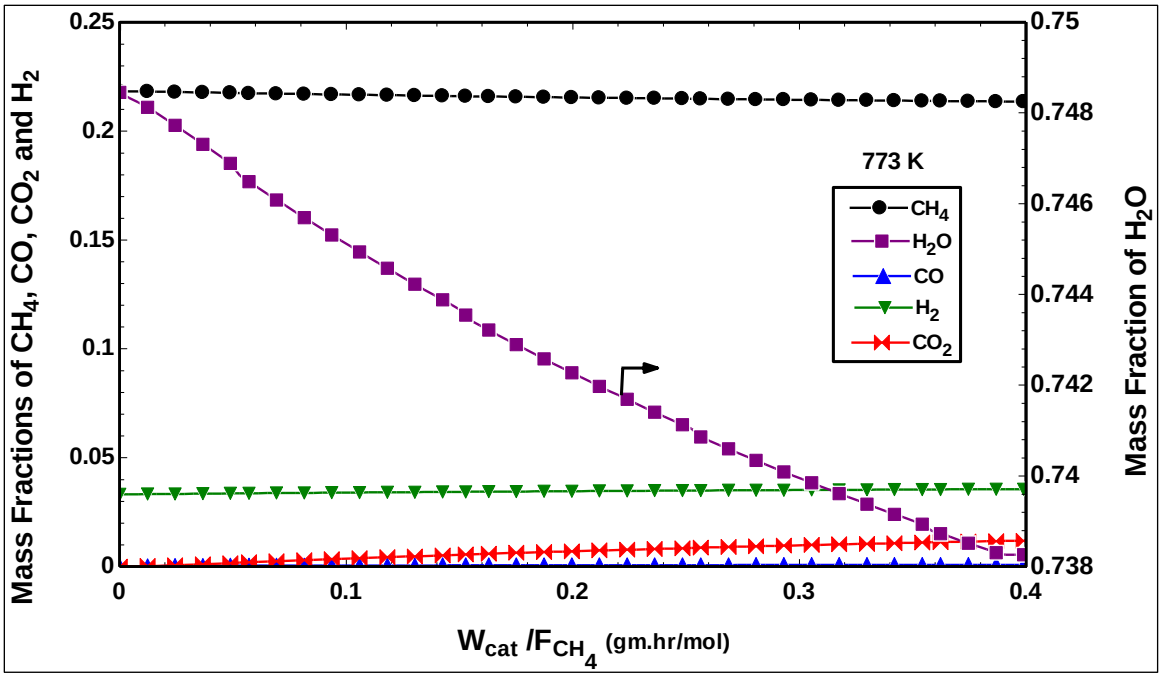

Figure 4.3: Mass Fraction of Species vs W_{cat}/F_{CH4} at F_{H2O}/F_{CH4} = 3, F_{H2}/F_{CH4} = 1.25 T = 773 K and P = 10 bar

The contours of hydrogen mass fraction at the various reforming temperatures considered for validation are shown in Figure 4.4. It is observed that there is an increase in the concentration of hydrogen along the axial length of the reactor as the reforming temperature is increased which is quite obvious since the steam methane reforming reactions (Eq. (1) & (3)) are highly endothermic. Nevertheless, the 2d plots also give an insight of the radial gradients of species concentration (if any) within the reactor which can help in determining the performance metrics of the reforming reactor and to study the thermal and chemical stability of the catalyst filled reactor.

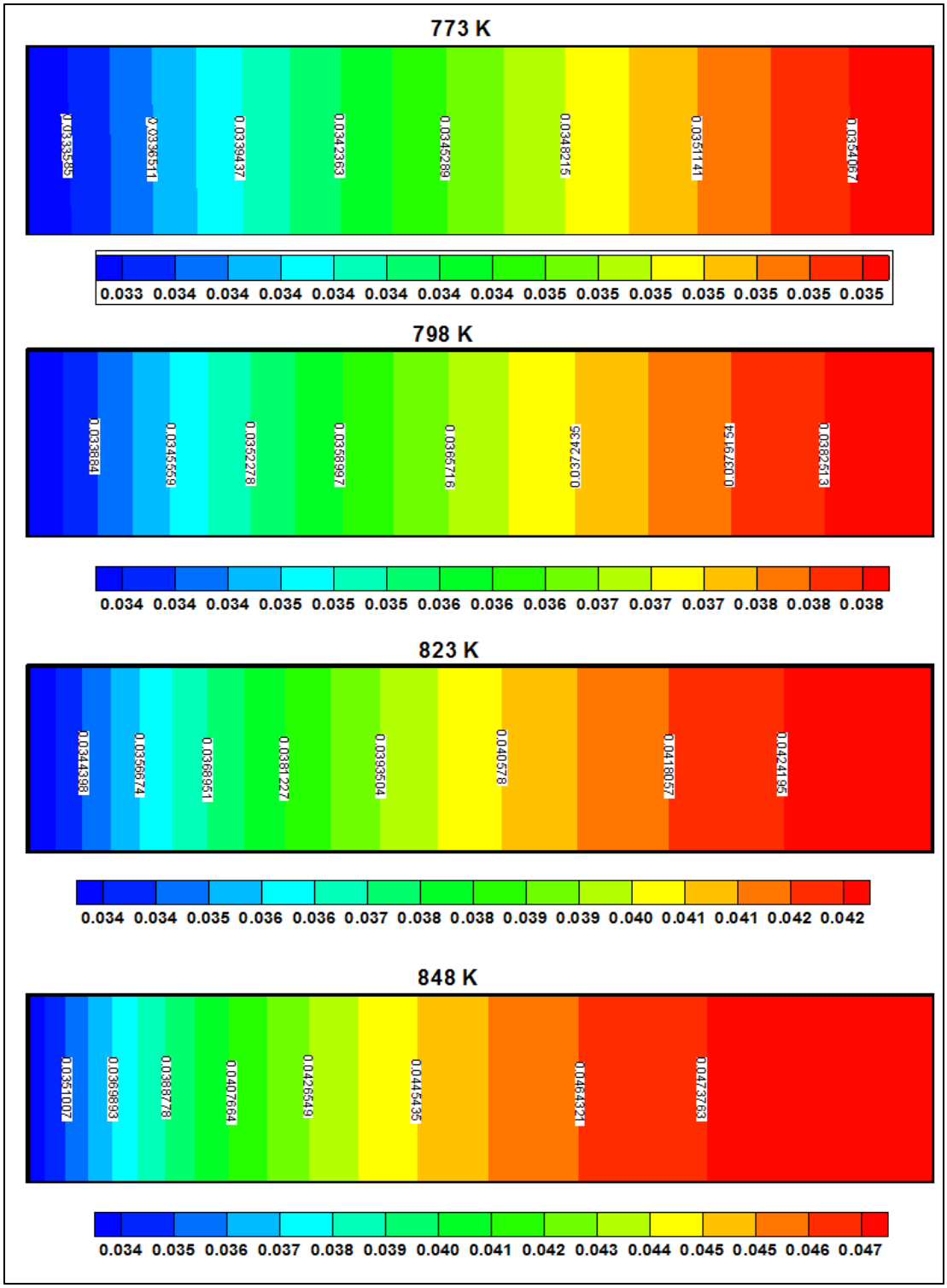

Figure 4.4: Contours of hydrogen mass fraction at different reforming temperatures for at $F_{H2O}/F_{CH4} = 3$, $F_{H2}/F_{CH4} = 1.25$ and P = 10 bar

The above comparisons (Figure 4.2) give enough confidence in the computational model developed for investigating the steam methane reforming reactions and the model can be further extended to study the effect of using a hydrogen permeation membrane which removes the hydrogen being formed by the SMR reaction.

4.2 Grid Independence

Further on, with regard to the membrane reactor model, a numerical mesh generator GAMBIT v2.2.30 is used to create the geometry (as in Figure 3.2) and mesh the domain using structured elements. A fine mesh is created at both sides near the membrane wall to capture the large gradients normal to the flow direction. Five different grids for membrane steam reforming reactor model shown in Figure 3.2 with 420, 680, 1248, 2850 and 3300 elements were created to examine the grid independence. These grids are named grid 1, grid 2, grid 3, grid 4 and grid 5 for further ease. Figure 4.5 compares the fractional methane conversion values obtained at the exit of the reactor using the five grids for the conditions of operating temperature = 773 K, pressure = 10 bar, steam to methane ratio = 1 and hydrogen to methane ratio of 0.1. The figure shows a good agreement (same values are obtained) between the fractional methane conversion values at fine grids 4 and 5 whereas a difference in the value is found at coarser grids of 1, 2 and 3.

Figure 4.6 shows the mass fraction of hydrogen through the membrane at the sweep side exit for the above mentioned grids and it can again be seen that for finer grids 4 and 5, the H_2 mass fractions are in good agreement giving the same values. Since grid 4 with a fine mesh produces results with the same accuracy as that with even more finer grid (grid 5), grid 4 with 2850 elements is used in further analysis to save computational time. Also,

from the above analysis, it can be concluded that the solution is grid independent for the selected grids.

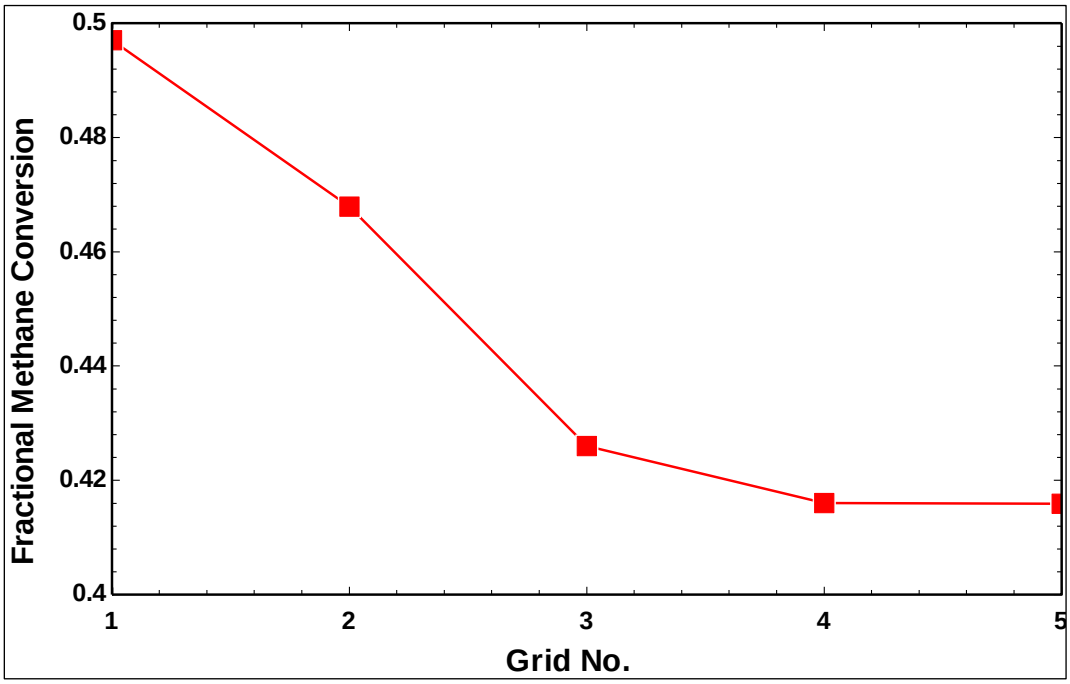

Figure 4.5: Grid Independence Results for Fractional Methane Conversion

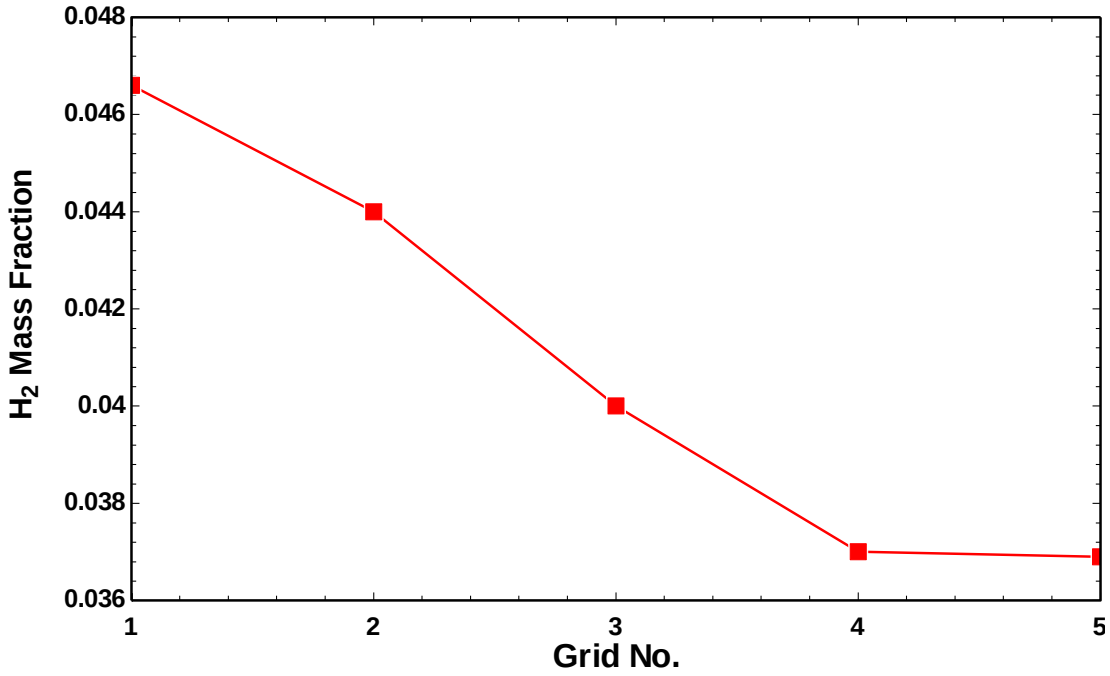

Figure 4.6: H_2 Mass Fraction at the sweep exit for different grid elements

CHAPTER 5

RESULTS & DISCUSSION

The aim of this work was to study the performance of the Pd membrane reactor in low temperature SMR operating in a temperature range obtainable by parabolic trough solar collectors (400-600 °C). In a practical situation, concentrated solar heat would be transferred from the parabolic trough using a molten salt as a heat transfer fluid [23, 88-90]. A detailed study of thermal effects, specifically addressing the issue of the effective heat supply by the molten salt, will be discussed later. Herein, the focus is on determining kinetic and transport limitations.

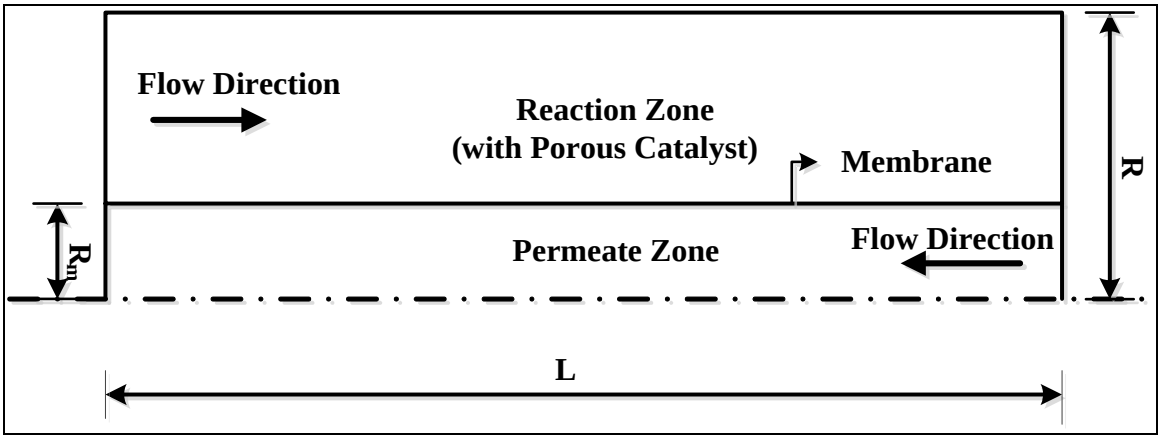

Figure 5.1: 2D CFD computational domain that represents a membrane reformer with tubular axisymmetric geometry.

In all simulations, dimensionless reformer geometry was defined by the reformer aspect ratio (2R/L = 0.12) and the membrane area-to-reformer volume ratio (A_M/V = 87.8 m^{-1}). Gas hourly space velocity (GHSV) is defined as the volumetric flow rate of CH_4 in the feed (defined at standard temperature and pressure) divided by the reformer volume:

$$GHSV = \frac{Q_{CH_4,f}^{STP}}{V} \quad (33)$$

Inlet feed consisted of (preheated to the reformer temperature) H_2O and CH_4 with a steam-to-carbon ratio S/C =1-3. Though the model does not account for carbon formation (which is expected to occur for S/C < 2 over Ni-based catalysts), the stoichiometric feed case (S/C = 1) was intentionally included in the analysis to evaluate the potential of the membrane reformer for low S/C operation. This is of particular importance for solar thermal reforming, wherein maximizing the reformer throughput is required to minimize capital cost investment. It should be mentioned here that the kinetic expressions used in the simulations were developed for MgO-promoted Ni/Al_2O_3, i.e. $Ni/MgAl_2O_4$, which is more stable against coking. Nevertheless, new catalysts, with superior stability against carbon deposition, should be developed for such applications. The pressure at the reaction zone outlet was fixed to P = 10 bar, whereas the pressure at the outlet of the permeation zone was P_M = 1 bar in all simulations.

The reformer performance was evaluated by fractional methane conversion (Eq. 32), H_2/CO ratio (accounting for combined H_2 flow at the outlet of the reaction and permeate zones) and H_2 recovery (the ratio of the molar rate of permeated H_2 (membrane outlet) to the feed CH_4 molar rate, Eq. 34). The H_2/CO ratio is more useful evaluation parameter for applications wherein the total reformer outlet is used as a fuel (for gas turbine) or as a chemical feedstock, while H_2 recovery is more relevant for applications that require an extra-pure H_2 flow (e.g. fuel cells, hydrogenation etc.).

$$R_{H_2} = \frac{F_{H_2,M,out}}{F_{CH_4,f}} \quad (34)$$

5.1 Co-Current vs Counter Current Flow:

Having selected the grid, further simulations were carried out to decide for the flow direction of sweep gas i.e. in the co-current or counter current direction of the reactants. Figure 5.2 shows the fractional methane conversion versus reforming temperature for both co-current and counter-current modes at steam to methane ratio of 3 and hydrogen to methane ratio of 1.25. Pressure at the reaction side was set to 10 bar whereas the permeate zone pressure was 1 bar. It can be noted (from Figure 5.2) that the counter-current mode gives always higher conversion than the co-current mode and the difference between the two modes is significant. In order to explain this methane conversion difference between the co-current and counter-current modes, it has to be taken into account the different flux configuration which is responsible for the different partial pressure profiles inside the reactor and the different permeation driving force between the two modes, resulting in a higher hydrogen recovery in the counter-current mode with respect to the co-current one. This higher hydrogen flux through the membrane gives a higher conversion for the counter-current mode with respect to the co-current one.

H_2/CO ratio (accounting for combined H_2 flow at the outlet of the reaction and permeate zones) and H_2 recovery (the ratio of the molar rate of permeated H_2 (membrane outlet) to the feed CH_4 molar rate) are important performance evaluation parameters for the reactor. The H_2/CO ratio is more useful evaluation parameter for applications wherein the total reformer outlet is used as a fuel (for gas turbine) or as a chemical feedstock, while H_2 recovery is more relevant for applications that require an extra-pure H_2 flow (e.g. fuel cells, hydrogenation etc.). Hydrogen recovery and hydrogen to carbon monoxide ratio for the co-current and counter current modes at different temperatures are shown in

Figure 5.3. The difference in both these parameters for the two flow regimes considered is significantly visible from the plots with hydrogen recovery showing much variation since permeation of hydrogen depends on partial pressure profile inside the reactor.

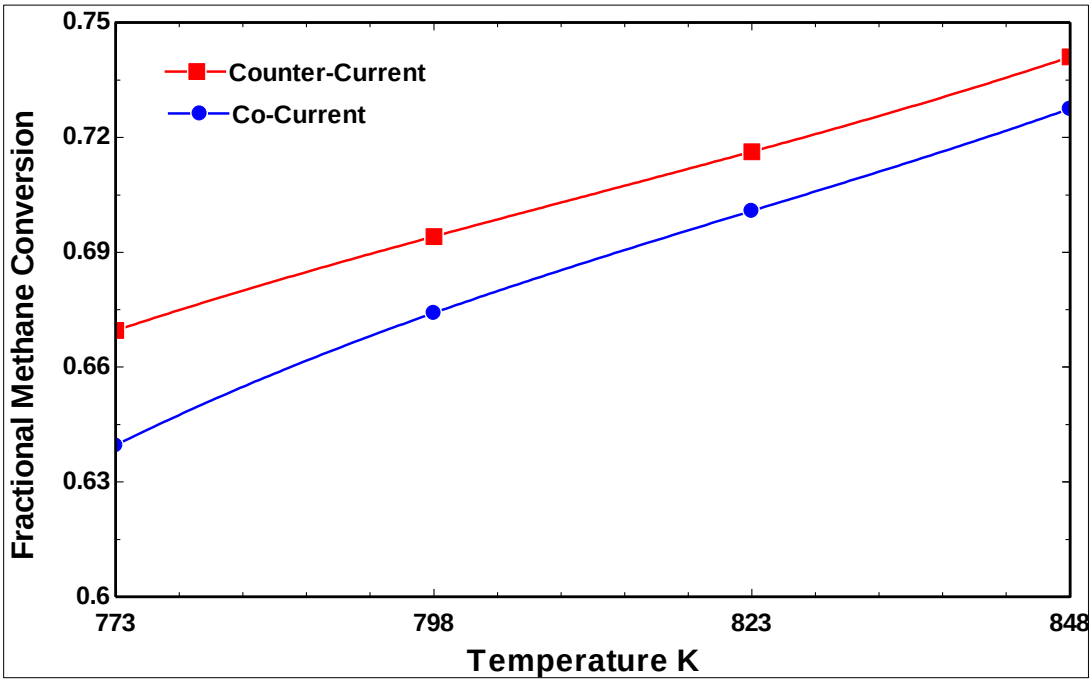

Figure 5.2: Variation of Fractional Methane Conversion vs Temperature at F_{H2O}/F_{CH4} = 3, F_{H2}/F_{CH4} = 1.25, P = 10 bar, P_M = 1 bar for Co-current and Counter current mode

The contours of hydrogen mass fraction for the case of T = 773 K, P = 10 bar and P_M = 1 bar for the co-current and counter current mode are shown in Figure 5.4. It is worthy to be noted from this 2d distribution that although the reaction conditions were the same for the two flow regimes, difference in hydrogen concentration within the reactor for both the modes is observed yielding to highest hydrogen mass fraction value of 0.083 (at the exit of permeate zone) for the co-current mode and correspondingly 0.098 for the counter current mode. As mentioned earlier, this variation in concentration of hydrogen is due to

the partial pressure profiles within the reactor which is quite high in the counter current mode, thus yielding to higher permeation.

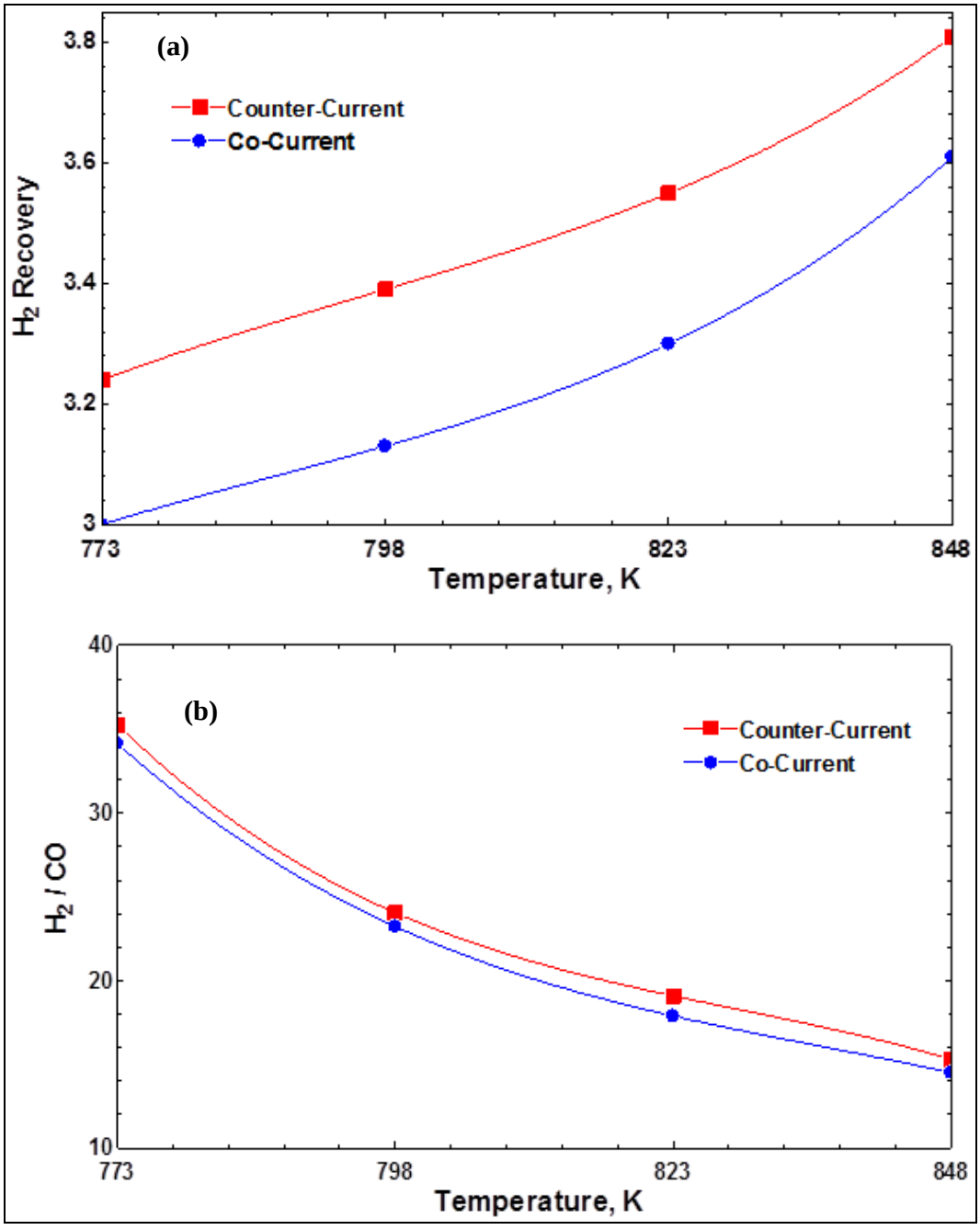

Figure 5.3: (a) Hydrogen Recovery vs Temperature and (b) H_2/CO vs Temperature at F_{H2O}/F_{CH4} = 3, F_{H2}/F_{CH4} = 1.25, P = 10 bar, P_M = 1 bar for Co-current and Counter current mode

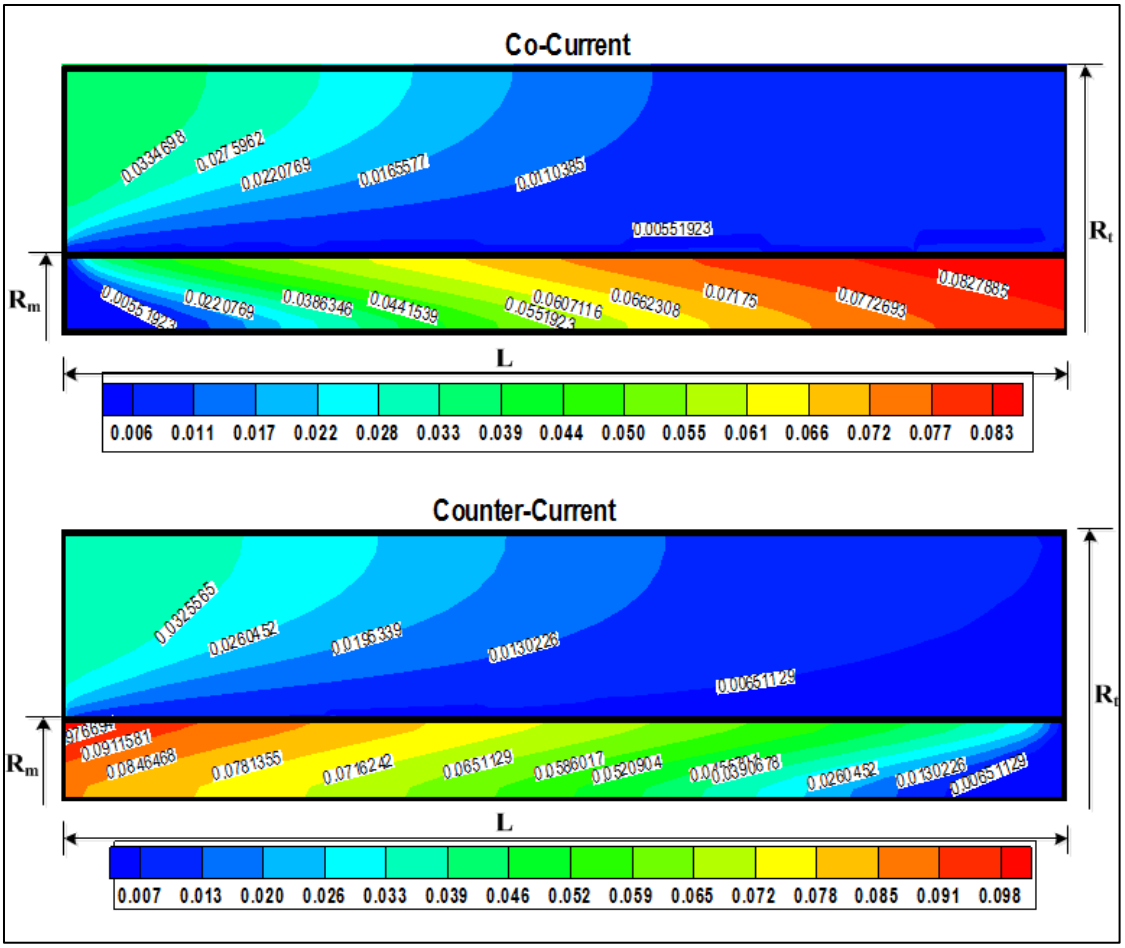

Figure 5.4: Simulated contours of H2 mass fraction for T = 773 K, P = 10 bar, P_M = 1 bar at F_{H2O}/F_{CH4} = 3, F_{H2}/F_{CH4} = 1.25 for Co-current and Counter current mode

5.2 Radial gradients

Figure 5.5 and Figure 5.6 presents typical results, showing simulated contours of the H_2 mass fraction within the computation domain for S/C = 1, 3 and T = 773, 848 K. The counter-current sweep flow was used to keep high H_2 partial pressure difference along the reformer (Figure 5.1), with the sweep gas mass flow rate equivalent to that of the feed. Since the flow of sweep gas is in the counter-current direction to the flow of reactants, the highest values of the H_2 mass fraction in the permeate zone are observed at the very inlet of the reactor, which is the exit for the sweep gas. These plots clearly

justify the use of the 2D model since strong radial gradients develop, leading to relatively low H_2 partial pressures at the membrane vicinity in the reaction zone. The buildup of the gradients is particularly pronounced in the beginning of the reaction zone in which the reforming reactions mostly take place. Since the driving force for H_2 separation is determined by the difference in H_2 partial pressures in the immediate vicinity of the membrane wall, concentration polarization limits the separation ability of the membrane and the overall performance of the membrane reformer in terms of CH_4 conversion and H_2 recovery.

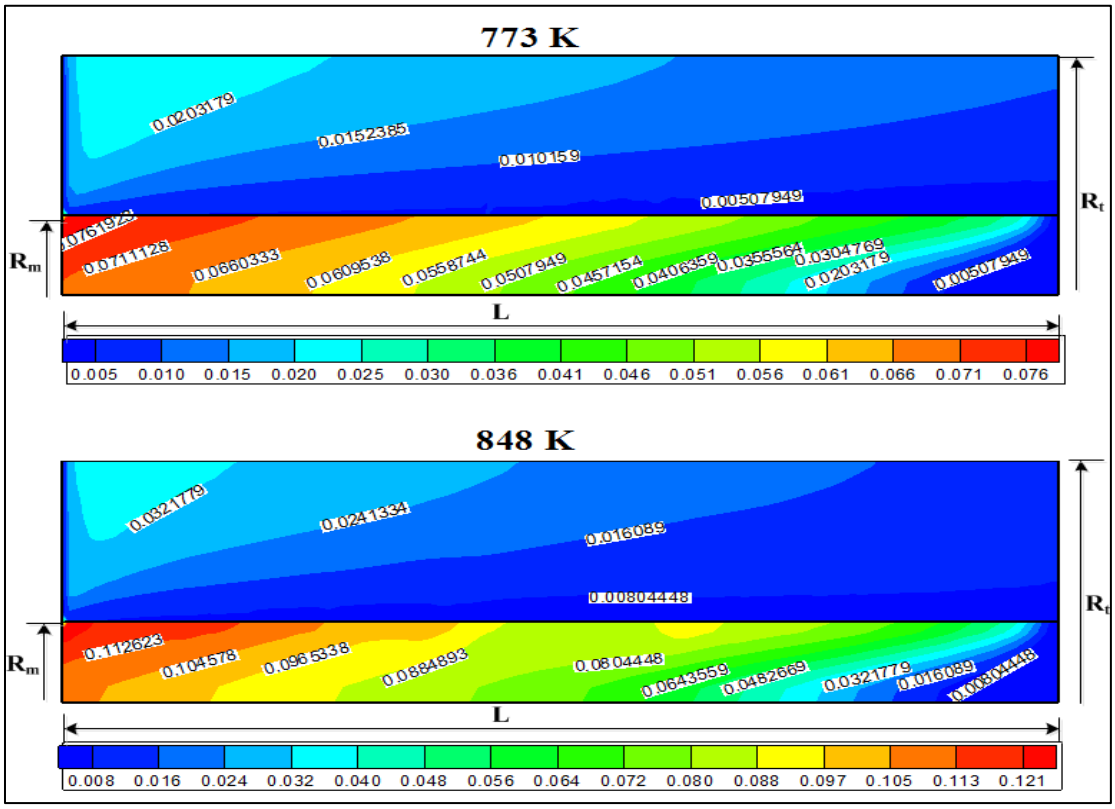

Figure 5.5: Simulated distributions of the H_2 mass fraction in the membrane reformer (not to scale) at T = 773 K and 848 K for S/C = 1 (b); GHSV = 6000 h^{-1}, P = 10 bar and P_M = 1 bar.

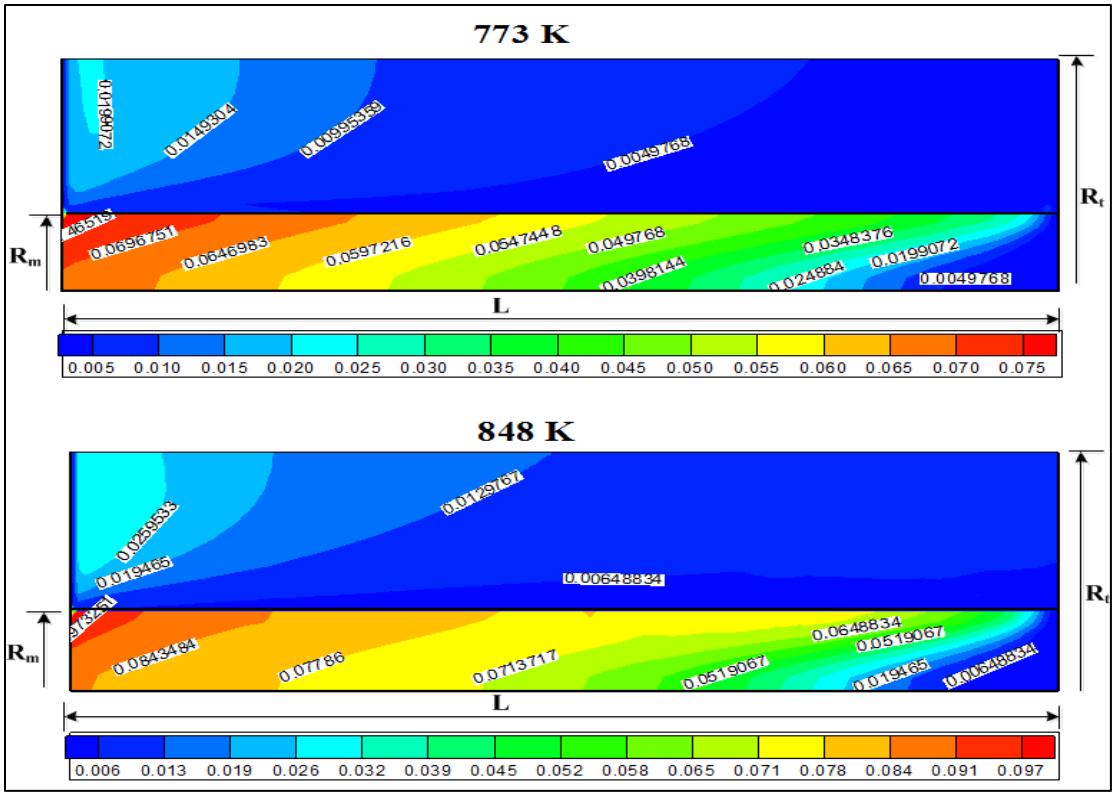

Figure 5.6: Simulated distributions of the H_2 mass fraction in the membrane reformer (not to scale) at T = 773 K and 848 K for S/C = 3 (b); GHSV = 6000 h^{-1}, P = 10 bar and P_M = 1 bar.

It can be seen from the contours (Figure 5.5 and Figure 5.6) that the mass fraction of hydrogen for steam to methane ratio of 1 is greater than that of 3. This is due to high amounts of steam present in the reaction system at higher steam to methane ratios which reduces the partial pressure of hydrogen due to dilution. Also, increase in hydrogen formation is observed at higher operating temperatures (848 K and constant S/C) which can be attributed to the fact that higher amounts of hydrogen is produced at high temperatures because of faster reaction kinetics since steam reforming of methane is highly endothermic. The contours also give an insight of hydrogen permeation through the membrane inside the catalyst filled reactor.

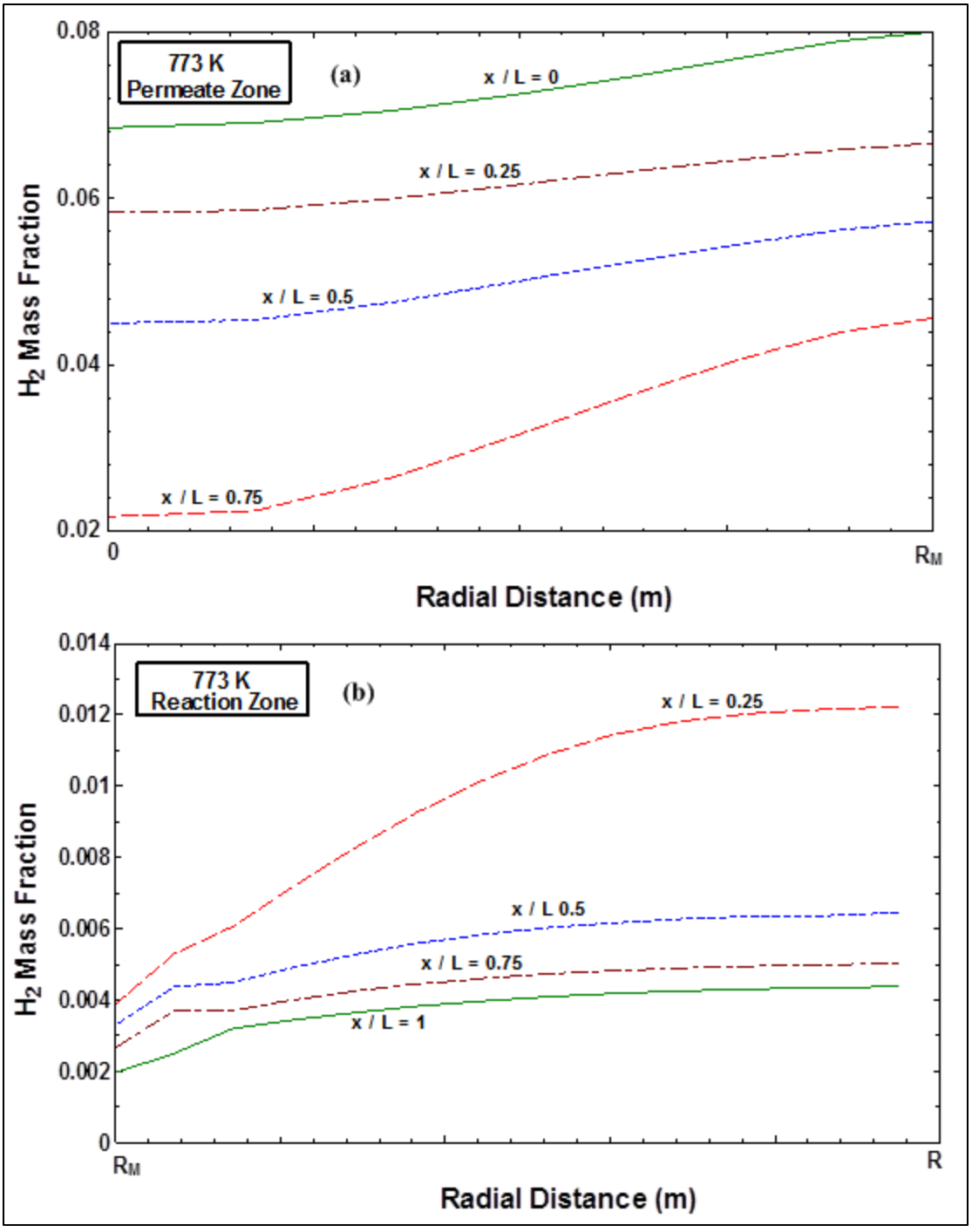

Figure 5.7: Simulated radial gradients of the H_2 mass fraction in the membrane interior (a) and the reformer reaction zone (b) at selected axial positions obtained at T = 773 K, S/C = 1 and GHSV = 6000 h^{-1}, P = 10 bar and P_M = 1 bar

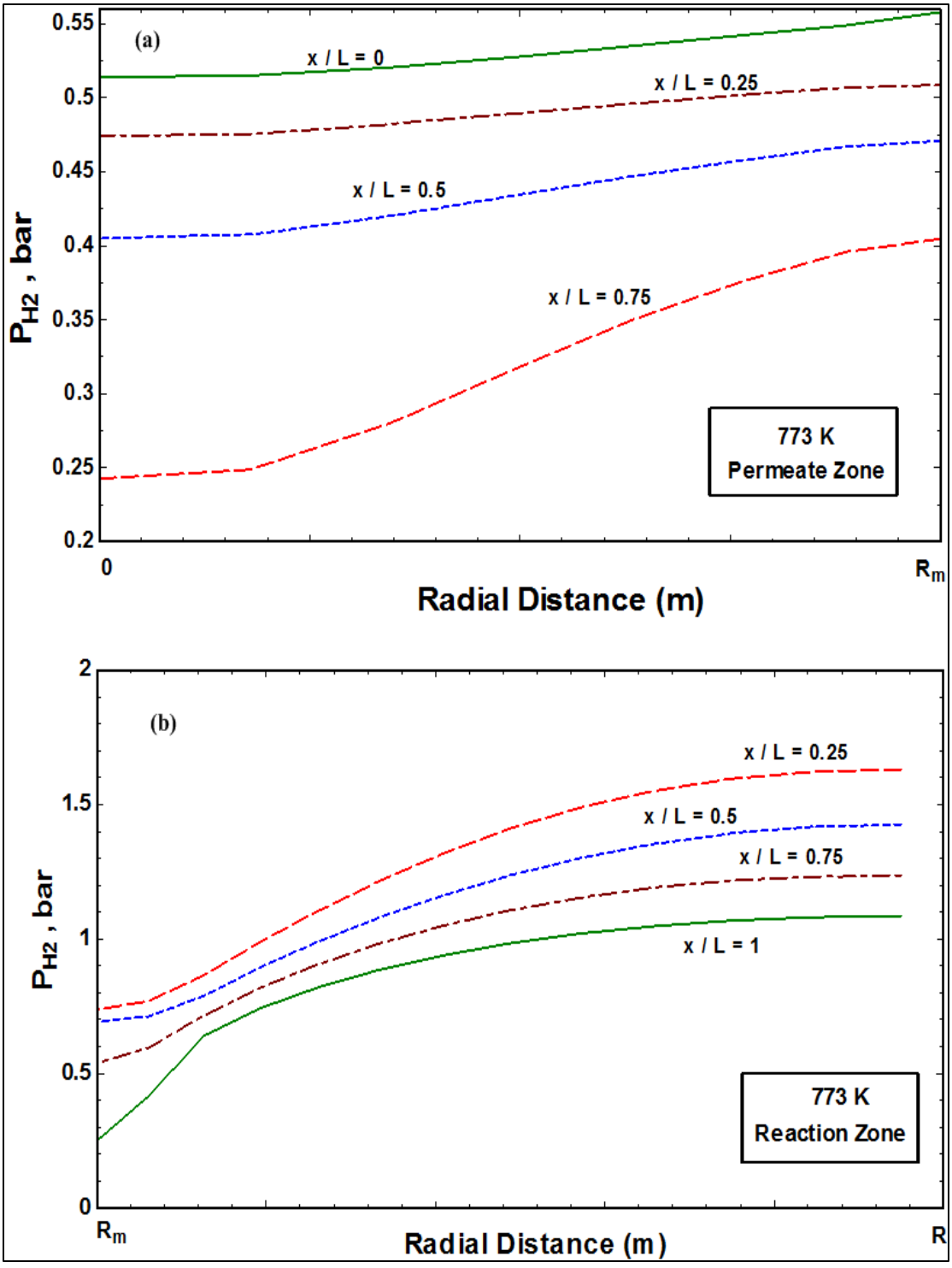

Figure 5.8 Simulated radial gradients of the H_2 partial pressure in the membrane interior (a) and the reformer reaction zone (b) at selected axial positions obtained at T = 773 K, S/C = 1 and GHSV = 6000 h^{-1}, P = 10 bar and P_M = 1 bar

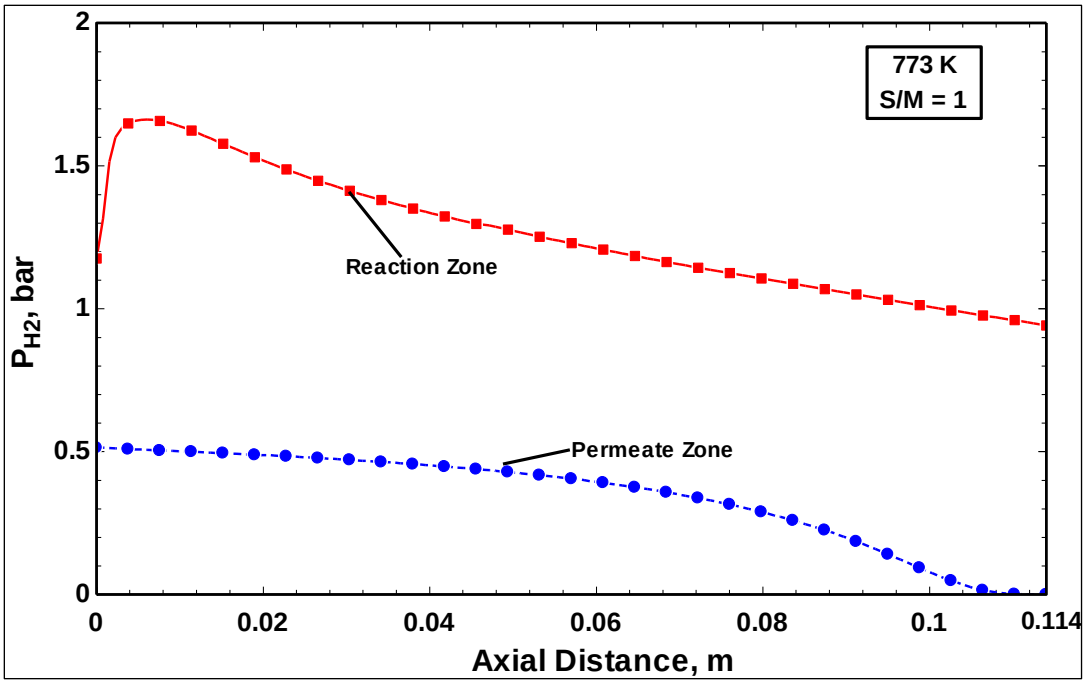

Figure 5.9: Partial pressure of H_2 in the membrane interior and reformer reaction zone at T = 773 K, S/C = 1, GHSV = 6000 h^{-1}, P = 10 bar and P_M = 1bar

Radial cuts of the 2D H_2 mass fraction distribution along the reactor length for the reaction and permeation channels are shown in Figure 5.7. Radial gradients are shown at four non-dimensional positions defined as x/L (x stands for the axial coordinate). The H_2 mass fraction decreases in both the reaction and permeate zones along the length of the reactor (in the direction of the reactants flow) as the H_2 formed by reforming reactions and WGS (Eqs. 1-3) permeates through the membrane and accumulates in the permeate zone. The existence of concentration polarization is evidently seen from Figure 5.7. Similarly, Figure 5.8 shows the radial partial pressure distribution of hydrogen at different axial positions of the reactor. Hydrogen partial pressure profile in the reaction and permeate zones along the length of the reactor is shown in Figure 5.9. The sweep gas in the permeate zone flows in the counter current direction (right to left in Figure 5.9),

thus giving larger values at the inlet of the reactor. An increase in partial pressure is observed in the initial length of the reaction zone which represents the formation of hydrogen through the SMR reactions (Eq. 1-3) followed by a gradual decrease due to hydrogen permeation and accumulation in the permeation zone. This partial pressure difference in the reaction and permeation zones is predominantly the main factor for the permeation of hydrogen according to Sivert's Law.

5.3 Methane conversion enhancement:

Figure 5.10 shows the simulated CH_4 conversion (Eq. 32) at a fixed GHSV of 6000 h^{-1} and different S/C ratios, in the low temperature SMR range relevant to the solar parabolic trough technology (~400-600 ^oC). As expected, CH_4 conversions obtained in the membrane reformers exceeds by far those obtainable in the non-membrane reformer over the tested range of temperature and steam-to-carbon ratios. This effect is due to the selective removal of H_2 by the Pd membrane that shifts the equilibrium towards products generation (Eqs. 1-3). This substantial increase in the CH_4 conversion compensates for low temperatures obtainable by solar parabolic troughs. For the given temperature, CH_4 conversion increases with steam-to-carbon ratio, both for membrane and non-membrane reactors (Figure 5.10), which is dictated by equilibrium.

Three different steam-to-carbon ratios, S/C=1, 2 and 3 are investigated. Though we aware of the tendency of the Ni catalyst to coke formation at S/C < 2 [4], a S/C = 1 is included as a reference value, which represents an ideal case with no coke formation (coking was not accounted for in the simulations). We note that CO is the main source of coking at low temperature (due to exothermic Boudouard coking and reverse gasification). Interestingly, the results presented in next sections show that very low CO concentrations

are obtained under certain operating conditions, thereby potentially allowing operation at low S/C ratios. Low CO concentrations can be attributed to low temperature regime of operation (since WGS is exothermic, Eq. 2) and to H_2 removal by the membrane.

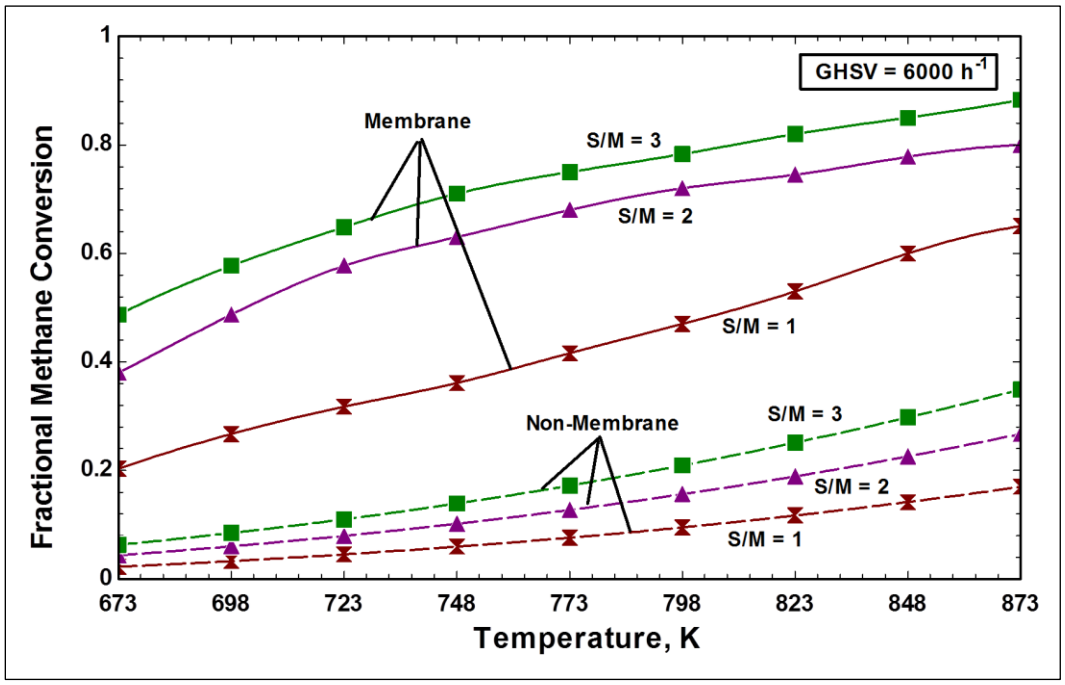

Figure 5.10: Fractional CH_4 conversion (Eq. 10) vs. temperature for different S/C ratios (steam-to-methane fed, S/M) at GHSV = 6000 h^{-1}, P = 10 bar and P_M = 1 bar.

Figure 5.11 shows the partial pressure profile of hydrogen in the reaction and permeation zones for T = 773 K and steam-to-carbon ratios of 1 and 3. It is observed that the partial pressure profile for both cases is similar in the permeation zone whereas variations of the same are observed in the reaction zone. Lower partial pressures are observed for a higher steam-to-carbon ratio (S/C = 3) than lower ones (S/C = 1). Dilution of hydrogen due to the presence of higher amounts of steam (H_2O) at higher steam-to-methane ratios in the reaction zone is attributed to this phenomenon which in turn reduces the partial pressure and thus negatively affects permeation. Although permeation is reduced due to lower

partial pressure difference, higher conversions are achieved at high steam-to-carbon ratios since probability of CH_4 reacting with steam increases, thus forming more hydrogen. Figure 5.12 shows a comparison of radial gradients of H_2 mass fraction distribution within the (a) reaction and (b) permeate zones at different axial positions (x/L = 0.25 and 0.75) for T = 848 K and steam-to-methane ratio of 1and 3.

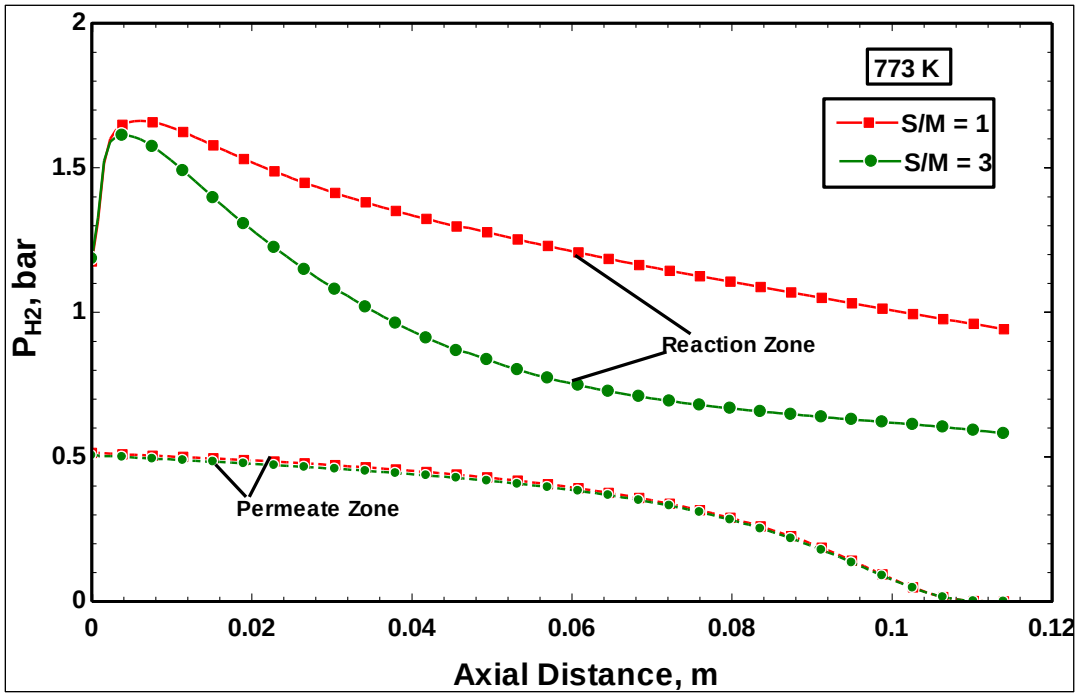

Figure 5.11: Comparison of H_2 partial pressure profiles in the membrane interior and reaction zone for S/M = 1 and 3 at T = 773 K, S/C = 1, GHSV = 6000 h^{-1}, P = 10 bar and P_M = 1bar

Similar to Figure 5.11, Figure 5.13 shows a comparison of hydrogen partial pressures for steam-to-carbon ratio of 1 and T = 773 and 873 K. Since steam reforming reactions are highly endothermic, higher temperatures tends the reaction (Eq. 1-3) to proceed in the forward direction i.e. towards the product side and yields to products formation. This is

why higher amounts of H_2 is produced (in the reaction zone) at high temperatures and thus higher partial pressures are observed.

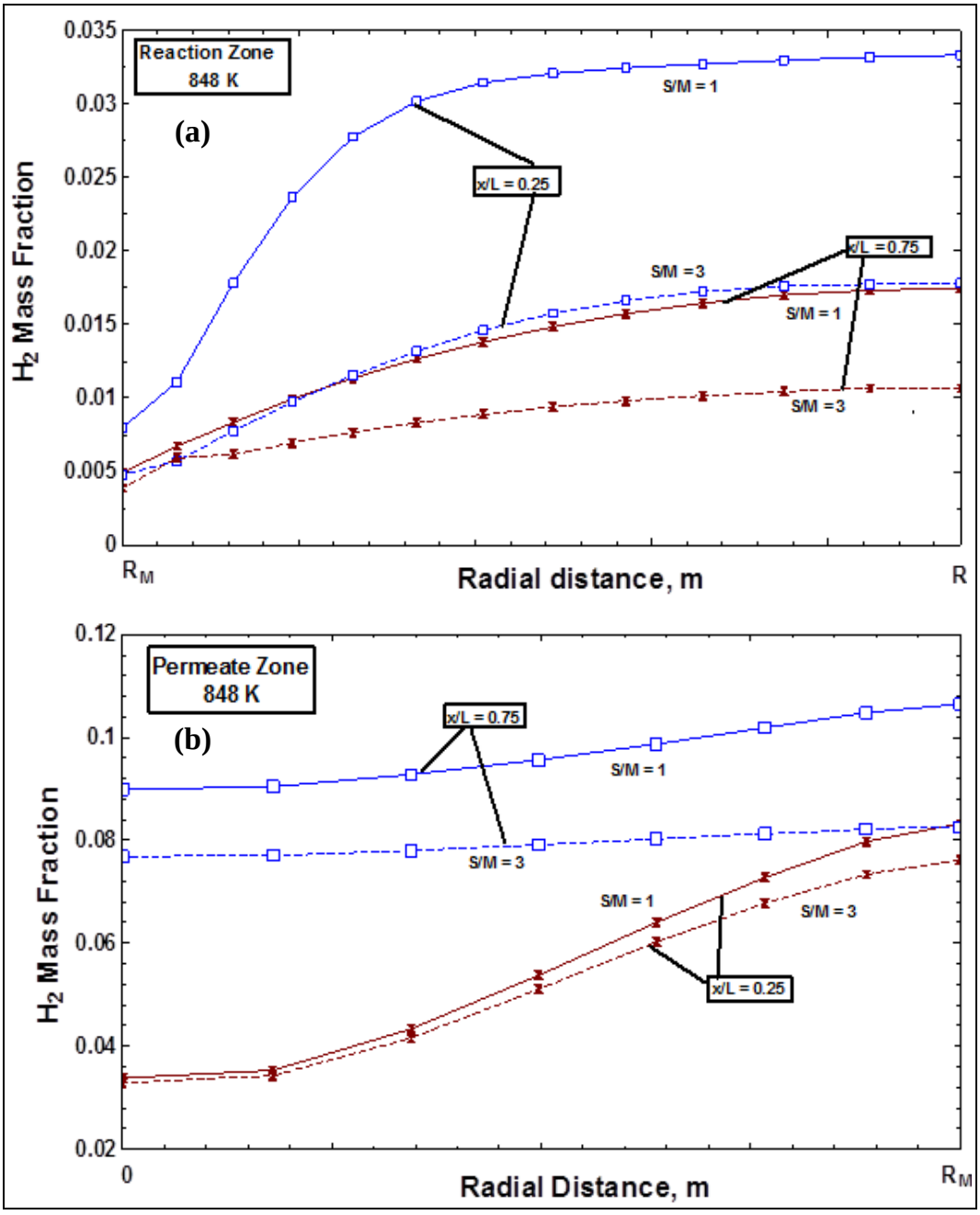

Figure 5.12: Comparison of radial gradients of H_2 mass fraction in the membrane interior (a) and the reformer reaction zone (b) at selected axial positions obtained at T = 848K, S/C = 1 & 3 and GHSV = 6000 h^{-1}, P = 10 bar and P_M = 1 bar

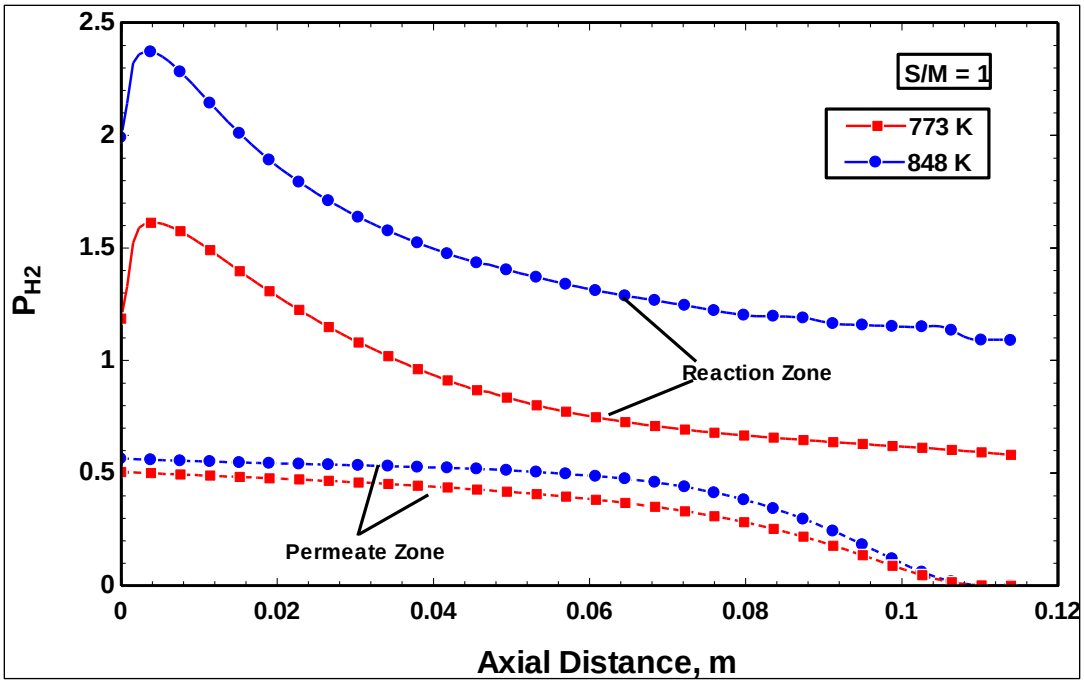

Figure 5.13: Comparison of H_2 partial pressure profiles in the membrane interior and reaction zone for T = 773 & 848 K at T = 773 K, S/C = 1, GHSV = 6000 h^{-1}, P = 10 bar and P_M = 1bar

Figure 5.14 shows a comparison of contours of hydrogen mass fraction for a non-membrane and membrane reactor. The difference in the amount of hydrogen produced (at same conditions) by both the reactors is clearly visible by the 2d contour plot. This increased amount of hydrogen produced by the membrane reactors is due to the equilibrium shift effect occurring by the selective removal of hydrogen from the reaction system which shifts the equilibrium towards the product side according to Le Chatelier's principle.

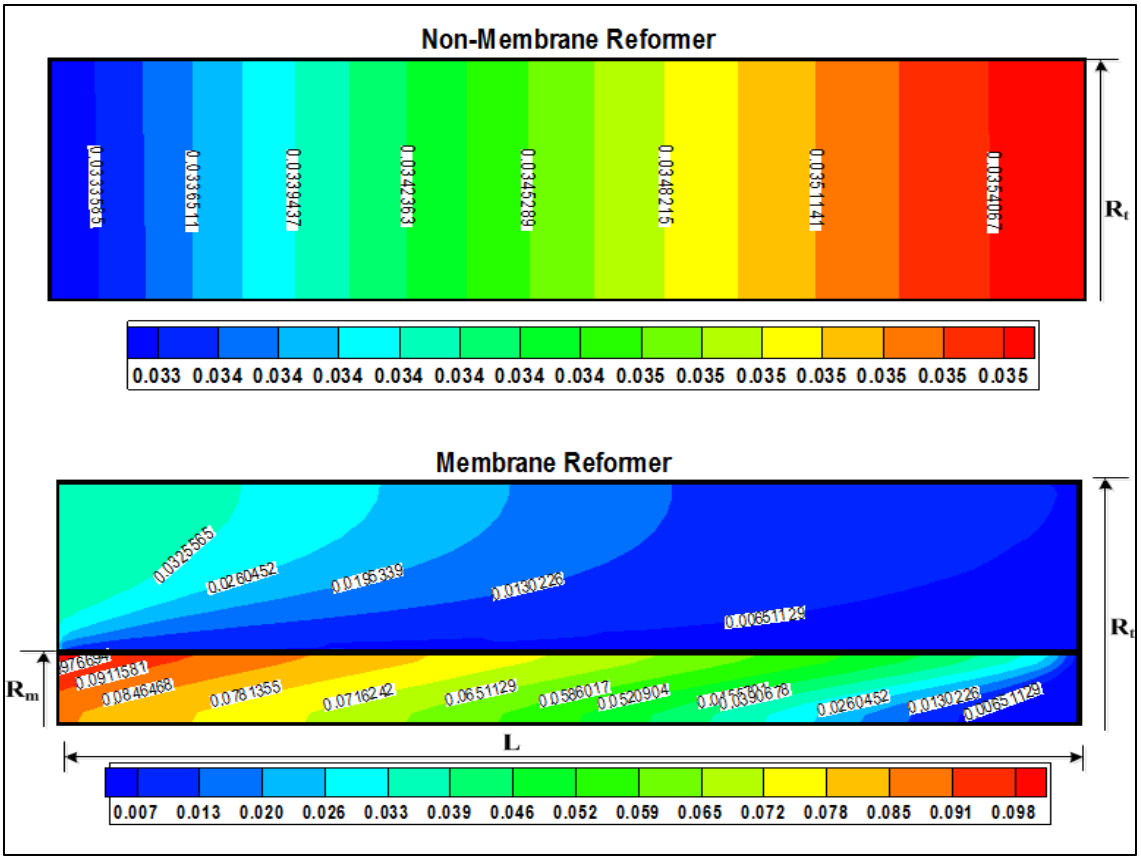

Figure 5.14: Comparison of hydrogen mass fraction for a non-membrane and membrane reformer at F_{H2O}/F_{CH4} = 3, F_{H2}/F_{CH4} = 1.25 T = 773 K, P = 10 bar and P_M = 1 bar

5.4 Effect of temperature and steam-to-carbon ratio

Hydrogen recovery and H_2/CO ratio at different operating temperatures and steam-to-methane ratios are shown in Figure 5.15. A general trend is observed showing that H_2 recovery increases for increasing temperature and S/C ratio (Figure 5.15a). This increase is due to the faster reaction and separation kinetics at high temperatures (see Eqs. 18 and 31) and an enhanced WGS reaction (Eq. 2) in the presence of excess steam for high S/C ratios. Though the increase in H_2 recovery is monotonic, three distinct ranges can be seen in Figure 5.15a. There is a slow increase for T = 673-723 K followed by a sharp (about two-fold) improved in the H_2 recovery for T = 723-773 K, while further increase in

temperature results in only minor improvement again. Such trend clearly indicates the existence of (at least two) different limiting factors. The maximum H_2 recovery for isothermal operation is 4, as dictated by the reaction stoichiometry (Eq. 3).

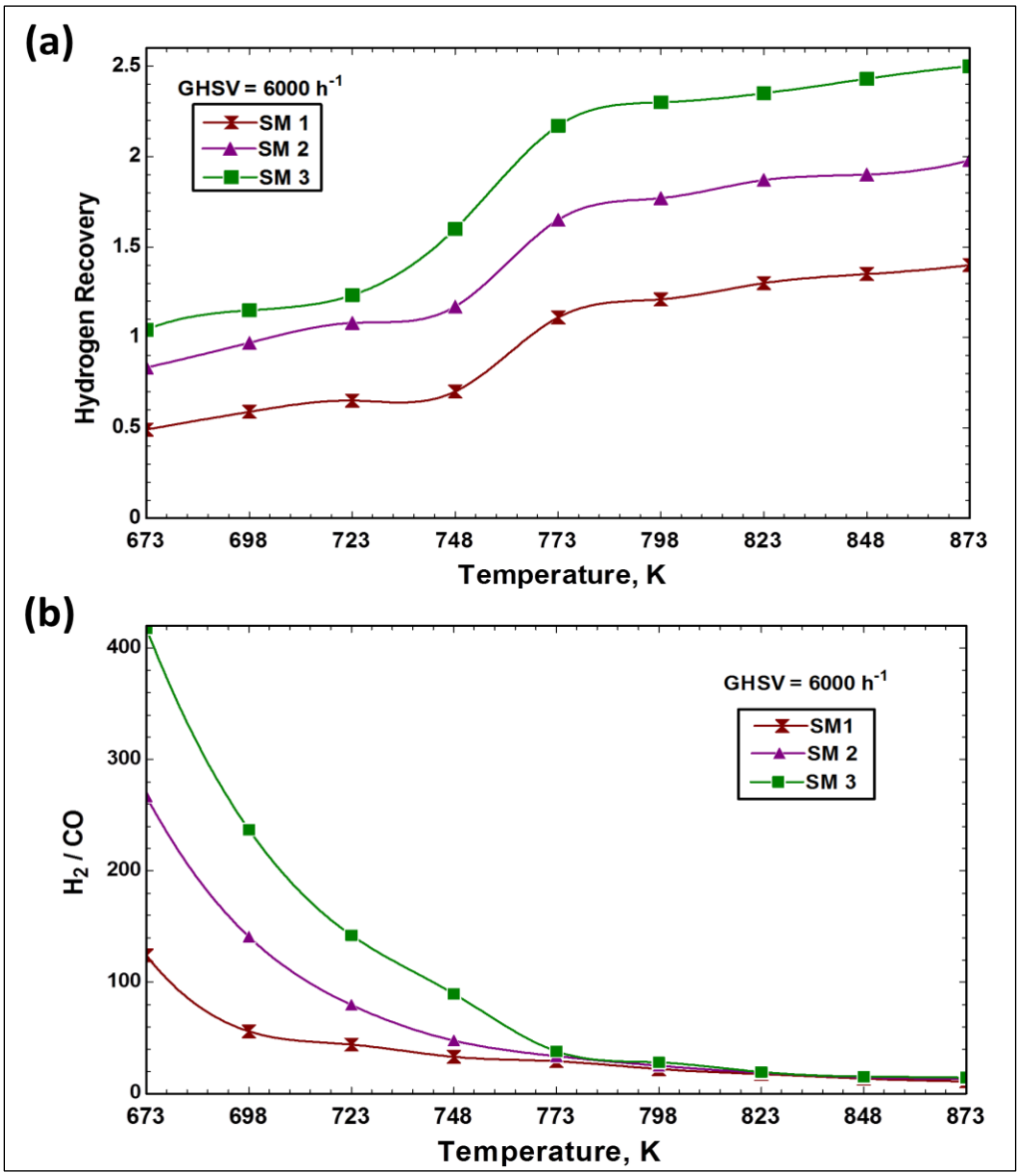

Figure 5.15: (a) H_2 recovery (Eq. 12) and (b) H_2/CO ratio as a function of temperature for different S/C ratios (steam-to-methane fed, SM); GHSV = 6000 h^{-1}, P = 10 bar and P_M = 1 bar.

At very low temperatures (T < 450 °C), the reformer performance is expected to be severely limited by the low activity of the Ni-based catalyst. The activation energy of the main reforming pathway is very high (E_1 = 240.1 kJ/mol, Eq.31a[33]), implying that the catalyst activity is very low below 450 °C, but increases drastically for T ~ 500 °C and above since the dependence of the reaction rate on temperature is highly nonlinear (Eqs. 31). This explains the two-fold increase in H_2 recovery for T = 450-500 °C in Figure 5.15a. The activation energy for H_2 separation is very low (E_{H_2} = 6.6 kJ/mol [91]) and is not expected to limit the reformer performance. The change in the slope of the H_2 recovery increase observed for T > 500 °C in Figure 5.15a should be rather attributed to the lack of the membrane area [34] (this subject is discussed in more detail in Section 5.5), but could be also the result of the more pronounced concentration polarization (see Figure 5.5 and Figure 5.6).

As expected, much higher H_2/CO ratios are obtained for higher steam-to-carbon ratio (Figure 5.15b), as the WGS reaction extent is enhanced by excess steam. Note that very low CO concentrations are produced below 500 °C. The decrease in H_2/CO ratio is observed with increasing operating temperatures, as it is expected from the exothermic nature of the WGS reaction. Comparing Figure 5.15 a and b shows that there is a tradeoff between high H_2 recovery and high H_2/CO ratio. Notably, T ~ 500 °C provides an optimal value to obtain both a relatively high H_2 recovery and an enhanced H_2/CO ratio. While high H_2 recovery is desirable for H_2 generation, low CO concentrations are preferable to prevent coking.

5.5 Effect of space velocity

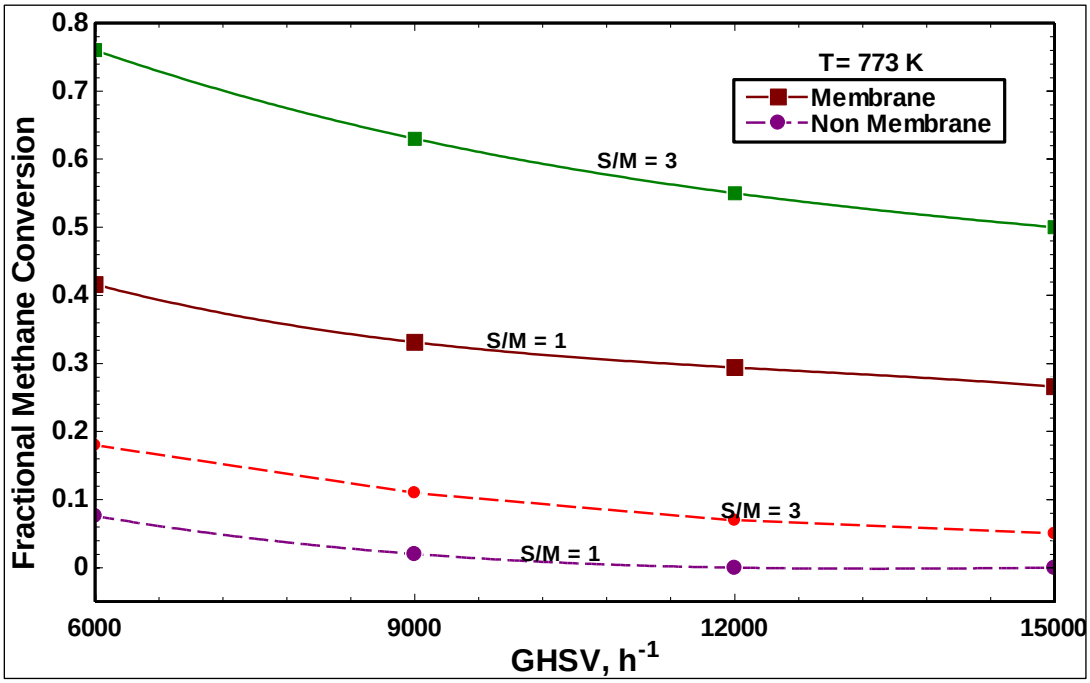

Figure 5.16: Comparison of performance of the membrane and non-membrane reformer in terms of CH_4 conversion (Eq. 10) as a function of GHSV (Eq. 11) for S/C = 1 and 3, T = 773 K, P = 10 bar and P_M = 1 bar.

Figure 5.16 shows the impact of space velocity (GHSV) on CH_4 conversion, comparing the performance of the membrane and non-membrane reformers. GHSV is defined as the ratio of the CH_4 volumetric feed flow rate (calculated at standard conditions, i.e. STP) to the reactor volume, Eq. 33. The reformer was simulated for GHSVs ranging from 6,000 h^{-1} to 15,000 h^{-1}, with S/C of 1 and 3, and operating temperatures of 773 K. Similarly to the results for a fixed GHSV shown before in Figure 5.10, it is evident that a substantial increase in the CH_4 conversion is achieved by the membrane reactor for high GHSVs. Evaluating the performance of membrane reformers in a range of space velocities applicable to industrial conditions is of great importance to assess their potential for

large-scale implementation. Importantly, although increasing GHSV leads to shorter contact times and lower CH_4 conversions, relatively high CH_4 conversions are still achievable by the membrane reformer for GHSV = 15,000 h^{-1} and S/C = 3 as evident from Figure 5.16.

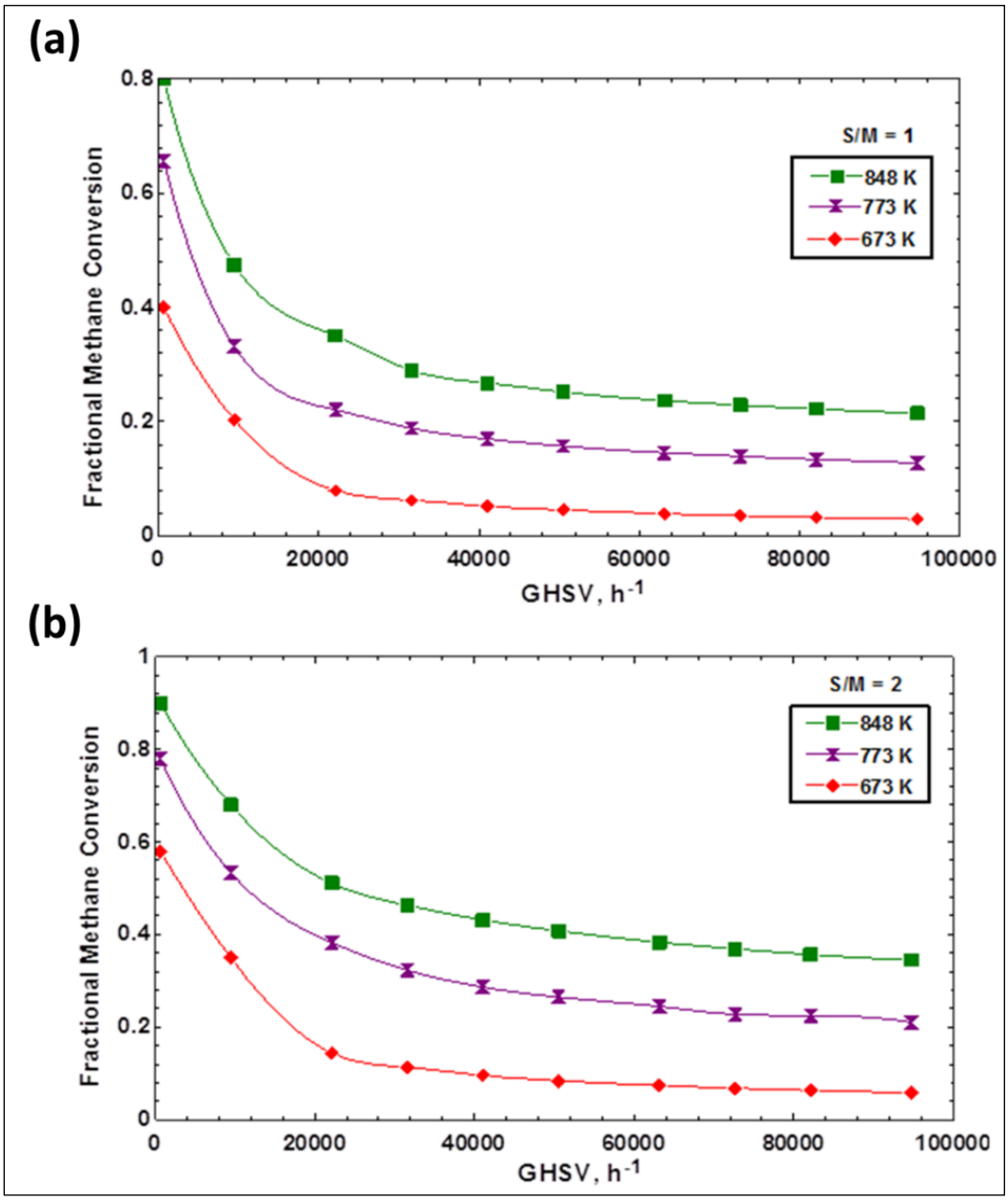

Figure 5.17: CH_4 conversion as a function of GHSV at various operating temperatures for (a) S/C = 1and (b) S/C = 2.

To determine the asymptotic limits of the reformer performance, numerical simulations were carried out in a wide range of space velocities, for GHSVs ranging from 500 h^{-1} to 100,000 h^{-1} (Figure 5.17). Low steam-to-carbon ratios (S/C = 1, 2) were used, which are of particular importance for solar thermal reforming applications, wherein maximizing the reformer throughput is required to compensate for high capital cost investment. Generation of excess steam will consume a lot of solar energy, which can be otherwise converted into chemical energy. Simulations were run for temperatures of 673 K, 773 K and 848 K, signifying the temperature range obtainable by solar parabolic troughs.

As shown in Figure 5.17, the equilibrium is approached as the GHSV tends to zero (infinite residence time). Membrane reactor equilibrium dictates nearly complete conversions for T > 500-550 °C (depending on the S/C ratio) [6]. Another (kinetic) asymptote is approached as the GHSV tends to infinity (zero residence time). There is a sharp decrease in CH_4 conversion for GHSV > 20,000 h^{-1}, while further increase in GHSV results in only minor further decrease of conversion, eventually attaining a plateau. In this regime, the reactor performance can be limited either kinetically (Ni catalyst activity) or by H_2 separation (membrane permeability and available membrane area), or both. For the reformer geometry analyzed in the present study, operation at GHSV < 10,000 h^{-1} would be recommended; in order to further increase the operating GHSV either a more active catalyst, a more permeable membrane or a larger membrane area would be required [6].

Figure 5.19 shows the variation of CH_4 conversion as a function of GHSV steam-to-carbon ratio of S/C = 1, 2 and 3, at T = 848 K. As it is dictated by the SMR-WGS equilibrium, higher CH_4 conversions are obtained for higher S/C ratios, due to the

presence of excess steam in the reaction system. While steam-to-carbon ratios lower than S/C = 2 are not recommended due to catalyst coking deactivation issues (at least for Ni-based catalysts), excessively high S/C ratios demand more steam production, increasing the cost of the entire process unit. Thus, a tradeoff between the cost of the system and the catalyst activity and stability must be carefully evaluated depending upon the final application of the process.

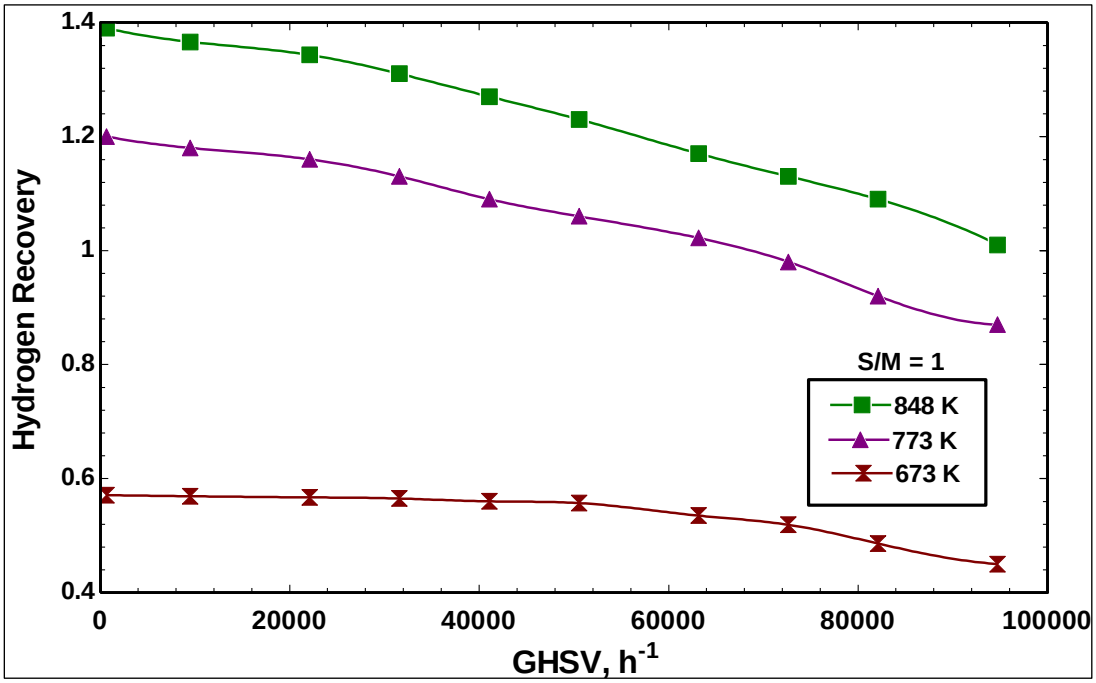

Figure 5.18: Variation of H_2 recovery as a function of GHSV for different temperatures (T = 673, 773 & 848 K) at S/C = 1, P = 10 bar and P_M = 1bar.

Interestingly, although there is a significant drop in CH_4 conversion as observed in Figure 5.19, the H_2 recovery values for S/C = 2 and 3 are still considerably high even for GHSV > 20,000 h^{-1} as shown in Figure 5.20a. This observation demonstrates one of the important advantages of membrane reactors over conventional, non-membrane reformers. Despite the drop of CH_4 conversion, H_2 separation by the membrane shifts the

equilibrium of the WGS reaction towards production of more H_2 by converting CO to CO_2. Excess of steam that results from the low SMR conversion at high GHSV is in fact favorable for WGS. This is evident from the significant increase in the H_2/CO ratio at elevated space velocities as observed in Figure 5.20b. As a result, H_2 recovery of higher than 2 is achievable even at GHSV = 100,000 h^{-1} for S/C > 2. Therefore, though the introduction of the H_2 selective membrane requires a significant capital cost investment, membrane reformers could allow to operate within the regimes wherein the performance of a conventional reformer would be very poor.

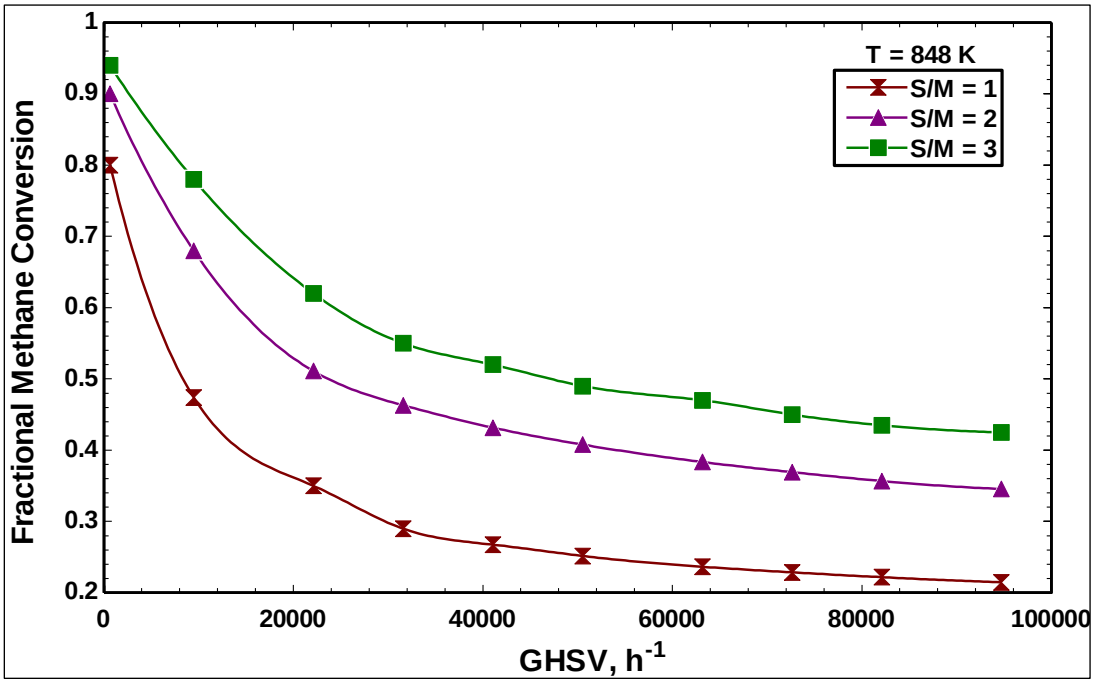

Figure 5.19: Variation of CH_4 conversion as a function of GHSV for different S/C ratios (steam-to-CH_4 feed, S/M = 1, 2 and 3) at T = 848 K, P = 10 bar and P_M = 1bar.

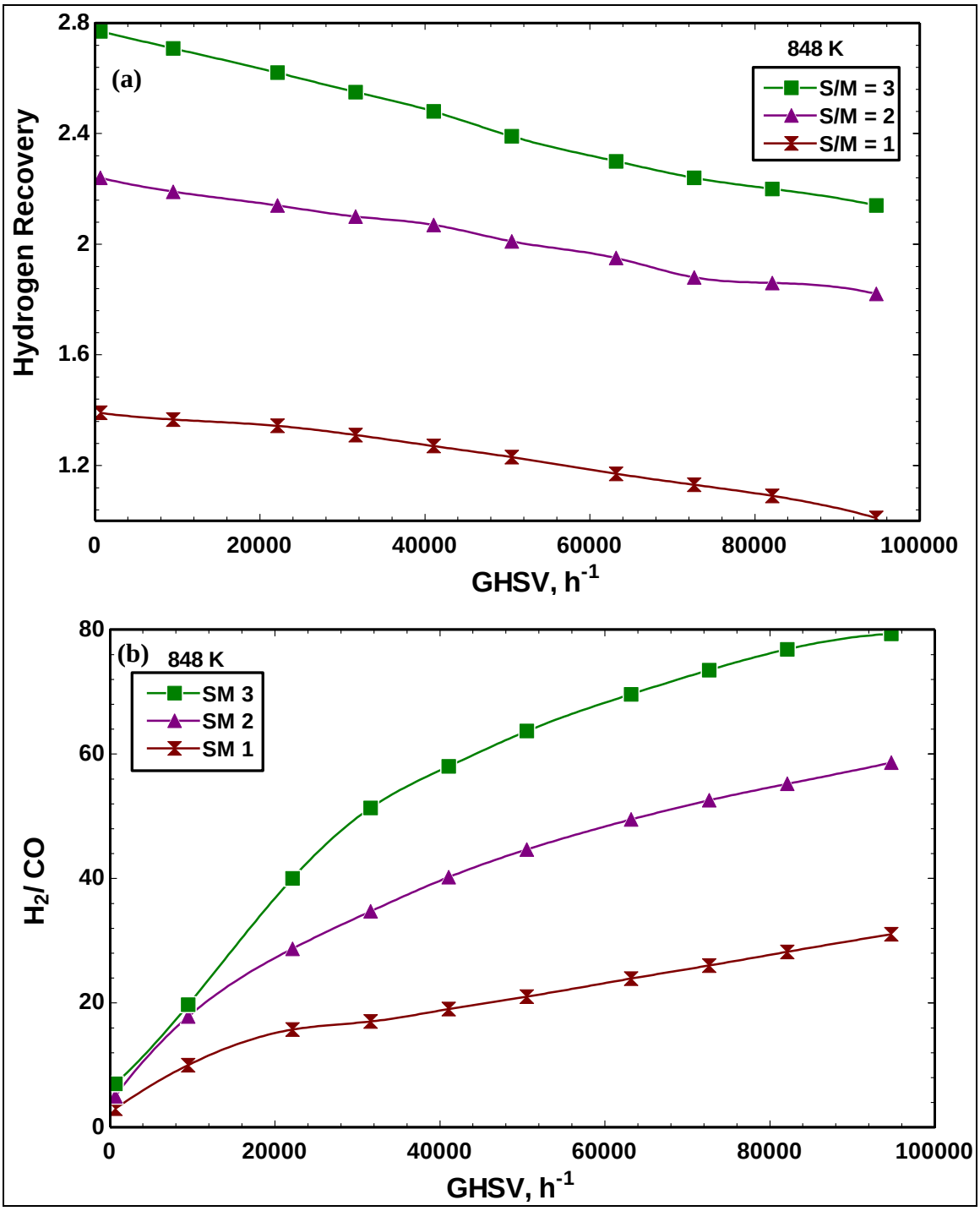

Figure 5.20 Variation of (a) H_2 recovery and (b) H_2/CO ratio as a function of GHSV for different S/C ratios (steam-to-CH_4 feed, S/M = 1, 2 and 3) at T = 848 K, P = 10 bar and P_M = 1bar.

5.6 Reformer performance limits

To summarize the findings and to generalize our results, a brief discussion is provided on the performance limits of Pd membrane reformers in low temperature SMR. As demonstrated and discussed in Section 5.3, H_2 recovery is limited by multiple factors (Figure 5.15a). It is clear that operation at T < 500 °C is disadvantageous because of low activity of the Ni-based catalyst that has very high activation energy and this limitation will be even more severe at elevated space velocities. To estimate the kinetic limit of the reforming process for the given catalyst, it is useful to calculate Damköhler number for the main steam reforming reaction [6] ($W_c = \rho_c(1-\varepsilon)V$, $F_{CH_4,f} = \rho_m Q^{STP}_{CH_4,f}$, ρ_m stands for molar density of ideal gas, k_1 is given in Eq. 31[5]):

$$Da_{SMR} = \frac{k_1}{F_{CH_4,f}/W_c} \equiv \frac{k_1 \rho_c (1-\varepsilon)}{\rho_m GHSV/3600} \tag{35}$$

Substituting the relevant values shows that $Da_{SMR} << 1$ for T < 500 °C even at low GHSV, implying that the process is severely limited by the reaction kinetics ($Da_{SMR} > 10$ is required for optimal performance).

For the membrane reformer, there is another useful dimensionless parameter, the membrane Péclet number (the ratio of the feed flow rate to the membrane separation rate) [6]:

$$Pe_M = \frac{F_{CH_4,f}}{A_M A_{H_2} \sqrt{P_{SR}} \exp\left(-E_{H_2}/R_g T\right)} \equiv \frac{\rho_m GHSV/3600}{(A_M/V) A_{H_2} \sqrt{P_{SR}} \exp\left(-E_{H_2}/R_g T\right)} \tag{36}$$

For the parameters of Figure 5.10, $Pe_M = 1.6-2$, depending on temperature, implying that the membrane reformer is slightly limited by H_2 separation ($Pe_M < 1$ is required for

optimal H_2 recovery [6]). As GHSV is increased (Figure 5.17 and Figure 5.19), Pe_M increases too, achieving $Pe_M \approx 5-7$ for GHSV = 20,000 h^{-1} and $Pe_M \approx 26-34$ for GHSV = 100,000 h^{-1}. Thus, a more permeable membrane (higher A_{H_2} and/or smaller E_{H_2} in Eq. 14) or a larger membrane area-to-reformer volume ratio (A_M/V in Eq. 14) are required to achieve high H_2 recovery and, therefore, to improve significantly CH_4 conversion.

CHAPTER 6

CONCLUSIONS & RECOMMENDATIONS

This chapter is divided into two sections. In the first section, the results in the previous chapter are summarized. In the second section, proposed directions for future research are presented.

6.1 Conclusions:

Low temperature methane reforming in a palladium membrane reactor was analyzed numerically using computational fluid dynamics, in a specific temperature range relevant to solar thermal reforming applications using parabolic trough solar collectors. The simulation results show a significant buildup of radial gradients of hydrogen concentration and concentration polarization, justifying the use of the two-dimensional formulation. Effects of temperature, steam-to-carbon ratio and space velocity on conversion, hydrogen recovery and carbon monoxide selectivity were specifically investigated.

Our results show that, depending on the operating conditions, the membrane reformer performance can be kinetically limited, due to the low activity of the Ni-based catalyst, or limited by transport, due to hydrogen separation. Transport limitations can be intrinsic and global, due to limitations by membrane permeability to hydrogen or insufficient membrane area, or local, due to concentration polarization. These finding emphasize the importance of development of more active catalysts and more permeable membranes for low temperature methane reforming applications.

A significantly high hydrogen recovery is achievable in the membrane reformer at elevated, industrially relevant space velocities, even when moderate to low methane conversions are obtained. This effect was attributed to the enhancement of the water gas shift reaction by hydrogen separation. Importantly, the water gas shift enhancement also reduces the concentration of carbon monoxide, the main source of coke formation at low temperatures. Further work in underway, to include thermal effects and specifically to analyze the efficiency of the solar heat supply by a molten salt flow.

6.2 Recommendations:

The use of membrane reforming technology shows potential for hydrogen production at low temperatures generated by solar parabolic troughs. A single membrane reforming reactor is studied in this work. However, a series of membrane reactors could be created such that the membrane surface area is split to a series of segments. This may lead to higher methane conversions at the reactor exit that makes membrane reforming more suitable in power cycles.

Also, the analysis is made considering the reaction kinetics developed for commercial $Ni–Al_2O_3$ catalyst. Reaction kinetics of the catalyst specially developed for the purpose of low temperature reforming if any can be considered in evaluating the reformer performance. Other major issues related to the effect of carbon deposition and soot formation on the membrane characteristics need detailed investigation.

Finally, cost analysis should be performed to evaluate the economic feasibility of the membrane reformer coupled with the solar parabolic trough system.

NOMENCLATURE:

a_0, a_1, a_2, a_3, a_4 Polynomial coefficients for calculating C_{pi}

A_i Pre exponential factor for Arrhenius equation, dimension of k_i

A_{H2} Membrane permeability to hydrogen, mol/(m^2 s $bar^{0.5}$)

A_M Membrane area, m^2

B_i Pre exponential factor for Van't Hoff equation, dimension of K_i

C_p Specific heat capacity of reaction mixture, KJ/kgK

C_{pi} Specific heat capacity of reaction mixture, KJ/kgK

$D_{i,e}$ Effective diffusion coefficient of species *i*, m^2/s

d_p Catalytic pellet diameter, m

E_{H2} Membrane activation energy for hydrogen permeability, kJ/mol

E_i Activation energy of reaction *i*, KJ/mol

f Fractional methane conversion

F_i Molar flow of species *i*, mol/s

g Gravitational acceleration, m/s^2

h_i Enthalpy of specie *i*, W/m.K

H_i Absorption enthalpy of specie *i*, KJ/mol

J_i Diffusive flux of specie *i*, kg/m^2s

J_{H2} Hydrogen flux through the membrane, mol/(m^2 s)

k_e Effective heat conduction coefficient, W/m.K

k_i Heat conduction coefficient of specie *i*, W/m.K

k_f Heat conduction coefficient of reaction mixture, W/m.K

k_s Heat conduction coefficient of catalyst, W/m.K

K_i Van't Hoff constant for specie *i*

k_i Rate constant of reaction *i*

L Reformer length, m

M_i Molecular weight of specie *i*, kg/mol

m_i Mass fraction of species *i*

p_i Partial pressure of specie *i*, bar

P Pressure of reaction zone mixture, bar

P_M Pressure of the permeate zone, bar

r_i Rate of reaction *i*, kmol/kg_{cat}.h

R Reformer tube radius, m

R_M Membrane tube radius, m

R_i Rate of reaction of specie *i*, mol/kg.s

R Universal gas constant, J/mol.K

S_i Source term, kg/m^3s

S/C Steam-to-Carbon feed ratio

T Temperature of reaction mixture, K

T_o Reference temperature for viscosity calculation, K

V Reformer volume, m^3

$\vec{V}$ Velocity of reaction mixture, m/s

Y_i Mass fraction of specie *i*

W Catalyst bed weight, kg

Greek Symbols:

η_i Effectiveness factor of reaction *i*

ρ_f Density of reaction mixture, kg/m^3

ρ_i Density of Specie *i*, kg/m^3

ρ_c Catalyst bed density, kg/m^3

ρ_c Ideal gas density, mol/m^3

τ Shear stress tensor, N/m^2

ε Porosity of catalyst bed

μ_f Viscosity of reaction mixture, kg/m.s

μ_i Viscosity of specie, kg/m.s

$\mu_{i,o}$ Viscosity of specie at reference temperature, kg/m.s

REFERENCES

1. Keller C.F. Global Warming 2007. An Update to Global Warming: The Balance of Evidence and Its Policy Implications. The Scientific World JOURNAL, 2007. **7**: p. 381-399.
2. World Petroleum Availability 1980-2000. A technical memorandum, NTIS order #PB81-145252
3. IPCC. Carbon Dioxide Capture and Storage. Special Report of the Intergovernmental Panel on Climate Change and Climatology. Cambridge University Press. 2005
4. IEA. Key World Statistics. Stedia Media, France. 2007.
5. Metz, B., et al., IPCC special report on carbon dioxide capture and storage. 2005, Intergovernmental Panel on Climate Change, Geneva (Switzerland). Working Group III.
6. http://www.upstreamonline.com/live/article195770.ece. 2014.
7. Steinberg M. and Cheng H.C. Modern and prospective technologies for hydrogen production from fossil fuels. International Journal of Hydrogen Energy, 1989. **14**(11): p. 797-820.
8. Joensen F. and Rostrup-Nielsen J.R. Conversion of hydrocarbons and alcohols for fuel cells. Journal of Power Sources, 2002. **105**(2): p. 195-201.
9. Rostrup-Nielsen J.R. Catalytic Steam Reforming. in Catalysis, D.J.R. Anderson and P.M. Boudart, Editors. 1984, Springer Berlin Heidelberg. p. 1-117.
10. Armor J.N. The multiple roles for catalysis in the production of H_2. Applied Catalysis A: General, 1999. **176**(2): p. 159-176.

11. Armor J.N. Catalysis and the hydrogen economy. Catalysis Letters, 2005. **101**(3-4): p. 131-135.

12. Lercher J.A, Bitter J.H, Steghuis A.G, Ommen J.G.V and Seshan K. Methane utilisation via synthesis gas generation - catalytic chemistry and technology, in Environmental Catalysis. 1999, p. 103-126.

13. Cheng Z.X, Zhao X.G, Li J.L. and Zhu Q.M. Role of support in CO_2 reforming of CH_4 over a Ni/γ-Al2O3 catalyst. Applied Catalysis A: General, 2001. **205**(1–2): p. 31-36.

14. Edwards J.H and Maitra A.M. The chemistry of methane reforming with carbon dioxide and its current and potential applications. Fuel Processing Technology, 1995. **42**(2–3): p. 269-289.

15. Stagg S.M, Romeo E, Padro C and Resasco D.E. Effect of Promotion with Sn on supported Pt catalysts for CO_2 Reforming of CH_4. Journal of Catalysis, 1998. **178**(1): p. 137-145.

16. Fathi, M. Bjorgum E, Vig T and Rokstad O.A. Partial oxidation of methane to synthesis gas:: Elimination of gas phase oxygen. Catalysis Today, 2000. **63**(2–4): p. 489-497.

17. Ayabe S, Omoto H, Utaka T, Kikuchi R, Sasaki K, Teraoka Y and Eguchi K. Catalytic autothermal reforming of methane and propane over supported metal catalysts. Applied Catalysis A: General, 2003. **241**(1–2): p. 261-269.

18. Pen˜a M.A, Gómez J.P and Fierro J.L.G. New catalytic routes for syngas and hydrogen production. Applied Catalysis A: General, 1996. **144**(1–2): p. 7-57.

19. Palm C, Cremer P, Peters R and Stolten D. Small-scale testing of a precious metal catalyst in the autothermal reforming of various hydrocarbon feeds. Journal of Power Sources, 2002. **106**(1–2): p. 231-237.

20. Sehested J, Johannes A.P.G, Ioannis N.R, Bengaard H and Norskov J.K. Sintering of nickel steam-reforming catalysts: effects of temperature and steam and hydrogen pressures. Journal of Catalysis, 2004. **223(**2): p. 432-443.

21. Parmaliana A, Frusteri F, Arena F, Mondello N and Giordano N. Activity and Characterization of Alkali Doped Ni/MgO Catalysts, in Studies in Surface Science and Catalysis, A.Z. Claudio Morterra and C. Giacomo, Editors. 1989, Elsevier. p. 739-748.

22. Bernardo C.A and Trimm D.L. The kinetics of gasification of carbon deposited on nickel catalysts. Carbon, 1979. **17**(2): p. 115-120.

23. Bernardo C.A, Alstrup I and Rostrup-Nielsen J.R. Carbon deposition and methane steam reforming on silica-supported Ni-Cu catalysts. Journal of Catalysis, 1985. **96**(2): p. 517-534.

24. Trimm D.L. Catalysts for the control of coking during steam reforming. Catalysis Today, 1999. **49**(1–3): p. 3-10.

25. Rakass S, Oudghiri-Hassani H, Rowntree P and Abatzoglou N. Steam reforming of methane over unsupported nickel catalysts. Journal of Power Sources, 2006. **158**(1): p. 485-496.

26. Laosiripojana N and Assabumrungrat S. Methane steam reforming over Ni/Ce–ZrO2 catalyst: Influences of Ce–ZrO2 support on reactivity, resistance toward

carbon formation, and intrinsic reaction kinetics. Applied Catalysis A: General, 2005. **290**(1–2): p. 200-211.

27. Matsumura Y. and Nakamori T. Steam reforming of methane over nickel catalysts at low reaction temperature. Applied Catalysis A: General, 2004. **258**(1): p. 107-114.

28. de Miguel N, Manzanedo J and Arias P L. Testing of a Ni-Al2O3 Catalyst for methane steam reforming using different reaction systems. Chemical Engineering & Technology, 2012. **35**(4): p. 720-728.

29. Ross J.R.H, Steel M.C.F and Zeini-Isfahani A. Evidence for the participation of surface nickel aluminate sites in the steam reforming of methane over nickel/alumina catalysts. Journal of Catalysis, 1978. **52**(2): p. 280-290.

30. Wong C and McCabe R.W. Effects of high-temperature oxidation and reduction on the structure and activity of $RhAl_2O_3$ and $RhSiO_2$ catalysts. Journal of Catalysis, 1989. **119**(1): p. 47-64.

31. Guo X, Sun Y, Yu Y, Zhu X and Liu C.J. Carbon formation and steam reforming of methane on silica supported nickel catalysts. Catalysis Communications, 2012. **19**: p. 61-65.

32. Zhai X, Ding S, Liu Z, Jin Y and Cheng Y. Catalytic performance of Ni catalysts for steam reforming of methane at high space velocity. International Journal of Hydrogen Energy, 2011. **36**(1): p. 482-489.

33. Ruojun S, Liangqu Z and Shendu G. Coking-Resistant nickel catalysts for hydrocarbon steam reforming. Studies in Surface Science and Catalysis, 1991, p. 243-247.

34. Sehested J, Carlsson A, Janssens T V W, Hansen P L and Datye A K. Sintering of nickel steam reforming catalysts on $MgAl_2O_4$ spinel supports. Journal of Catalysis, 2001. **197**(1): p. 200-209.

35. Sehested J. Four challenges for nickel steam-reforming catalysts. Catalysis Today, 2006. **111**(1–2): p. 103-110.

36. Snoeck J.W, Froment G.F and Fowles M. Steam/CO_2 reforming of methane. Carbon formation and gasification on catalysts with various potassium contents. Industrial & Engineering Chemistry Research, 2002. **41**(15): p. 3548-3556.

37. Teixeira S.C and Giudici R. Deactivation of steam reforming catalysts by sintering: experiments and simulation. Chemical Engineering Science, 1999. **54**(15–16): p. 3609-3618.

38. Li C and Chen Y.W. Temperature-programmed-reduction studies of nickel oxide/alumina catalysts: effects of the preparation method. Thermochimica Acta, 1995. **256**(2): p. 457-465.

39. Kuo H.K, Ganesan P and De Angelis R.J. The sintering of a silica-supported nickel catalyst. Journal of Catalysis, 1980. **64**(2): p. 303-319.

40. Hou K, Hughes R. The kinetics of methane steam reforming over a Ni/α-Al_2O catalyst. Chemical Engineering Journal, 2001. **82**(1): p. 311-328.

41. Münster P and Grabke H.J. Kinetics of the steam reforming of methane with iron, nickel, and iron-nickel alloys as catalysts. Journal of Catalysis, 1981. **72**(2): p. 279-287.

42. Nikolla E, Schwank J. and Linic S. Comparative study of the kinetics of methane steam reforming on supported Ni and Sn/Ni alloy catalysts: The impact of the

formation of Ni alloy on chemistry. Journal of Catalysis, 2009. **263**(2): p. 220-227.

43. Ross J.R.H and Steel M.C.F. Mechanism of the steam reforming of methane over a coprecipitated nickel-alumina catalyst. Journal of the Chemical Society, Faraday Transactions 1: Physical Chemistry in Condensed Phases, 1973. **69**(0): p. 10-21.

44. Ko K.D, Lee J.K, Park D and Shin S.H. Kinetics of steam reforming over a Ni/alumina catalyst. Korean Journal of Chemical Engineering, 1995. **12**(4): p. 478-480.

45. Xu J and Froment G.F. Methane steam reforming, methanation and water-gas shift: 1. Intrinsic kinetics. AIChE J, 1989. **35**: p. 88-96.

46. Xu J and Froment G.F. Methane steam reforming: II. Diffusional limitations and reactor simulation. AIChE Journal, 1989. **35**(1): p. 97-103.

47. Pantoleontos G, Kikkinides E.S and Geordiadis M. C. A heterogeneous dynamic model for the simulation and optimisation of the steam methane reforming reactor. International Journal of Hydrogen Energy, 2012. **37**(21): p. 16346-16358.

48. Seo Y.S, Seo D.J, Seo Y.T and Yoon W L. Investigation of the characteristics of a compact steam reformer integrated with a water-gas shift reactor. Journal of Power Sources, 2006. **161**(2): p. 1208-1216.

49. Zhai X, Ding S, Cheng Y, Jin Y and Cheng Y. CFD simulation with detailed chemistry of steam reforming of methane for hydrogen production in an integrated micro-reactor. International Journal of Hydrogen Energy, 2010. **35**(11): p. 5383-5392.

50. Irani M, Alizadehdakhel A, Pour A N, Hoseini N and Adinehnia M. CFD modeling of hydrogen production using steam reforming of methane in monolith reactors: Surface or volume-base reaction model? International Journal of Hydrogen Energy, 2011. **36**(24): p. 15602-15610.

51. Vakhshouri K and Motamed Hashemi M.M.Y. Simulation Study of Radial Heat and Mass Transfer inside a Fixed Bed Catalytic Reactor. World Academy of Science, Engineering and Technology, 2007. 34: p. 180-187.

52. Shayegan J, Motamed Hashemi M.M.Y and Vakhshouri K. Operation of an industrial steam reformer under severe condition: A simulation study. The Canadian Journal of Chemical Engineering, 2008. **86**(4): p. 747-755.

53. Alberton A.L, Schwaab M, Fontes C.E, Bittencourt R.C and Pinto J.C. Hybrid Modeling of Methane Reformers. 1. A Metamodel for the Effectiveness Factor of a Catalyst Pellet with Complex Geometry. Industrial & Engineering Chemistry Research, 2009. **48**(21): p. 9369-9375.

54. Schwaab M, Alberton A.L, Fontes C.E, Bittencourt R.C and Pinto J.C. Hybrid Modeling of Methane Reformers. 2. Modeling of the Industrial Reactors. Industrial & Engineering Chemistry Research, 2009. **48**(21): p. 9376-9382.

55. Marín P, Yolanda P, Diez F.V and Ordonez S. Modelling of hydrogen perm-selective membrane reactors for catalytic methane steam reforming. International Journal of Hydrogen Energy, 2012. **37**(23): p. 18433-18445.

56. De Wilde J and Froment G.F. Computational Fluid Dynamics in chemical reactor analysis and design: Application to the ZoneFlow™ reactor for methane steam reforming. Fuel, 2012. **100**: p. 48-56.

57. Zanfir M. and Gavriilidis A. Catalytic combustion assisted methane steam reforming in a catalytic plate reactor. Chemical Engineering Science, 2003. **58**(17): p. 3947-3960.

58. Soliman M.A, El-Nashaie S.S.E.H, Al-Ubaid A.S and Adris A. Simulation of steam reformers for methane. Chemical Engineering Science, 1988. **43**(8): p. 1801-1806.

59. Pedernera M.N, Pina J, Borio D and Bucala V. Use of a heterogeneous two-dimensional model to improve the primary steam reformer performance. Chemical Engineering Journal, 2003. **94**(1): p. 29-40.

60. Pina J, Noemi S.S, Bucala V and Borio D. Influence of the heat-flux profiles on the operation of primary steam reformers. Industrial & Engineering Chemistry Research. 2001. **40**(23): p. 5215-5221.

61. Coroneo M, Montante G and Paglianti A. Numerical and experimental fluid-dynamic analysis to improve the mass transfer performances of Pd−Ag membrane modules for hydrogen purification. Industrial & Engineering Chemistry Research, 2010. **49**(19): p. 9300-9309.

62. Grashoff G. J, Pilkington C.E and Corti C.W. The purification of hydrogen: a review of the technology emphasizing the current status of palladium membrane diffusion. Report 27 (4), 1983: p. 157–169.

63. Holleck G.L. Diffusion and solubility of hydrogen in palladium and palladium--silver alloys. The Journal of Physical Chemistry, 1970. **74**(3): p. 503-511.

64. Gallucci F, Fernandez E, Corengia F and van Sint Annaland M. Recent advances on membranes and membrane reactors for hydrogen production. Chemical Engineering Science, 2013. **92**: p. 40-66.

65. Siemens - Steam Turbine.

66. Spiewak I. Applications of solar reforming technology. 1993.

67. Buck R, Muir J F and Hogan R E. Carbon dioxide reforming of methane in a solar volumetric receiver/reactor: the CAESAR project. Solar Energy Materials, 1991. **24**(1–4): p. 449-463.

68. Muir J F, Hogan Jr R E, Skocypec R D and Buck R. Solar reforming of methane in a direct absorption catalytic reactor on a parabolic dish: I—Test and analysis. Solar Energy, 1994. **52**(6): p. 467-477.

69. Böhmer M, Langnickel U and Sanchez M. Solar steam reforming of methane. Solar Energy Materials, 1991. **24**(1–4): p. 441-448.

70. Becker M and Raumfahrt L. GAST: The gas-cooled solar tower technology program : Proceedings of the final presentation, May 30-31, Lahnstein, Federal Republic of Germany. 1988: Springer-Verlag. 396.

71. Spiewak I, Epstein M and Segal A. The Weizmann Institute of Science 480-KW reformer system," IEA SSPS Task V, Proceedings of the workshop on methane Reforming. Koeln, 1991.

72. Diver R B, Fish J D, Levitan R, Levy M, Meirovitch E and Rosin H. Solar test of an integrated sodium reflux heat pipe receiver/reactor for thermochemical energy transport. Solar Energy, 1992. **48**(1): p. 21-30.

73. Gokon N, Oku Y, Kaneko H and Tamaura Y. Methane reforming with CO_2 in molten salt using FeO catalyst. Solar Energy, 2002. **72**(3): p. 243-250.

74. Berman A, Karn R K and Epstein M. Steam reforming of methane on a Ru/Al_2O_3 catalyst promoted with Mn oxides for solar hydrogen production. Green Chemistry, 2007. **9**(6): p. 626-631.

75. De Maria G, D'Alessio L, Coffari E, Paolucci M and Tiberio C.A. Thermochemical storage of solar energy with high-temperature chemical reactions. Solar Energy, 1985. **35**(5): p. 409-416.

76. De Maria G, Tiberio C.A, D'Alessio L, Piccirilli M, Coffari E and Paolucci M. Thermochemical conversion of solar energy by steam reforming of methane. Energy, 1986. **11**(8): p. 805-810.

77. Chibane L and Djellouli B. Methane Steam Reforming Reaction Behaviour in a Packed Bed Membrane Reactor. International Journal of Chemical Engineering Applications, 2011. 2: p. 147-156.

78. Fernandes F.A.N and Soares Jr A.B. Methane steam reforming modeling in a palladium membrane reactor. Fuel, 2006. **85**(4): p. 569-573.

79. Falco M.D, Marrelli L and Iaquaniello G. Membrane reactors for hydrogen production processes. 2011: Springer Science & Business Media. 244.

80. Simakov D.S.A and Sheintuch M. Demonstration of a scaled-down autothermal membrane methane reformer for hydrogen generation. International Journal of Hydrogen Energy, 2009. **34**(21): p. 8866-8876.

81. Simakov D.S.A and Sheintuch M. Model-based optimization of hydrogen generation by methane steam reforming in autothermal packed-bed membrane reformer. AIChE Journal, 2011. **57**(2): p. 525-541.

82. Coroneo M, Montante G, Giacinti Baschetti M and Piaglianti A. CFD modelling of inorganic membrane modules for gas mixture separation. Chemical Engineering Science, 2009. **64**(5): p. 1085-1094.

83. Goto S, Assabumrungrat S, Tagawa T and Praserthdam P. The effect of direction of hydrogen permeation on the rate through a composite palladium membrane. Journal of Membrane Science, 2000. **175**(1): p. 19-24.

84. Staudacher M, Harasek M, Brinkmann T, Hilgendorff W and Friedl A. CFD simulation of mass transfer effects in gas and vapour permeation modules. Desalination, 2002. **146**(1–3): p. 237-241.

85. Fluent Inc. User's Guide. 2006.

86. Xu J and Froment G.F. Methane steam reforming, methanation and water-gas shift: I. Intrinsic kinetics. AIChE Journal, 1989. **35**(1): p. 88-96.

87. Patankar S. Numerical Heat Transfer and Fluid Flow. 1980: CRC Press. 218.

88. Giaconia A, Falco M.D, Caputo G, Grena R, Tarquini P and Marrelli L. Solar steam reforming of natural gas for hydrogen production using molten salt heat carriers. AIChE Journal, 2008. **54**: p. 1932-1944.

89. Giaconia A, Turchetti L, Monteleone G, Morico B, Iaquaniello G and Shabtai K. Development of a solar-powered, fuel-flexible compact steam reformer: The CoMETHy Project. Chemical Engineering Transactions, 2013. **35**: p. 433-438.

90. Chen W.J, Sheu F.R and Savage R.L. Catalytic activity of coal ash on steam methane reforming and water-gas shift reactions. Fuel Processing Technology, 1987. **16**(3): p. 279-288.

91. Sehested J. Sintering of nickel steam-reforming catalysts. Journal of Catalysis, 2003. **217**(2): p. 417-426.

VITAE

Name	:Mohammed Waseeuddin
Nationality	:Indian
Date of Birth	:10/14/1988
Email	:wasee_mech@yahoo.com
Address	:KFUPM Student Housing, KFUPM, Dhahran-31261, KSA..
Academic Background	:Master of Science (M.S) in Mechanical Engineering 2014, GPA: 3.53/4.0, KFUPM, KSA.
	Bachelors in Mechanical Engineering (B.E.), Percentage 85/100, Osmania University, 2010, INDIA.